DESIGNING IMMOBILIZED CATALYSTS FOR CHEMICAL TRANSFORMATIONS: NEW PLATFORMS TO TUNE THE ACCESSIBILITY OF ACTIVE SITES

A Dissertation
Presented to
The Academic Faculty

by

Wei Long

In Partial Fulfillment
of the Requirements for the Degree
Doctor of Philosophy in the
School of Chemistry & Biochemistry

Georgia Institute of Technology
August 2012

DESIGNING IMMOBILIZED CATALYSTS FOR CHEMICAL TRANSFORMATIONS: NEW PLATFORMS TO TUNE THE ACCESSIBILITY OF ACTIVE SITES

Approved by:

Dr. Christopher W Jones, Advisor
School of Chemical & Biomolecular Engineering and School of Chemistry & Biochemistry
Georgia Institute of Technology

Dr. Charles L Liotta
School of Chemistry & Biochemistry
Georgia Institute of Technology

Dr. E. Kent Barefield
School of Chemistry & Biochemistry
Georgia Institute of Technology

Dr. John Zhang
School of Chemistry & Biochemistry
Georgia Institute of Technology

Dr. William J Koros
School of Chemical & Biochemical Engineering
Georgia Institute of Technology

Date Approved: June 20, 2012

“Perseverance, character and character, hope.” – Romans 5:4

“Two roads diverged in a wood and I – I took the one less traveled by.” – Robert Frost

ACKNOWLEDGEMENTS

First I would like to thank Dr. Chris Jones, for his invaluable guidance. It is his advice and motivation along the journey which constantly help improve my skills and mindset in research. The ideas, questions, and suggestions from him enlightened me for these scientific challenges undertaken. Furthermore, I would like to thank the team members. It is a great memory to have the opportunity of working with them together and build the friendship to cherish forever. Thank them for bringing joy and happiness to the lab. Particular thanks go to Chris Gill, Krishnan Venkatasubbaiah, Nicholas Brunelli, Mariefel Valenzuela Olarte, Eric Ping, Jeff Drese, Genggeng Qi, Jun Huang and Xunjin Zhu for their mentorship and advice.

Thanks to my parents, Wangxiang Long and Guihua Chen, for their loving parenting and sound advice throughout my life. They taught me integrity, love, self-responsibility, and many others, which guide me all the time. These virtues helped me a lot both in personal lives and in the research work. And special thanks to my husband Wei Zhang, who has always kept my spirits high and encouraged me to follow my dream. This past year and a half has been difficult without him nearby, but our love thrived, becoming stronger with the distance and time.

TABLE OF CONTENTS

Page

ACKNOWLEDGEMENTS iv

LIST OF TABLES x

LIST OF FIGURES xii

LIST OF SYMBOLS AND ABBREVIATIONS xvi

SUMMARY xviii

CHAPTER

1 INTRODUCTION 1

1.1 General Remarks 1

1.2 Why Immobilize A Catalyst? 3

1.3 Immobilization Techniques 4

1.3.1 Covalent binding 4

1.3.2 Adsorption 6

1.3.3 Entrapment 7

1.4 Support Materials 8

1.4.1 Silica materials 9

1.4.2 Magnetic nanoparticles 10

1.4.3 Inorganic-polymer composites 13

1.5 Commercial Applications of Immobilized Catalysts 14

1.6 Optimization of Immobilized Catalysts 15

1.7 Catalyst Systems Studied in This Work 17

1.7.1 Magnetic nanoparticles (MNP) supported catalysts for ring-opening reactions 17

1.7.2 Silica-polymer composite supported catalysts 19

1.8 Thesis Goals 20

1.9 References 22

2 MAGNETIC NANOPARTICLE SUPPORTED ALUMINUM ISOPROPOXIDE FOR RING-OPENING POLYMERIZATION OF Є-CAPROLACTONE 26

2.1 Introduction 26

2.2 Experimental Section 28

2.2.1 Chemicals and materials 28

2.2.2 Characterization 28

2.2.3 Catalyst preparation 29

2.2.4 Polymerization 29

2.2.5 Catalyst recycles 30

2.3 Results and Discussions 31

2.3.1 Catalyst preparation and characterization 31

2.3.2 Kinetics of the fresh catalyst 34

2.3.3 Leaching tests 35

2.3.4 Polymerization 35

2.3.5 Recyclability of the catalysts 42

2.4 Conclusions 45

2.5 Acknowledgment 46

2.6 References 47

3 CATALYTIC REGIOSELECTIVE EPOXIDE RING OPENING WITH PHENOL USING HOMOGENEOUS AND SUPPORTED ANALOGUES OF DIMETHYLAMINOPYRIDINE 51

3.1 Introduction 51

3.2 Experimental Methods 53

3.2.1 Chemicals 53

3.2.2 Synthesis of N-methyl-N-(3-(triethoxysilyl)propyl)pyridin-4-amine 53

3.2.3 Mesoporous SBA-15 silica synthesis 54

3.2.4 N-methyl-N-(3-(triethoxysilyl)propyl)pyridin-4-amine grafting 55

3.2.5 Magnetic nanoparticle synthesis 55

3.2.6 Materials characterization 56

3.2.7 Catalysis 57

3.3 Results and Discussions 59

3.3.1 Homogeneous reactions 59

3.3.2 Heterogeneous catalysts 63

3.3.2.1 Materials characterization – SBA_MPAP 63

3.3.2.2 Materials characterization – MNP_MPAP 67

3.3.3 Heterogeneous catalysis 70

3.4 Conclusions 75

3.5 Acknowledgements 76

3.6 References 77

4 HYBRID SULFONIC ACID CATALYSTS BASED ON SILICA-SUPPORTED POLY(STYRENE SULFONIC ACID) BRUSH MATERIALS AND THEIR APPLICATION IN ESTER HYDROLYSIS 81

4.1 Introduction 81

4.2 Experimental Section 84

4.2.1 Chemicals and materials 84

4.2.2 Synthesis of the new ATRP initiator silane 85

4.2.3 Preparation of catalysts 87

4.2.4 Characterization 88

4.2.5 Catalytic hydrolysis of ethyl lactate 89

4.3 Results and Discussions 90

4.3.1 Synthesis of the ATRP initiator silanes 90

4.3.2 Preparation of the supported initiator 91

4.3.3 Surface initiated ATRP of styrene 93

4.3.4 Sulfonation of the poly(styrene) brushes 95

4.3.5 Catalytic hydrolysis of ethyl lactate 100

4.4 Conclusions 106

4.5 Acknowledgements 106

4.6 References 107

5 AMINOPOLYMER-SILICA COMPOSITE SUPPORTED PALLADIUM CATALYSTS FOR SELECTIVE HYDROGENATION OF ALKYNES 110

5.1 Introduction 110

5.2 Experimental Section 113

5.2.1 Chemicals and materials 113

5.2.2 Characterization 114

5.2.3 Preparation of aminopolymer-silica composites 115

5.2.4 Preparation of supported palladium catalysts 117

5.2.5 Selective hydrogenation of alkynes 118

5.2.6 Catalyst regeneration 119

5.3 Results and Discussions 120

5.3.1 Preparation and characterization of aminopolymer-silica composites 120

5.3.2 Preparation and catalytic performance of Pd-HAS 123

5.3.3 Catalytic performance of Pd-SiO_2-gt-PEI 129

5.3.4 Investigation on recoverability and recyclability 137

5.4 Conclusions 138

5.5 Acknowledgements 139

5.6 References 139

6 SUMMARY AND FUTURE WORK 144

6.1 Summary 144

6.2 Suggested future work 147

6.2.1 Further investigation on the modification effects of polymer composites 149

6.2.2 Characterization of aminopolymer composite supported Pd nanoparticles using XAS 150

6.2.3 Development of Pd nanoparticles on polymer brush sulfonic acid for the direct synthesis of hydrogen peroxide 150

6.3 References 151

LIST OF TABLES

Page

Table 1.1: E factors. 1

Table 1.2: Comparison of three main immobilization techniques. 7

Table 1.3: Summary comparison of the synthetic methods. 12

Table 2.1: ROP of ε-caprolactone. 39

Table 2.2: EA results of fresh and recycled catalysts. 42

Table 2.3: ROP of ε-caprolactone with fresh and recycled catalyst. 44

Table 2.4: Hydrodynamic particle size of bare MNP and Al-MNP catalysts. 45

Table 3.1: Conversion and regioselectivity for the epoxide ring opening of epoxy hexane with phenol using homogenous DMAP 59

Table 3.2: Conversion and regioselectivity comparison for different solvents for the epoxide ring opening of epoxy hexane using phenol with homogeneous DMAP 60

Table 3.3: Conversion and regioselectivity of epoxide ring-opening reactions using homogeneous DMAP using different nucleophiles and epoxides. 62

Table 3.4: Physical and chemical characteristics of the different functionalized mesoporous and magnetic materials. 65

Table 3.5: Conversion and regioselectivity comparison for different heterogeneous catalysts. 71

Table 4.1: Loading and density of the supported initiator. 92

Table 4.2: Physical characteristics of the polymer brush materials prepared via surface initiated ATRP. 95

Table 4.3: Compositions of solid polymer brush materials after sulfonation. 98

Table 4.4: EA of the fresh SiO_2@alkyl-PS-SO_3H and the recycled ones. 103

Table 4.5: EA of the fresh SiO_2@ester-PS- SO_3H and the recycled ones. 103

Table 4.6: EA of the fresh SiO_2@ester-PS- SO_3H_2 and the recycled catalysts. 105

Table 5.1: Compositions of aminopolymer-silica composites. 122

Table 5.2: Physical characteristics of aminopolymer-silica composites. 123

Table 5.3: Catalytic performance of Pd-HAS (H_2 reduction) with different substrates. 124

Table 5.4: Catalytic performance of aminopolymer-silica supported Pd catalysts and comparison to catalysts described in the literature. 128

Table 5.5: Composition of the catalysts. 130

Table 5.6: Binding energies (BE) of different peaks in XPS spectra of aminopolymer-silica supported catalysts. 133

Table 5.7: Catalytic performance of aminopolymer-silica composite supported Pd catalysts. 136

Table 5.8: Comparison of compositions of the fresh and used catalysts. 137

Table 5.9: Comparison of activity of fresh, used and regenerated catalysts. 138

LIST OF FIGURES

Page

Figure 1.1: Cartoon of different types of catalysts. 3

Figure 1.2: Post-grafting and co-condensation method in meso-structured silica materials. 5

Figure 1.3: Polymeric supports for catalysts immobilization. 6

Figure 1.4: Examples of immobilized catalysts for commercial applications. 15

Figure 1.5: MNP supported catalysts for ROP. 18

Figure 1.6: Silica-polymer brush sulfonic acids for the hydrolysis of ethyl lactate. 19

Figure 1.7: Aminopolymer-silica composite supported Pd catalysts. 20

Figure 2.1: ROP of ε-caprolactone. 27

Figure 2.2: XRD pattern of the $CoFe_2O_4$ nanoparticle support. 31

Figure 2.3: TEM images of the bare MNP (a) and the fresh catalyst (b). 32

Figure 2.4: Preparation of MNP supported aluminum catalysts. 33

Figure 2.5: FT-IR spectra of bare MNP, fresh catalyst and recycled catalyst. 34

Figure 2.6: Kinetics for ROP of ε-caprolactone with MNP supported aluminum catalyst. 35

Figure 2.7: ^{1}H NMR spectrum of poly (ε-caprolactone). 37

Figure 2.8: GPC curves of poly(caprolactone) produced with the MNP supported aluminum catalyst. 38

Figure 2.9: Mn (GPC) vs conversion for ROP of ε-CL. 40

Figure 2.10: GPC curves of poly(caprolactone) produced with the MNP supported aluminum catalyst. 41

Figure 2.11: Kinetics for ROP of ε-caprolactone with fresh and recycled catalysts. 43

Figure 2.12: TEM images of fresh catalyst (a), catalyst after one cycle (b), catalyst after two cycles (c) and catalyst after three cycles (d). 45

Figure 3.1: Base catalysts used for the epoxide ring opening, (a) homogeneous DMAP, (b) MPAP organosilane, (c) polyBMAP, (d) MNP_MPAP, and (e) SBA_MPAP. 53

Figure 3.2: Base catalyzed epoxide ring opening. 58

Figure 3.3: Kinetics of the reaction of 1,2-epoxyhexane with phenol catalyzed with homogeneous DMAP (10 mol%) at 80°C in toluene. 61

Figure 3.4: X-ray diffraction pattern of SBA-15 before (Bare) and after functionalization and silanol capping (SBA_MPAP_HMDS). 63

Figure 3.5: Nitrogen physisorption comparison of the silica material before and after grafting of the organosilane. 64

Figure 3.6: TGA curve for the mesoporous silica organosilane (SBA_MPAP) and the bare mesoporous material (SBA_Bare). After three ERO reaction cycles, the material was analyzed for the increase in organic content (SBA_MPAP Post ERO). 66

Figure 3.7: ^{13}C CP MAS NMR of SBA_MPAP. 66

Figure 3.8: FTIR comparison of the bare silica (SBA-15), MPAP functionalized silica before reaction (SBA_MPAP) and after 3 reaction cycles (SBA_MPAP Post ERO), and the MPAP and HMDS functionalized silica before (SBA_MPAP_HMDS) and after 3 reaction cycles (SBA_MPAP_HMDS Post ERO). 67

Figure 3.9: FTIR spectra of magnetic nanoparticles with oleic acid capping ligands (Fe_3O_4 Oleic Acid), after silica coating (Fe_3O_4 SiO_2), after functionalization with the PMAP organosilane (Fe_3O_4 PMAP), and after 3 reaction cycles (Fe_3O_4 PMP Post ERO). 68

Figure 3.10: X-ray diffraction pattern of the as-synthesized Fe_3O_4 nanoparticles before (Fe_3O_4) and after silica coating (Fe_3O_4 SiO_2). 69

Figure 3.11: TEM image of the silica coated magnetic nanoparticles. 69

Figure 3.12: TGA curve for the as-synthesized Fe_3O_4 magnetic nanoparticles (MNP_Bare) and for organic functionalized, silica coated nanoparticles (MNP_MPAP). 70

Figure 3.13: TGA curve for the bare mesoporous material before (SBA_Bare) and after one reaction cycle with homogeneous DMAP (SBA_Bare+Homogeneous DMAP). 73

Figure 3.14: FTIR spectra of the bare mesoporous material before (SBA_Bare) and after one ERO reaction cycle with homogeneous DMAP (SBA_Bare_Homogeneous DMAP). 73

Figure 3.15: ^{13}C CP MAS NMR of SBA_MPAP_HMDS. 75

Figure 3.16: TGA curve for the mesoporous silica functionalized with the organosilane and with the silanols capped through an HMDS (SBA_MPAP_HMDS) and the bare mesoporous material (SBA_Bare). After three ERO reaction cycles with the functionalized silica, the recovered material was analyzed for the increase in organic content (SBA_MPAP_HMDS Post ERO). 75

Figure 4.1: Silica-supported poly(styrene sulfonic acid) brush materials. 84

Figure 4.2: Synthesis of ethyl 2-chloro-2-methyl-7-(trimethoxysilyl) heptanoate. 91

Figure 4.3: FT-IR of SiO_2@ester initiator (a); SiO_2@alkyl initiator (b); SiO_2@ester-PSt (c). 92

Figure 4.4: XPS spectra of SiO_2@alkyl initiator (a); SiO_2@ester initiator (b). 93

Figure 4.5: TEM images of SiO_2@alkyl-PS (a); SiO_2@ester-PS (b). 95

Figure 4.6: Preparation of SiO_2@alkyl-PS-SO_3H. 95

Figure 4.7: FT-IR of Amberlyst 15 (a); SiO_2@alkyl-PS-SO_3H (b); SiO_2@ester-PS-SO_3H (c). Amberlyst 15 is sulfonic acid resin based on cross-linked styrene-divinylbenzene copolymers. 98

Figure 4.8: XPS spectra of SiO_2@alkyl-PS-SO_3H (a); SiO_2@ester-PS-SO_3H (b). 99

Figure 4.9: TGA of SiO_2@alkyl-PS-SO_3H. 99

Figure 4.10: Kinetics of ethyl lactate hydrolysis. 100

Figure 4.11: Kinetics of the catalysts during recycles: SiO_2@alkyl-PS-SO_3H (a); SiO_2@ester-PS-SO_3H (b). 101

Figure 4.12: FT-IR spectra of SiO_2@alkyl-PS-SO_3H (a); SiO_2@alkyl-PS-SO_3H after run 1 (b). 102

Figure 4.13: FT-IR spectra of SiO_2@ester-PS-SO_3H (a); SiO_2@ester-PS-SO_3H after run 1 (b). 102

Figure 4.14: Normalized carbon content of the catalysts after each cycle. 104

Figure 4.15: Kinetics of SiO_2@ester-PS-SO_3H_2 during recycles. 105

Figure 5.1: Reaction routes of selective hydrogenation of di-substituted alkynes. 113

Figure 5.2: Preparation of aminopolymer-silica composites. 121

Figure 5.3: FT-IR of HAS (a); SBA-gt-PEI (b); MCF-gt-PEI (c). 122

Figure 5.4: Preparation of aminopolymer-silica supported Pd catalysts. 124

Figure 5.5: Solution UV-Vis of PEI (a); Pd(II)-PEI (b); Pd(0)-PEI (c); $Pd(OAc)_2$ (d). 126

Figure 5.6: Solid UV-Vis of HAS (a); Pd(II)-HAS (b); Pd-HAS (H_2 reduction) (c); Pd-HAS ($NaBH_4$ reduction) (d). 126

Figure 5.7: TEM of Pd-SBA-gt-PEI (a); Pd-MCF-gt-PEI (b); Pd-HAS ($NaBH_4$ reduction) (c); Pd-SBA-gt-PEI (used) (d). 131

Figure 5.8: Reaction profiles of Pd-HAS ($NaBH_4$ reduction). 133

Figure 5.9: Reaction profiles of Pd-SBA-gt-PEI. 134

Figure 5.10: Reaction profiles of Pd-MCF-gt-PEI. 134

LIST OF SYMBOLS AND ABBREVIATIONS

atm	atmosphere
ATRP	atom transfer radical polymerization
BET	Brunauer-Emmet-Teller
CP-MAS	cross-polarization magic angle spinning
DMAP	4-dimethylaminopyridine
DSC	differential scanning calorimetry
EA	elemental analysis
FID	flame ionization detector
FT	Fourier transform
GC	gas chromatography
GPC	gel permeation chromatography
h	hour(s)
IR	infrared spectroscopy
MCF	mesocellular foam
min	minute(s)
MNP	magnetic nanoparticles
NMR	nuclear magnetic resonance
ROP	ring-opening polymerization
SBA-15	Santa Barbara mesoporous silica material #15
SEM	scanning electron microscopy
TEOS	tetraethylorthosilicate
TEM	transmission electron microscopy
TGA	thermogravimetric analysis

TOF	turnover frequency
UV-Vis	ultraviolet-visible
XRD	X-ray diffraction
XPS	X-ray Photoelectron Spectroscopy
XAS	X-ray absorption spectroscopy

SUMMARY

Chemical catalysts are divided into two traditional categories: homogeneous and heterogeneous catalysts. Although homogeneous (molecular) catalysts tend to have high activity and selectivity, their wide application is hampered by the difficulties in catalyst separation. In contrast, the vast majority of industrial scale catalysts are heterogeneous catalysts based on solid materials. Immobilized catalysts, combining the advantages of homogeneous and heterogeneous catalysts, have developed into an important field in catalysis research.

This dissertation presents synthesis, characterization and evaluation of several novel immobilized catalysts. In the first part, MNP supported aluminum isoproxide was developed for ROP of ϵ-caprolactone to achieve facile magnetic separation of catalysts from polymerization system and reduce toxic metal residues in the poly(caprolactone) product. Chapter 3 presents a silica coated MNP supported DMAP catalyst that was synthesized and displayed good activity and regio-selectivity in epoxide ring opening reactions. In Chapter 4, hybrid sulfonic acid catalysts based on polymer brush materials have been developed. The unique polymer brush architecture permits high catalyst loadings as well as easy accessibility of the active sites to be achieved in this catalytic system. In Chapter 5, aminopolymer-silica composite supported Pd catalysts with good activity and selectivity were developed for the selective hydrogenation of alkynes. In this case, the aminopolymer composite works as a stabilizer for palladium nanoparticles, as well as a modifier to tune the catalyst selectivity. All in all, the general theme of the thesis is developing new immobilized catalysts with improved activity/selectivity as well as easy separation via rational catalyst design.

CHAPTER 1

INTRODUCTION

1.1 General Remarks

The chemical industry manufactures all kinds of chemicals from plastics, lubricants, oils, perfumes, etc. to agrochemicals and drug precursors, which are indispensable to our common lives. During chemical manufacturing, a large amount of waste was generated, which increases the environmental pollution as well as the process cost of handling the waste products. According to the E-factor (tons of waste generated per ton of product manufactured) developed by Sheldon[1] (Table1.1), from oil refining, bulk chemicals to fine chemicals and pharmaceuticals, with the increase in added value, the generation of waste is also increased. This is one of the major challenges facing us today. How can we produce chemical products in a more environmentally friendly way?

Table 1.1. E factors (tons of waste generated per ton of product)[1]

Industry segment	Annual product tonnage	E factor
Oil refining	$10^6 – 10^8$	Approx. 0.1
Bulk chemicals	$10^4 – 10^6$	< 1-5
Fine chemicals	$10^2 – 10^4$	5 – 50+
Pharmaceuticals	$10 – 10^3$	50– 100+

Also, in the chemical industry, the majority of chemical feedstocks is based on petroleum. However with the dwindling reserves of fossil resources, it is urgent to find other resources as substitutes to the petroleum feedstock. One important alternative resource is biomass, which has attracted tremendous attention in recent years.

Catalysis is a key to all the important issues. Catalysts allow chemical reactions to be performed under mild conditions to save energy, increase the product yields to reduce waste, and open the door for new transformation routes in exploring alternative chemical feedstocks. Chemical catalysts could be divided into two main categories: catalysts in the same phase with reactants (homogeneous), and catalysts in a different phase from reactants and products (heterogeneous). Heterogeneous catalysts, such as metal oxides, zeolites, and supported metals, are among the most important catalytic systems and have wide applications in industry. They are normally multi-sited and could be easily separated from the products. Homogeneous catalysts, such as mineral acids, metal-ligand complexes, are generally well defined chemical compounds. They act under mild conditions and normally display very high activity and selectivity. Combining the advantages of homogeneous catalysts (high activity and selectivity, easy tunability) and heterogeneous catalysts (easy separation) leads to the development of immobilized molecular catalysts, which have attracted a lot of attention and developed into an important field in the catalysis research[2–8] (Figure 1.1).

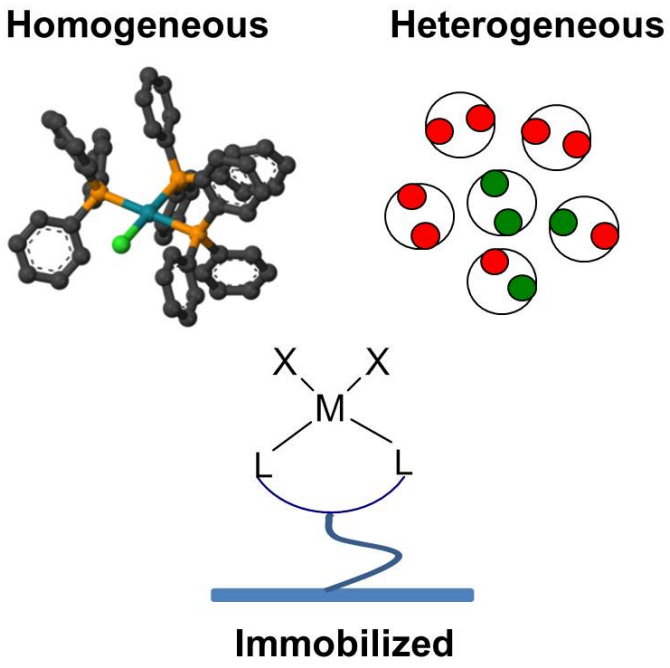

Figure 1.1. Cartoon of different types of catalysts.

1.2 Why Immobilize A Catalyst?

It normally takes extra efforts to prepare immobilized catalysts, which increase the synthesis complexity as well as the cost. One might ask how to justify the additional efforts for the preparation of immobilized catalysts. Here are several reasons. Compared to homogeneous catalysts, it is always much easier to separate immobilized catalysts (filtration, centrifuge, magnetic separation, etc.), making it more realistic to reuse the catalysts. It is also more efficient for the product isolation and purification as well as removal of the catalyst residues, which is especially important for the catalytic systems involving toxic metals.

Immobilization of the homogeneous metal-ligand molecular complexes can help isolation of the surface active species to prevent agglomeration of the catalysts and

maintain their activities for a longer time. Sometimes the supports could also interact with the immobilized functional groups to benefit the overall catalytic reactions. The immobilized catalysts can be easily applied in different reactors, such as fixed bed reactors, membrane reactors, etc., making it easier to incorporate the catalysts into the industrial chemical processes.

1.3 Immobilization Techniques

Different immobilization methods have been used in the literature to heterogenize organic groups or metal complexes onto solid supports.[9] Covalent attachment is the most widely used immobilization strategy. Other immobilization techniques, such as adsorption and entrapment, are also commonly used. The major immobilization techniques are summarized here (Table 1.2).

1.3.1 Covalent binding

The covalent binding method is used to build a robust attachment between the functional groups and the solid supports. Compared to the non-covalent interactions, catalysts prepared with this method can be used in a wider range of reaction conditions and the potential catalyst leaching problem can also be prevented. Depending on the solid supports, different strategies have been used for the covalent attachment of active species to the solid surface. Silicas and organic polymers are the two most commonly used supports for the catalyst immobilization.

For silica materials[10], two main methods have been extensively described in the literature to incorporate active sites into the solid matrices: post-grafting and co-condensation (direct synthesis). The post-grafting method (Figure 1.2) is based on the modification of the silica surface via silylation, which is a chemical reaction between surface silanols (isolated, germinal, or vicinal) and alkoxy- or chloro- organosilanes. In this method, organic groups or ligands with defined structures are attached onto the solid surface, thus avoiding potential side reactions and formation of undesirable chemical species. Catalysts via co-condensation method are prepared by sol-gel co-condensations of the siloxanes and the desired organosiloxanes, often in the presence of structure directing agents. The post-grafting method tends to produce materials with better defined structures, while the co-condensation method yields materials with a more uniform surface coverage of functional groups.

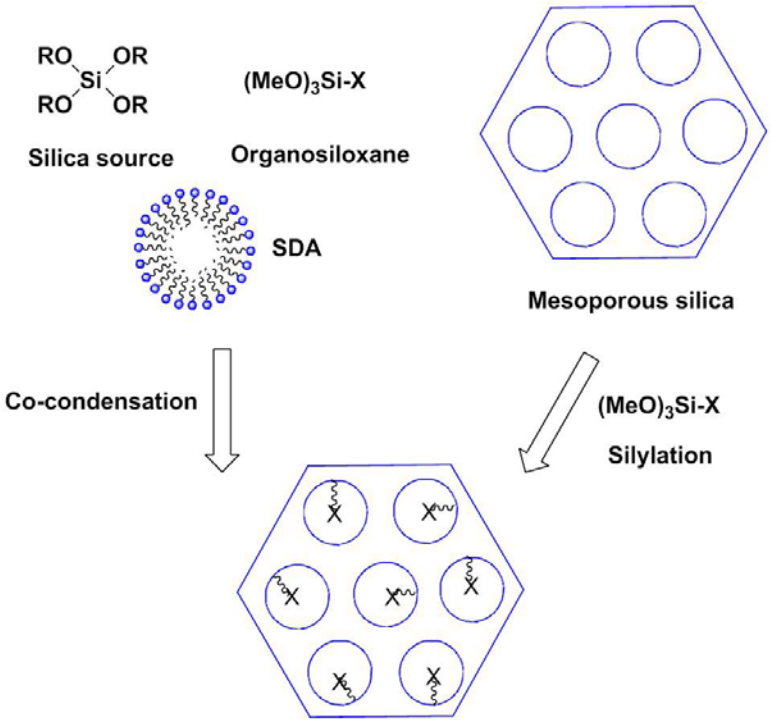

Figure 1.2. Post-grafting and co-condensation method in mesostructured silica materials.

For polymeric materials, similar strategies are also used (Figure 1.3) to prepare the polymer supported catalysts: copolymerization of monomers, co-monomers and crosslinking agents (direct synthesis); or attachment of functional groups to the anchor points in the pre-formed resins (post-grafting).

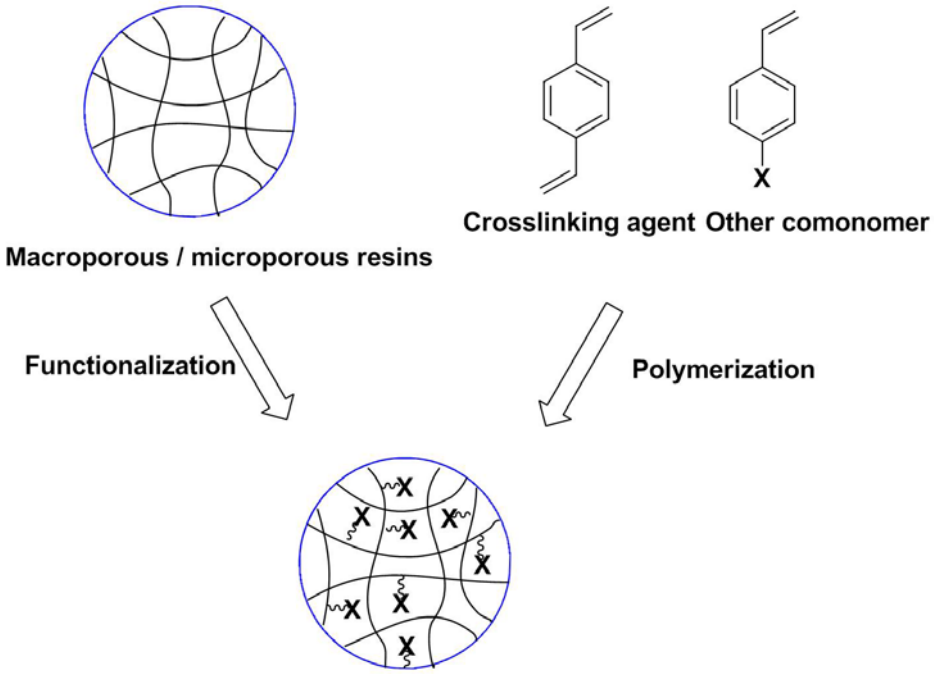

Figure 1.3. Polymeric supports for catalysts immobilization.

1.3.2 Adsorption

Adsorption is another common immobilization technique for catalytically active species. By contacting preformed solids with organic species or metal complexes, the catalytic species could be bond to the surface via physisorption, which is normally very weak, or chemisorption, e.g. anionic or cationic bonding, or metal-ligand interactions, which is much stronger than physisorption. The adsorption method is relatively easier to use compared to the covalent binding method, since there is no need to modify the

organic ligands for immobilization. However catalysts prepared with the adsorption method could only be used in limited reaction solvents and temperatures, and the catalytic species tend to be leached into the reaction solution to some extent.

Table 1.2. Comparison of three main immobilization techniques.

Immobilization techniques	Examples	Pros/Cons
Covalent binding	Silica supported propyl sulfonic acids;[10] polymer resin supported Co(III)-Salen catalysts.[11]	Stable attachment, less leaching, increased complexity to synthesize the immobilization precursors.
Adsorption	Heteropoly acids as anchoring agents between supports and metal complexes.[12]	Limited reaction conditions, prone to be leached.
Entrapment	Polysaccharide supported metal nanoparticles;[13] Ni-Salen complexes inside zeolites.[14]	Diffusion limitation.

1.3.3 Entrapment

One unique example of the entrapment method is "ship in a bottle". For catalysts prepared in this manner, catalysts are assembled and thereby entrapped inside the cage-like pores of porous materials, such as zeolites, MCM-41, etc. The dimension of the metal complexes/organic groups is typically larger than the size of the pore mouth to

prevent the diffusion of the active species out of the pores. However catalysts prepared with this method normally have limitations on the diffusion of reactants and products as well as constraints on the interactions between substrates and active sites, which means that this approach could not be generally adopted.

Another good example of entrapment is demonstrated in the case of supported metal nanoparticle catalysts.[13,15,16] Since nanoparticles are prone to agglomeration naturally, with the help of a polymeric network, nanoparticles can be entrapped inside the polymer matrix to prevent aggregation while keeping good activity.

1.4 Support Materials

One common type of support materials for the immobilized catalysts are inorganic oxides, such as silicas, aluminas, zeolites, metal oxides (MgO, TiO_2, ZrO_2, etc), clays, and layered double hydroxides. Polymeric supports are also widely used for the catalyst immobilization. It is normally beneficial to use materials with defined and ordered structures for the catalyst immobilization to achieve an even distribution of active sites, as well as to provide a uniform local environment around the active species. Materials with high surface areas and large pore sizes would lead to the improved accessibility of the active sites. Besides that, the support materials should also be inert during the immobilization procedures and be stable when used in the catalytic reactions. Several commonly used materials for the catalyst immobilization, which are also used in this thesis work, are introduced here.

1.4.1 Silica materials

Silica materials possess most of the desired properties of the catalyst supports, and as such have been extensively used in the preparation of immobilized catalysts. They have good thermal stability and can withstand a wide range of pressures. They are typically stable in most chemical reactions. They have high surface areas and high densities of surface silanols, which could be readily reacted with organosilanes for the catalyst immobilization. Although amorphous silicas possess the above traits, the disordered nature of the material complicates the characterization of the catalysts and the analysis of the catalytic performance. It is also difficult to obtain a uniform distribution of the active sites in the material due to the wide distributions of the pore sizes in the amorphous silicas.

The explosive development in the mesoporous silicas during 1990s introduced a series of ordered silica materials, with an unprecedented control over the porosity as well as the extremely high surface areas. MCM (Mobile Crystalline Material) and SBA (Santa Barbara mesoporous silica material) are two common members of the family of mesoporous silicas. MCM, discovered by Beck and his co-workers in 1992,[17] extended the pore size of ordered silicas into the mesoporous range. MCM-41 and MCM-48 are two of the most widely used mesoporous molecular sieves in the MCM series. MCM-41 is synthesized using quaternary ammonium surfactants, which form rod-shaped micelles in the acidic solution. The silica precursors polymerize around the micelles to form the silica material. After synthesis, the surfactants are removed by calcination to get an ordered silica material with a hexagonal array of unidirectional pores and a narrow pore size distribution. The pore size (in the range of 15 Å to larger than 100 Å) can be adjusted

by varying the alkyl chain length of the surfactant and a really high surface area (>700 m^2/g) could be achieved.

SBA was developed by Zhao and Stucky in 1998,[18,19] in an effort to increase the thermal stability of mesoporous silicas via increasing wall thickness compared to the MCM type materials. SBA-15, one member of the SBA family, is commonly employed in the immobilized catalysts. SBA-15 is synthesized in a similar manner as MCM-41, but its synthesis uses triblock copolymer of poly(ethylene oxide)-poly(propylene oxide)-poly(ethylene oxide) as the template instead of the quaternary ammonium surfactant. The materials consist of unidirectional, hexagonally arranged pores (40 Å -300 Å) with very high surface areas of 690 -1040 m^2/g.

Using mesoporous silica as the template, Ryong Ryoo's group synthesized highly ordered carbon molecular sieves[20] in recent years. Similar nanocasting concept was also applied to prepare a range of highly structured mesoporous materials, such as CeO_2, Co_3O_4, In_2O_3, etc., which were impossible or at least very difficult to synthesize with the conventional methods.[21]

1.4.2 Magnetic nanoparticles

Another interesting material worth mentioning is the magnetic nanoparticle.[22,23] When the nanoparticle size is below a critical value, which is typically around 10-20 nm and varies with the material, each nanoparticle becomes a single magnetic domain and shows superparamagnetic behavior when the temperature is above the blocking temperature. In this case, every nanoparticle behaves like a giant paramagnetic atom with a quick response to the applied magnetic field. Negligible remanence (residual

magnetization in zero magnetic field) and coercivity (the field required to bring the magnetization to zero) are observed. With these unique features, magnetic nanoparticles are very attractive for a broad range of applications, including catalysis. The advantages of immobilized catalysts based on magnetic nanoparticles are summarized as follows: (1) the catalysts could be recovered under an external magnetic field, providing a new and energy efficient catalyst separation method compared to the traditional filtration and centrifugation methods; (2) high external surface areas could be achieved on nanoparticles; (3) the active sites are distributed on the outer surface of the magnetic nanoparticle, thus alleviating the internal diffusion problems; (4) the nanoparticles are highly dispersible in solvents due to the small particle size, leading to the easy accessibility of the active sites.

Spinel ferrites with the general formula MFe_2O_4 are the most widely used and studied magnetic materials. The magnetic moments of spinel ferrites are intrinsically related to the compositions of the particles. For example, the magnetic anisotropy is enhanced in $CoFe_2O_4$ compared to Fe_3O_4 with a similar particle size. Metals (Fe, Co, Ni) and alloys (FePt, $FePt_3$) are also commonly used magnetic materials. However, it is normally difficult to synthesize pure metal nanoparticles since they are readily oxidized under air.

A wide variety of methods, such as co-precipitation, thermal decomposition, microemulsion, and hydrothermal synthesis are applied for the synthesis of magnetic nanoparticles. Co-precipitation is considered to be the simplest method to produce iron oxides. The synthesis is typically carried out in an aqueous solution containing Fe(II) and Fe(III) salts and base is added under inert gas at room temperature. Surfactants or

associated ions are also used to stabilize the formed iron oxide nanoparticles. Thermo decomposition is also successfully employed for producing iron oxide nanoparticles.[24–26] For example, mono-dispersed Fe_3O_4 nanoparticles were synthesized via decomposition of iron(III) precursors at high temperatures with oleic acid an oleylamine as stabilizers.[25] Different synthesis methods of magnetic nanoparticles are summarized and compared in Table 1.3. More detailed information on the synthesis and characterization of magnetic nanoparticles and their applications in catalysis could be found in several reviews published recently.[23,27,28]

Table 1.3. Summary comparison of the synthetic methods. (reproduced with permission from reference[23])

Synthetic method	Synthesis	Reaction temp. / °C	Reaction period	Solvent	Size distribution	Shape control	Yield
co-precipitation	very simple, ambient conditions	20-90	minutes	water	relatively narrow	not good	high/ scalable
thermal decomposition	complicated, inert atmosphere	100-320	hours-days	organic compound	very narrow	very good	high/ scalable
microemulsion	complicated, ambient conditions	20-50	hours	organic	relatively narrow	good	low
hydrothermal synthesis	simple, high pressure	220	hours-days	water-ethanol	very narrow	very good	medium

1.4.3 Inorganic-polymer composites

Inorganic-polymer composites can be considered as a unique derivative of organic-inorganic hybrid materials. The polymer component can be used for the attachment of active sites or be working as the catalytic species or part of the catalytic species. Different inorganic particles have been employed for the preparation of the inorganic-polymer composites, including: metals (Au, Fe, Al, etc.), metal oxides (Al_2O_3, TiO_2, etc.), nonmetal oxide (SiO_2), and others (SiC).[29] Compared to the polymeric resins, the inorganic-polymer composites typically do not have dramatic shrinking or swelling in solvents due to the structural rigidity imparted by the inorganic supports, and tend to have better thermal and mechanical properties and good long term stability.[30] They can also achieve high catalyst loadings as well as good flexibility and easy accessibility of the active sites.[31–33]

"Grafting from" and "grafting to" are two common approaches for the covalent functionalization of inorganic materials with polymers.[34–36] The "grafting-from" method is based on the initial immobilization of initiators onto the surface of the inorganic materials, followed by the surface initiated polymerization. This method could be used to prepare polymer composites with high grafting density. However it is normally require a strict control of the initiator numbers and monomer concentrations to obtain the desired materials. The "grafting to" method is based on the attachment of the pre-formed polymers to the functional groups on the solid surface via appropriate chemical reactions. For this method, polymers with known molecular weights and structures could be synthesized or obtained commercially before attachment, thus simplifying the synthesis procedures. However the main limitation of this technique is that the initially grafted

polymers would sterically hinder the diffusion of more polymer chains to the surface for further attachment, thus leading to the relative low polymer loadings.

Although the preparation, characterization, processing techniques, and thermal, mechanic and electric properties of inorganic-polymer composites have been extensively studied, only a limited amount of examples of their applications in catalysis could be found in literature,[31–33,37–46] indicating more efforts are needed to develop the inorganic-polymer composites supported catalysts.

1.5 Commercial Applications of Immobilized Catalysts

It has been over thirty years since the first immobilized catalyst was reported. Although many publications and patents showed potential applications of immobilized catalysts in the chemical industry, just a few of them are known to be used at commercial scale.[47,48] Here are several examples of immobilized catalysts used in production processes or sold as commercial products. The Acetica process introduced by Chiyoda and UOP, which is used for production of acetic acid via carbonylation of methanol, uses a poly(vinyl pyridine) resin supported rhodium complex[49,50] (Figure 1.4). FibreCat, developed by Johnson Matthey, has four series of the catalysts commercially available now. The FibreCat 1000 series are palladium catalysts for the coupling reactions. The 2000 series consist of rhodium catalysts for the hydrogenation reactions. The 3000 series includes one ruthenium catalyst for the selective oxidation and two osmium catalysts for the dihydroxylation reactions. The 4000 series has one platinum catalyst for the

hydrosilylation reactions. EnCat, produced via Reaxa, are Pd(0) or Pd(II) species encapsulated in a poly(urea) matrix[51] for C-C coupling reactions and reduction processes.

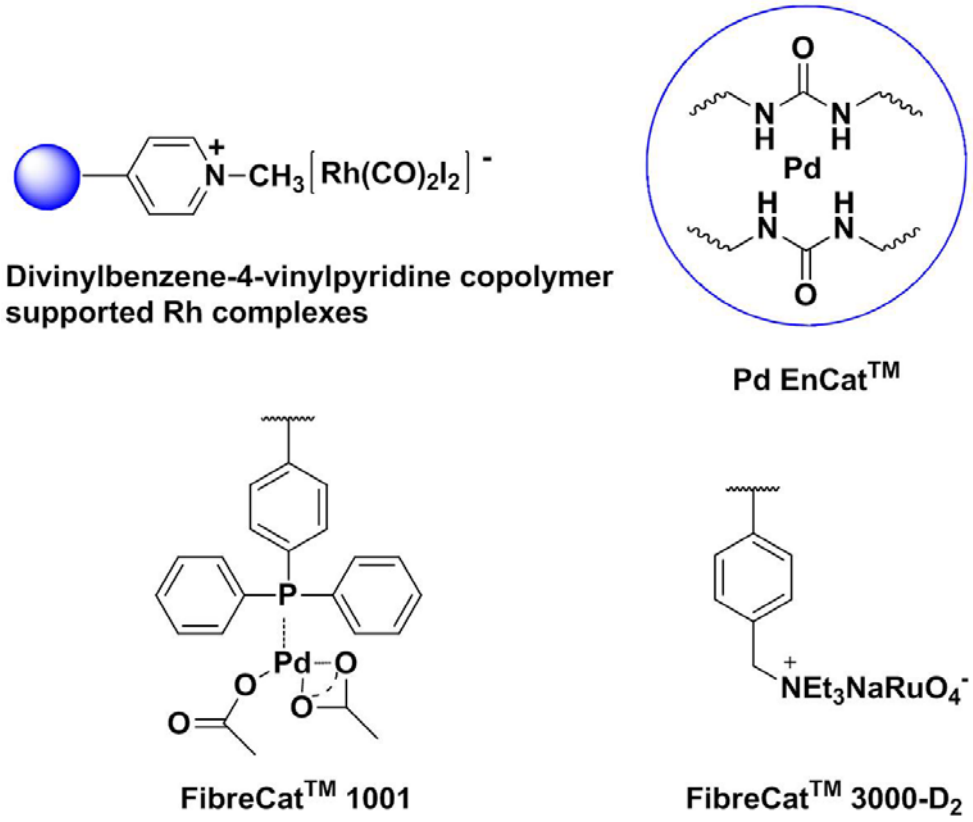

Figure 1.4. Examples of immobilized catalysts for commercial applications. (adapted from reference[48])

1.6 Optimization of Immobilized Catalysts

Development of immobilized catalysts is not just about anchoring techniques. The trickiest part is to design the right catalysts for the specific substrates and necessary reaction conditions. Although immobilized catalysts bring the convenience of easier catalyst separation, there are still several shortcomings that have to be addressed. Generally speaking, due to the difference in the local chemical environment, the activity

and selectivity of immobilized catalysts are normally changed compared to their homogeneous analogues. How to maintain similar activity and selectivity as the homogeneous catalysts is one of the biggest problems that must be solved. However, what's more interesting is to develop unique catalytic properties or to improve catalytic performance via intelligently optimizing the interaction of supports and active sites or the interactions between different active species immobilized on the same support.

When organic groups or metal-ligand complexes are immobilized to the surface of the solid supports, the catalyst normally will experience a different local environment compared to the homogeneous analogues in an organic solvent. For example, the silica surface is normally quite polar and hydrophilic, which would have an influence on the activity of the catalyst. Tailoring the surface polarity introduces different interactions of reactants/products with the active species, leading to some ability to alter the catalytic performance. Thus it is necessary to carefully design the active sites of the catalysts to ensure optimum activity and selectivity.

One efficient and simple approach is using "spectator groups" to modify the surface. These groups are normally non-reactive, and are able to tune the surface polarity, thereby minimizing active site-surface interactions and improving reactant adsorption/product desorption processes. For example, hybrid MCM-41 materials containing both sulfonic acids and alkyl (methyl or propyl) groups[52] were developed for the esterification of glycerol with lauric and oleic acids. Maximum catalytic activity per sulfonic acid could be achieved by adjusting the alkyl/sulfonic acid group ratios to tune the hydrophobicity of the catalyst. Another interesting example is demonstrated in a new Pd/Ph-Al-MCM-41 catalyst used in Ullmann coupling reactions in an aqueous medium.[53]

The catalyst exhibited higher activity, better selectivity and stronger durability than other supported palladium catalysts, which is attributed to the increased surface hydrophobicity resulting from the surface modification of MCM-41 with phenyl groups, and the improved surface Lewis acidity owing to the Al-modification.

In contrast to the homogeneous catalysts, two mutually incompatible functional groups could also be incorporated onto the same surface in the immobilized catalysts. For example, the Davis group developed acid-base bifunctional catalysts[54,55] by grafting amine and acid sites on the silica surface with spatial separation. Aldol condensation of nitrobenzaldehyde with acetone based on these bifunctional catalysts showed improved activity compared to similar materials with only acid or base sites.

1.7 Catalyst Systems Studied in This Work

1.7.1 Magnetic nanoparticle (MNP) supported catalysts for ring-opening reactions

Nanoscale magnetically separable catalysts are very attractive because of their high external surface areas and easy recovery under a magnetic field, which is superior compared to the traditional separation methods. Magnetic nanoparticle supported catalysts can be used to bridge the gap between homogeneous and heterogeneous catalysts, retaining the advantages of both.[28]

In Chapters 2, MNP supported aluminum isopropoxide (MNP-AlO^{i}Pr) is developed for the ring-opening polymerization (ROP) of ε-caprolactone. In the traditional porous solid supported catalytic systems, the pores of the catalysts tend to be filled with

polymer products, which slows down the reaction rate, affects the structure of the polymer product and also hampers the recovery of the catalysts.[5,56] To address the pore clogging and internal diffusion problems, MNPs are identified as a promising catalyst support for use in polymerization reactions due to their nonporous nature, easy recoverability under a magnetic field, high external surface area and potential for facile surface modifications. Without an external magnetic field, the magnetic nanoparticles could be evenly suspended in the solution at the beginning of the catalytic reaction. After polymerization, in the presence of a magnetic field, the catalysts could be readily separated from the reaction solutions (Figure 1.5), yielding polymer products with reduced metal residues. The activity of the new catalyst, polymerization characteristics, recoverability and recyclability of the catalytic systems are studied in detail.

Chapter 3 reports the catalytic regioselective epoxide ring-opening using supported analogues of dimethylaminopyridine (DMAP). A MNP-supported DMAP catalyst is developed and tested in comparison to the similar catalysts based on the more traditional and familiar polymer and silica supports in terms of activity, selectivity as well as recyclability.

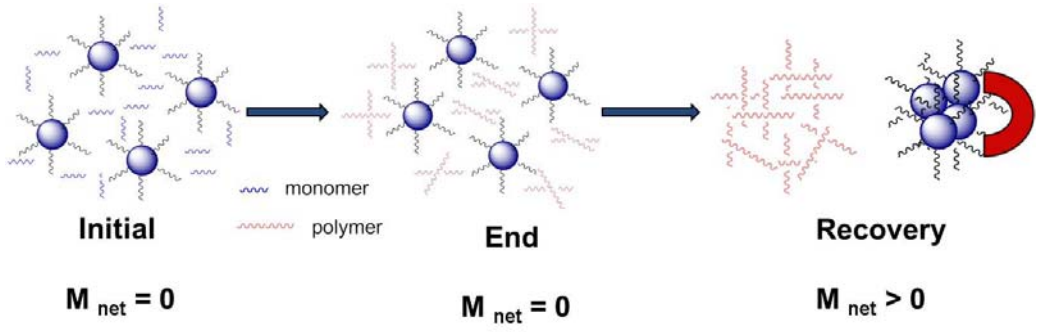

Figure 1.5. MNP supported catalysts for ROP.

1.7.2 Silica-polymer composite supported catalysts

Chapter 4 and Chapter 5 describe two unique examples of immobilized catalysts based on silica-polymer composites. In Chapter 5, new polymer brush supported sulfonic acid catalysts are built on the silica surface with the surface initiated atom transfer radical polymerization (ATRP) method[57,58] to achieve high loadings of active sites while allowing good accessibility of the active centers to the substrates (Figure 1.6). These new catalysts are used for the catalytic hydrolysis of ethyl lactate, with emphasis on understanding the catalytic performance and catalyst stability in the aqueous media.

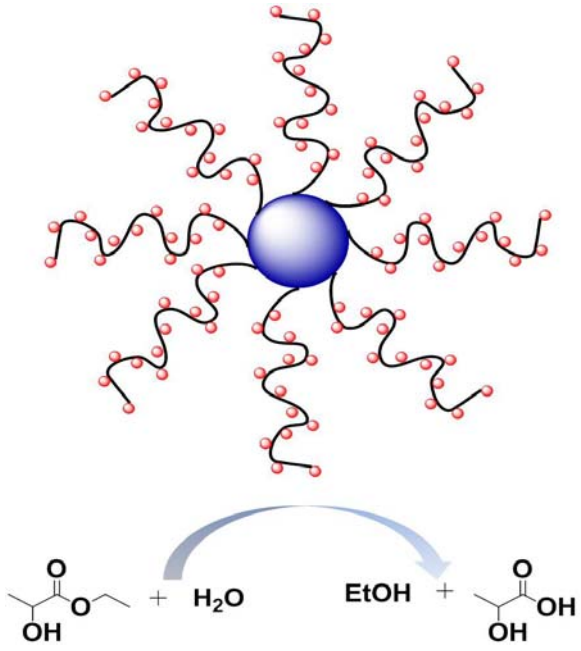

Figure 1.6. Silica-polymer brush sulfonic acids for the hydrolysis of ethyl lactate.

In Chapter 5, aminopolymer-silica composite supported palladium catalysts are developed for the selective hydrogenation of alkynes. The aminopolymer composite has a dual effect on the palladium nanocluster active species, working as a stabilizer to keep good dispersion of the palladium nanoparticles, as well as a modifier to tune the catalyst

selectivity (Figure 1.7). Activity and selectivity of the new catalysts are studied in detail to develop a better understanding of the modification effect of the aminopolymers. Recoverability and recyclability of the catalysts are also investigated.

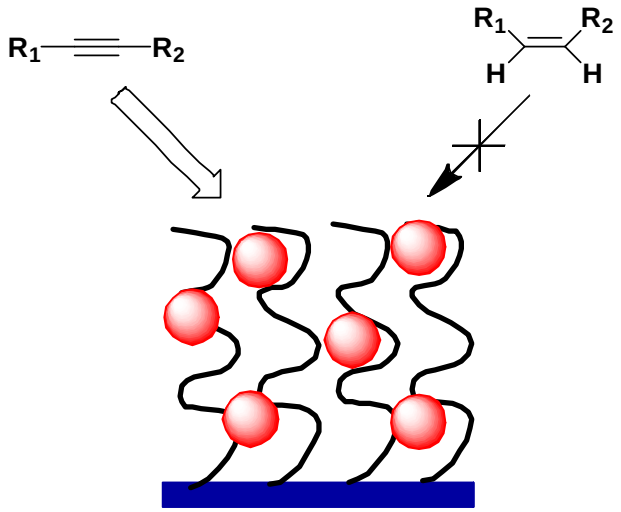

Figure 1.7. Aminopolymer-silica composite supported Pd catalysts.

1.8 Thesis Goals

The general theme to my PhD work is on developing new immobilized catalysts to produce organic species typical of fine or specialty chemicals and polymers, with the following specific goals:

(1) Identify novel materials or architectures to build immobilized catalysts with new or unique properties, which are difficult or even impossible to obtain on conventional materials;

(2) Intelligently design immobilized catalysts to tune the accessibility of active sites to achieve better activity/selectivity;

(3) Investigate the recoverability and recyclability of the catalytic systems and understand the deactivation mechanisms.

The following several chapters present three main topics: (1) magnetically recoverable nanoparticle supported catalysts for ring-opening reactions; (2) polymer brush sulfonic acids; (3) polymer composite supported Pd catalysts for selective hydrogenation, shedding light onto the three above mentioned goals.

1.9 References

(1) Sheldon, R. A. *Chemtech* **1994**, *24*, 38.

(2) Song, C. E.; Lee, S. *Chem. Rev.* **2002**, *102*, 3495.

(3) Benaglia, M.; Puglisi, A.; Cozzi, F. *Chem. Rev.* **2003**, *103*, 3401.

(4) McMorn, P.; Hutchings, G. J. *Chem. Soc. Rev.* **2004**, *33*, 108.

(5) Jones, C. W.; McKittrick, M. W.; Nguyen, J. V.; Yu, K. *Top Catal.* **2005**, *34*, 67.

(6) Corma, A.; Garcia, H. *Adv. Synth. Catal.* **2006**, *348*, 1391.

(7) Jones, C. W. *Top Catal.* **2010**, *53*, 942.

(8) Wight, A. P.; Davis, M. E. *Chem. Rev.* **2002**, *102*, 3589.

(9) McMorn, P.; Hutchings, G. J. *Chem. Soc. Rev.* **2004**, *33*, 108.

(10) Melero, J. A.; Grieken, R. V.; Morales, G. *Chem. Rev.* **2006**, *106*, 3790.

(11) Venkatasubbaiah, K.; Zhu, X.-J.; Jones, C. W. *Top Catal.* **2010**, *53*, 1063.

(12) Augustine, R.; Tanielyan, S.; Anderson, S.; Yang, H. *Chem. Commun.* **1999**, 1257.

(13) White, R. J.; Luque, R.; Budarin, V. L.; Clark, J. H.; Macquarrie, D. J. *Chem. Soc. Rev.* **2009**, *38*, 481.

(14) Ferreira, R.; García, H.; de Castro, B.; Freire, C. *Eur. J. Inorg. Chem.* **2005**, 4272.

(15) Kralik, M.; Biffis, A. *J. Mol. Catal. A: Chem.* **2001**, *177*, 113.

(16) Corain, B. *J. Mol. Catal. A: Chem.* **2001**, *173*, 99.

(17) Beck, J. S.; Vartuli, J. C.; Roth, W. J.; Leonowicz, M. E.; Kresge, C. T.; Schmitt, K. D.; Chu, C. T.; Olson, D. H.; Sheppard, E. W.; McCullen, S. B.; Higgins, J. B.; Schlenkert, J. L. *J. Am. Chem. Soc.* **1992**, *114*, 10834.

(18) Zhao, D.; Feng, J. L.; Huo, Q.; Melosh, N.; Fredrickson, G. H.; Chmelka, B. F.; Stucky, G. D. *Science* **1998**, *279*, 548.

(19) Zhao, D.; Huo, Q.; Feng, J.; Chmelka, B.; Stucky, G. D. *J. Am. Chem. Soc.* **1998**, *120*, 6024.

(20) Ryoo, R.; Joo, S. H.; Jun, S. *J. Phys. Chem. B* **1999**, *103*, 7743.

(21) Lu, A.-hui; Schüth, F. *Adv. Mater.* **2006**, *18*, 1793.

(22) Laurent, S.; Forge, D.; Port, M.; Roch, A.; Robic, C.; Vander Elst, L.; Muller, R. N. *Chem. Rev.* **2008**, *108*, 2064.

(23) Lu, A.-hui; Salabas, E. L.; Schüth, F. *Angew. Chem. Int. Ed.* **2007**, *46*, 1222.

(24) Hyeon, T.; Lee, S. S.; Park, J.; Chung, Y.; Na, H. B. *J. Am. Chem. Soc.* **2001**, *123*, 12798.

(25) Sun, S.; Zeng, H. *J. Am. Chem. Soc.* **2002**, *124*, 8204.

(26) Sun, S.; Zeng, H.; Robinson, D. B.; Raoux, S.; Rice, P. M.; Wang, S. X.; Li, G. *J. Am. Chem. Soc.* **2004**, *126*, 273.

(27) Fan, J.; Gao, Y. *J. Exp. Nanosci.* **2006**, *1*, 457.

(28) Shylesh, S.; Schünemann, V.; Thiel, W. R. *Angew. Chem. Int. Ed.* **2010**, *49*, 3428.

(29) Hussain, F.; Hojjati, M.; Okamoto, M.; Gorga, R. *J. Compos. Mater.* **2006**, *40*, 1511.

(30) Hughes, M.; Miranda, P.; Nielsen, D.; Rosenberg, E.; Gobetto, R.; Viale, A.; Burton, S. *Macromol. Symp.* **2006**, *235*, 161.

(31) Gill, C. S.; Long, W.; Jones, C. W. *Catal. Lett.* **2009**, *131*, 425.

(32) Gill, C. S.; Venkatasubbaiah, K.; Phan, N. T. S.; Weck, M.; Jones, C. W. *Chem. Eur. J.* **2008**, *14*, 7306.

(33) Long, W.; Jones, C. W. *ACS Catalysis* **2011**, *1*, 674.

(34) Coleman, J. N.; Khan, U.; Gun'ko, Y. K. *Adv. Mater.* **2006**, *18*, 689.

(35) Liu, P. *Eur. Polym. J.* **2005**, *41*, 2693.

(36) Guillet-Nicolas, R.; Marcoux, L.; Kleitz, F. *New J. Chem.* **2010**, *34*, 355.

(37) Choi, M.; Kleitz, F.; Liu, D.; Lee, H. Y.; Ahn, W.-S.; Ryoo, R. *J. Am. Chem. Soc.* **2005**, *127*, 1924.

(38) Zhao, B. I. N.; Jiang, X.; Li, D.; Jiang, X.; Lenick, T. G. O.; Li, B.; Li, C. Y. *J. Polym. Sci., Part A: Polym. Chem.* **2008**, *46*, 3438.

(39) Jiang, X.; Wang, B.; Li, C. Y.; Zhao, B. I. N. *J. Polym. Sci., Part A: Polym. Chem.* **2009**, *47*, 2853.

(40) Costantini, F.; Bula, W. P.; Salvio, R.; Huskens, J.; Gardeniers, H. J. G. E.; Reinhoudt, D. N.; Verboom, W. *J. Am. Chem. Soc.* **2009**, *131*, 1650.

(41) Costantini, F.; Benetti, E. M.; Tiggelaar, R. M.; Gardeniers, H. J. G. E.; Reinhoudt, D. N.; Huskens, J.; Vancso, G. J.; Verboom, W. *Chem. Eur. J.* **2010**, *16*, 12406.

(42) Li, C.; Yang, J.; Wang, P.; Liu, J.; Yang, Q. *Micropor. Mesopor. Mater.* **2009**, *123*, 228.

(43) Martín, a.; Morales, G.; Martínez, F.; van Grieken, R.; Cao, L.; Kruk, M. *J. Mater. Chem.* **2010**, *20*, 8026.

(44) Okayasu, T.; Saito, K.; Nishide, H.; Hearn, M. T. W. *Chem. Commun.* **2009**, 4708.

(45) Okayasu, T.; Saito, K.; Nishide, H.; Hearn, M. T. W. *Green Chem.* **2010**, *12*, 1981.

(46) Jiang, Y.; Gao, Q. *J. Am. Chem. Soc.* **2006**, *128*, 716.

(47) Blaser, H.-U. *Top Catal.* **2010**, *53*, 997.

(48) Nichole, E.; Kai-Uwe, S. *Topics in Current Chemistry* **2004**, *242*, 241.

(49) Yoneda, H.; Shiroto, Y.; Hameto, K.; Asaoka, S.; Maejima, T. *Eur Pat Appl Ep567331* **1993**.

(50) Yoneda, N.; Mimami, T.; Weiszmann, J.; Spehlmann, B. *Stud. Surf. Sci. Catal.* **1999**, *121*, 93.

(51) Ley, S. V.; Mitchell, C.; Pears, D.; Ramarao, C.; Yu, J.-Q.; Zhou, W. *Org. Lett.* **2003**, *5*, 4665.

(52) Diaz, I.; Marquez-Alvarez, C.; Mohino, F.; Perez-Pariente, J.; Sastre, E. *J. Catal.* **2000**, *193*, 295.

(53) Li, H.; Chen, J.; Wan, Y.; Chai, W.; Zhang, F.; Lu, Y. *Green Chem.* **2007**, *9*, 273.

(54) Zeidan, R. K.; Davis, M. E. *J. Catal.* **2007**, *247*, 379.

(55) Zeidan, R. K.; Hwang, S.-jong; Davis, M. E. *Angew. Chem. Int. Ed.* **2006**, *45*, 6332.

(56) Wilson, B. C.; Jones, C. W. *Macromolecules* **2004**, *37*, 9709.

(57) Coessens, V.; Pintauer, T.; Matyjaszewski, K. *Prog. Polym. Sci.* **2001**, *26*, 337.

(58) Barbey, R.; Lavanant, L.; Paripovic, D.; Schüwer, N.; Sugnaux, C.; Tugulu, S.; Klok, H.-A. *Chem. Rev.* **2009**, *109*, 5437.

CHAPTER 2

MAGNETIC NANOPARTICLE SUPPORTED ALUMINUM ISOPROPOXIDE FOR RING-OPENING POLYMERIZATION OF Є-CAPROLACTONE*

2.1 Introduction

Polymerization catalysts are routinely single use catalysts, as neither homogeneous (no easy recoverable mechanism), nor traditional heterogeneous catalysts (polymer clogs catalysts pores and entraps the active sites) are easily recoverable and recyclable. Although many commercial catalysts are so active that a single use is acceptable,[1] catalyst residue can be an issue for some specialized polymer products, such as polymers for biomedical application. A few supported catalysts for atom transfer radical polymerization (ATRP) have recently been reported to be recoverable and recyclable.[2-4] However, ATRP catalysis does not involve direct covalent attachment between active centers and polymer chains, which makes recovery and recycle much easier. For the polymerization systems in which the polymer bonds covalently to the catalysts during chain growth, catalyst recovery and recycle are still a major challenge.

Poly(esters) with biodegradability and biocompatibility are of great interest due to their wide potential applications in biomedical and related industries. Ring-opening

---

* Reproduced in part with permission from W. Long, C.S. Gill, S. Choi, C.W. Jones, *Dalton Trans.* **2010**, 39, 1470. Copyright (2010), Royal Society of Chemistry.

polymerization (ROP) of cyclic lactone monomers (Figure 2.1) is a common route to produce these polymers. The most widely investigated catalysts for the ROP of caprolactones and lactides are homogeneous metal complexes,[5-11] such as metal-ligand complexes of aluminum, tin, yttrium, scandium, or other Lewis acids. However it is very difficult to recover these homogeneous metal catalysts from reaction solutions or from polymer products, and this can lead to an increase in process costs and/or metal contamination of the polymers. Some research groups have developed homogeneous catalysts based on small molecular organic species[12-24] or low toxicity metal complexes,[16,25-31] to address the metal contamination problem. Besides these methods, use of heterogeneous catalysts has also recently emerged as an alternative approach to produce polymers with reduced metal contamination.[32-41] However, for catalytic systems based on use of traditional solid porous supports, the pores tend to become filled with polymers over the course of the polymerization, slowing down the reaction rate, potentially affecting the structure of polymers and also hampering the recycle of the catalysts. To address the pore clogging and internal diffusion problems, magnetic nanoparticles(MNPs), are identified here as an intriguing catalyst support for use in polymerizations due to their nonporous nature, easy recoverability under a magnetic field, high external surface area and potential for facile surface modification.

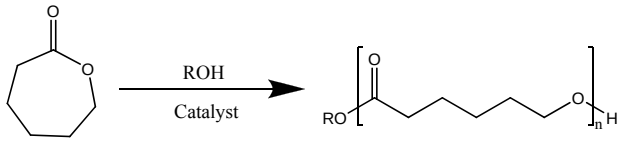

Figure 2.1. ROP of ε-caprolactone.

In this work, MNP supported aluminum isopropoxide (MNP-AlO^{i}Pr) was synthesized and demonstrated in the ROP of ε-caprolactone. The catalysts were easily recovered under an external magnetic field and subsequently reused for additional polymerizations, yielding poly(caprolactone) with negligible metal residue, but with reduced reaction rates. The polymerization characteristics of the catalytic system were investigated in detail. The recyclability of the catalysts is described and the mechanisms associated with the decreased activity of recycled catalysts are enumerated.

2.2 Experimental Section

2.2.1 Chemicals and materials

ε-Caprolactone (Aldrich, 97%) and dodecane (Acros, 99%) were dried over CaH_2 and distilled at reduced pressure. Toluene (Aldrich, 99.8%) was dried by refluxing over sodium benzophenone and then distilled under Argon. Isopropyl alcohol (^{i}PrOH, Aldrich, 99.5%) was dried over CaH_2 and distilled at reduced pressure. Aluminum isopropoxide (Aldrich, 98+ %), cobalt(II) chloride (Alfa Aesar, anhydrous, 99.5%), iron(II) chloride (Alfa Aesar, anhydrous, 99.5%) were used as received.

2.2.2 Characterization

The polymers were measured by gel permeation chromatography to determine the molecular weights and molecular weight distributions (two Varian PLgel Mixed E columns, THF eluent, 30 °C, poly(styrene) calibration standards, refractive index and UV detectors). ^{1}H NMR measurements were performed on a Varian Mercury Vx 400 ($CDCl_3$

solvent). The polymerization reaction conversion was monitored by gas chromatography (Shimadzu GC-2010, FID detector, SHRX5 column). Transmission electron microscopy (TEM) measurements were performed on a JEOL 100CX-2 and HF2000. Elemental analysis (EA) was performed by Columbia Analytical Services (Tucson, AZ). FT-IR spectra were obtained on a Bruker Vertex 80 optical bench using KBr Pellets. X-ray diffraction (XRD) patterns were collected on a PAN analytical X'Pert Pro powder X-ray diffractometer with a Cu*K*α source. Dynamic light scattering measurements (DLS) were performed in a DynaPro instrument with an incident irradiation at 784 nm and a scattering angle of 90º. Surface area was assessed via nitrogen physisorption analysis using a Micromeritics ASAP 2010. Thermogravimetric analysis (TGA) was performed on a Netzsch STA409.

2.2.3 Catalyst preparation

The synthesis of cobalt spinel ferrite nanoparticles ($CoFe_2O_4$) followed a published microemulsion method.[42] $CoFe_2O_4$ support (0.7 g), which was dried under vacuum (180 °C, overnight) prior to use, was suspended in dry toluene (27 ml). Then, aluminum isopropoxide (1.1 g) was added into the solution. The mixture was stirred at room temperature for 24 h. The solid was then recovered under a magnetic field, washed with toluene three times, and dried under vacuum (150 °C, overnight).

2.2.4 Polymerization

A typical procedure is as follows: A pressure tube was charged with ε-caprolactone (12.1 mmol), ^{i}PrOH (0.55 mmol), dodecane (0.515 g), catalysts (1.77 mol %) and toluene (10 ml). The reaction mixture was stirred under nitrogen (100 °C) while a

GC was used to monitor the conversion. At set time intervals, 120 μL aliquots of the polymerization solution were taken. Of this amount, a 20 μL sample was added into acetone for GC analysis. THF (1 ml) and iPrOH (0.1mL) were added into the vial with the remaining 100 μL sample for GPC analysis (catalysts in the samples were removed before measurement). Once the expected conversion was reached, the reaction was terminated by addition of excess ^{i}PrOH, followed by toluene. The reaction vessel was put on a magnet to recover all the catalysts. The clean reaction solution was recovered and excess solvent was removed by rotovap, leaving an oily liquid. Polymers were then precipitated with cold hexane, washed with cold hexane and cold methanol a few times, and then dried under vacuum. When polymerization was complete, the reaction mixture was quenched with ^{i}PrOH and toluene. Catalysts were attracted to the bottom of the flask by an external magnet, washed three times with toluene, and then dried under vacuum (150 °C, overnight). The recovered catalysts were then added into the reactor and reused according to the typical polymerization procedure.

2.2.5 Catalyst recycles

When polymerization was complete, the reaction mixture was quenched with ^{i}PrOH and toluene. Catalysts were attracted to the bottom of the flask by an external magnet, washed three times with toluene, and then dried under vacuum (150 °C, overnight). The recovered catalysts were then added into the reactor and reused according to the typical polymerization procedure.

2.3 Results and Discussions

2.3.1 Catalyst preparation and characterization

Cobalt spinel ferrite ($CoFe_2O_4$), which was used as the catalyst support, was synthesized according to a published microemulsion method.[42] The obtained MNPs were washed repeatedly with DI H_2O and ethanol and then dried under vacuum at 180 °C overnight. XRD of the MNPs (Figure 2.2) displayed patterns consistent with that of $CoFe_2O_4$ previously reported in the literature.[42] Analysis of nitrogen physisorption data obtained using the MNPs yielded a BET surface area of 40 m^2/g. From the TEM images (Figure 2.3), the average particle radius is approximately 20 nm. Assuming nonporous, spherical particles, simple surface area calculation showed that a surface area of 40 m^2/g corresponds to a primary particle size of ~14 nm in radius, which is similar to the particle size observed in the TEM images.

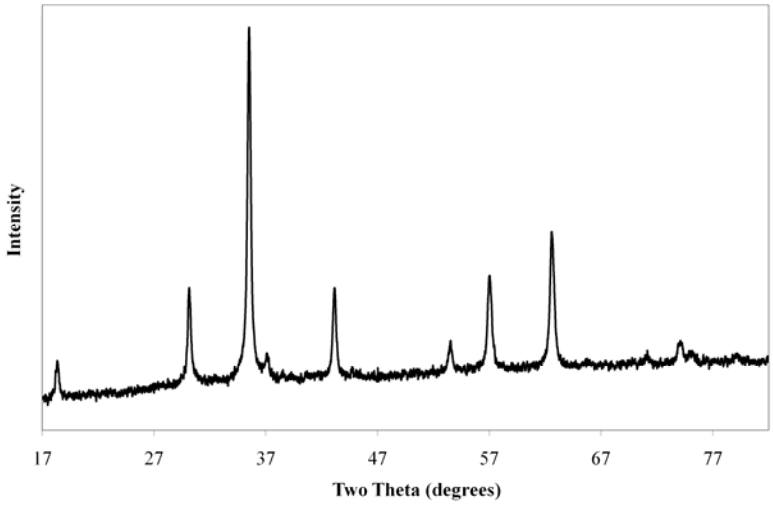

Figure 2.2. XRD pattern of the $CoFe_2O_4$ nanoparticle support.

In the synthesis process (Figure 2.4), the metal atoms on the MNP surface that have positive charges are counterbalanced by OH^- from the reaction medium (e.g. basic aqueous solution). Thus, metal-OH groups exist on the MNP surface, although the density of surface hydroxyl groups varies with different synthesis methods. After synthesis, the MNPs were dried at 180 °C overnight and stored in a glove box. Aluminium isopropoxide was mixed with the dried MNP in anhydrous toluene and stirred at room temperature for 24 h. Aluminum sites were thus grafted onto the surface, likely via the reaction of isopropoxide ligands with the hydroxyl groups on the nanoparticle surface.[43] The solids were then separated from the reaction solution by an external magnet and washed repeatedly with toluene to remove excess aluminium isopropoxide. The recovered catalysts were dried at 150 °C overnight and stored in a glove box for subsequent use.

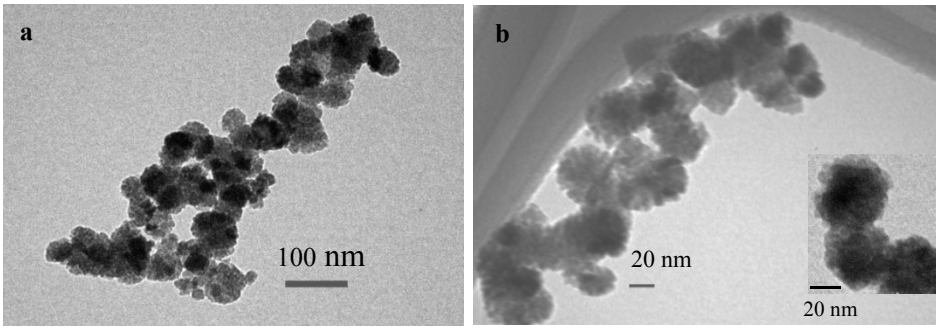

Figure 2.3. TEM images of the bare MNP (a) and the fresh catalyst (b).

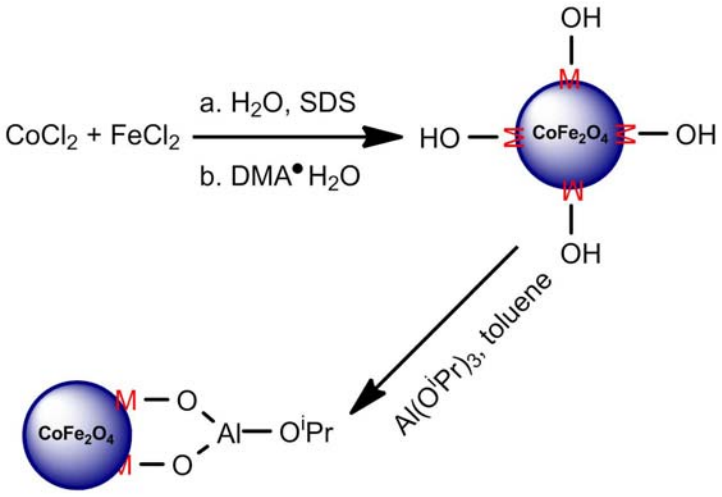

Figure 2.4. Preparation of MNP supported aluminum catalysts. (The exact structure of the aluminum active sites on the surface remains unclear. For simplicity, we illustrate an isolated, Lewis acidic, 3-coordinate aluminum isopropoxide.)

Due to the superparamagnetic nature of the nanoparticles, nuclear magnetic resonance (NMR) techniques could not be used to confirm surface modifications of the catalyst. Instead, TEM, FT-IR and elemental analysis results were combined to develop a picture of the structure of the catalysts. From the TEM images, the magnetic nanoparticle after modifications displayed similar particle size and distribution compared to the bare MNPs. In the FT-IR spectra (Figure 2.5), two sharp peaks at 593 and 398 cm^{-1} are assigned to the M-O vibration of the $CoFe_2O_4$. After modification with aluminum, sharp peaks around 2850- 3000 cm^{-1} were observed, corresponding to C-H stretches in isopropoxide ligands. Elemental analysis gave a catalyst loading of 0.85 mmol Al per gram of solid. It was assumed that one aluminum atom bears one isopropoxide ligand, on average. However, the structures of the active species on the surface remain unclear. Some aluminum centers may have two bound isopropoxide ligands, while others may not have any remaining organic ligands. Furthermore, we cannot rule out the possibility of

aluminum species in aggregated forms. Thus, the number of actual active centers is likely less than the stoichiometric estimate calculated from the aluminum content and thus turnover frequencies (TOFs) calculated per Al atom must be considered lower bounds of the activity.

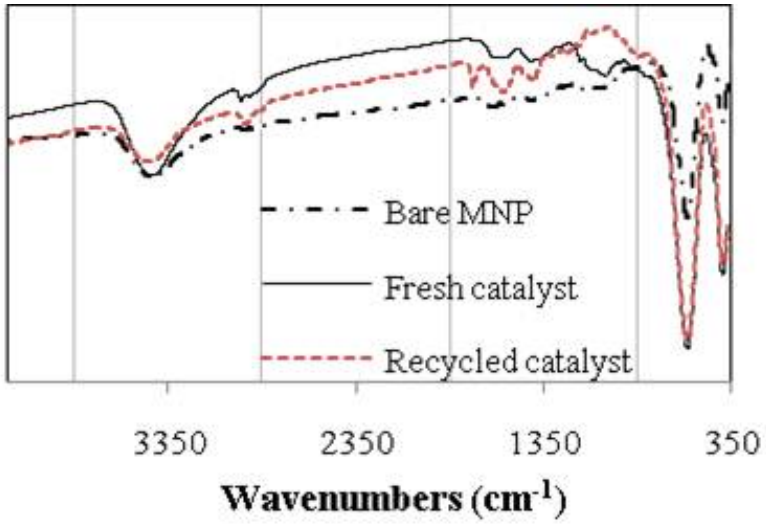

Figure 2.5. FT-IR spectra of bare MNP, fresh catalyst and recycled catalyst.

2.3.2 Kinetics of the fresh catalyst

Polymerization of ε-caprolactone was performed with MNP supported aluminum catalysts in toluene under nitrogen at 100 °C. The reaction conversion reached 95% after 10.5 h (Figure 2.6). A linear relationship was observed when plotting $\ln([M]_0/[M])$ with time, revealing a first order dependence on the monomer concentration in the polymerization.

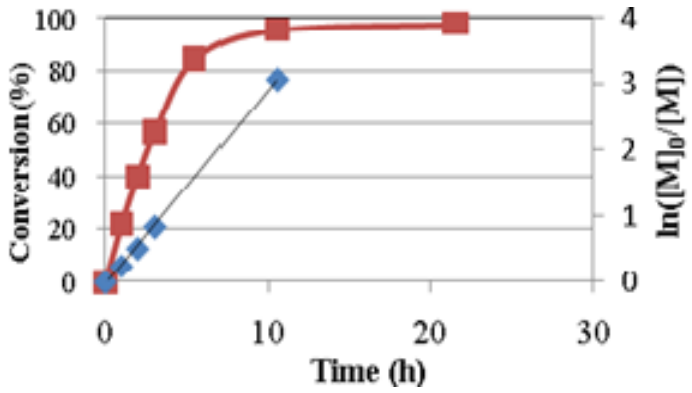

Figure 2.6. Kinetics for ROP of ε-caprolactone with MNP supported aluminum catalyst. (Conversions are plotted as squares. Reaction conditions: toluene, 100 °C, $[Al]_0$= 1.77 mol%, [Monomer]/[^{i}PrOH]=22.)

2.3.3 Leaching tests

For heterogeneous catalysts, it is critical to assess if the active sites might migrate from the solid supports to the reaction solution. To investigate whether any potential leached metal contributed to the polymerization, leaching tests were performed. A polymerization reaction was run at 100 °C for 1 h under nitrogen. At this point, 24% conversion was achieved. Then the reaction was stopped, the catalysts were separated with a magnet and the clean solution was added into another flask to continue the reaction under the same conditions. After 8 h, the conversion (27%) was virtually unchanged. It is suggested based on this result that the catalytic activity was mainly attributed to the surface active sites on the MNPs.

2.3.4 Polymerization

For the MNP supported aluminum catalysts, the polymerization is suggested to follow the generally accepted coordination-insertion mechanism. First, the monomer is activated by coordination of the carbonyl group to the Lewis acidic center (aluminum

center), which decreases the Lewis acidity of the metal center, weakens the C=O bond of the monomer, and increases the nucleophilicity of the alkoxide ligand. Then the acyl-oxygen bond of ε-CL ring is cleaved and inserted into the Al-O bond. In the polymerization, free alcohols were added as chain transfer agents. This type of polymerization has been referred to as an "immortal" polymerization,[44,45] in which a rapid and reversible chain transfer reaction is involved, with an advantage of producing more polymer molecules than initiators molecules, in contrast to a "living" polymerization.

At the end of the polymerization, excess alcohol was added to terminate the reaction. The MNP supported aluminum catalyst was separated from the polymerization solution by use of an external magnet. The clear reaction solution was poured out and excess solvent was evaporated by rotovap. White polymer product was precipitated by adding cold hexane and the polymers were washed by cold methanol. The polymer products were analyzed by ^{1}H NMR, DSC, elemental analysis and GPC. Figure 2.7 shows a typical ^{1}H NMR of the poly(ε-caprolactone) produced. The signals of isopropyl groups (δ C*H*$_3$ at 1.22ppm, δ $(CH_3)_2$C*H* at 4.99ppm) were easily identified in this spectrum, which was consistent with the coordination-insertion mechanism proposed above. DSC measurement of the melting point showed two distinct peaks at 55 and 59 °C for the polymer product, in good agreement with the values from the literature.[46]

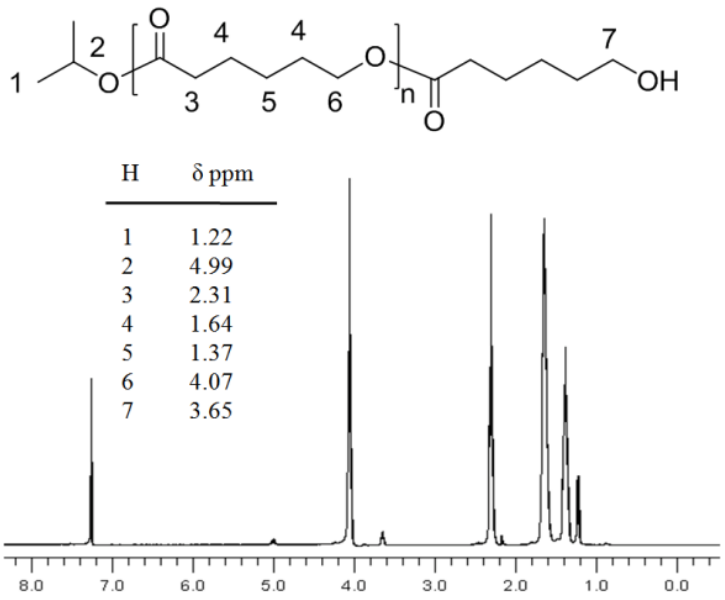

Figure 2.7.[1]H NMR spectrum of poly (ε-caprolactone).

The recovered polymer product was sent for elemental analysis to assess the possible presence of metal residues. In the poly(caprolactone) produced by the MNP supported aluminum catalysts, aluminum was not detected. Cobalt and iron, which are the main components of the MNP support, were also not detectable. The polymer was analyzed by ICP-OES and the metal compositions were all below the detection limits: Al < 120 ppm, Co < 10 ppm, Fe < 20 ppm. These observations suggested that there was no or only a small amount of metal residue in the resulting polymer when using the MNP supported aluminum catalysts.

The molecular weights and PDI of the polymer products were determined by GPC. Poly(styrene) standards were used for GPC calibration and molecular weights of the poly(caprolactone) were corrected according to the Mark-Houwink equation.[47] The

molecular weight of the poly(caprolactone) produced by MNP supported aluminum catalyst was also estimated by ^{1}H NMR to be comparable with the value obtained from GPC. For example, for a specific polymer, a molecular weight (Mn=2229) was calculated from ^{1}H NMR based on the ratios of the peaks of repeat units and end groups in the polymer. The same sample was analyzed by GPC and a similar number (Mn, average = 2334) was obtained.

In the GPC profile (Figure 2.8), a primary peak was observed with a low molecular weight (MW). Besides this main peak, a small amount of high MW polymer was also observed. To gain further insights into the surface active sites and the polymerization process, the low MW and high MW polymer peaks are discussed below separately.

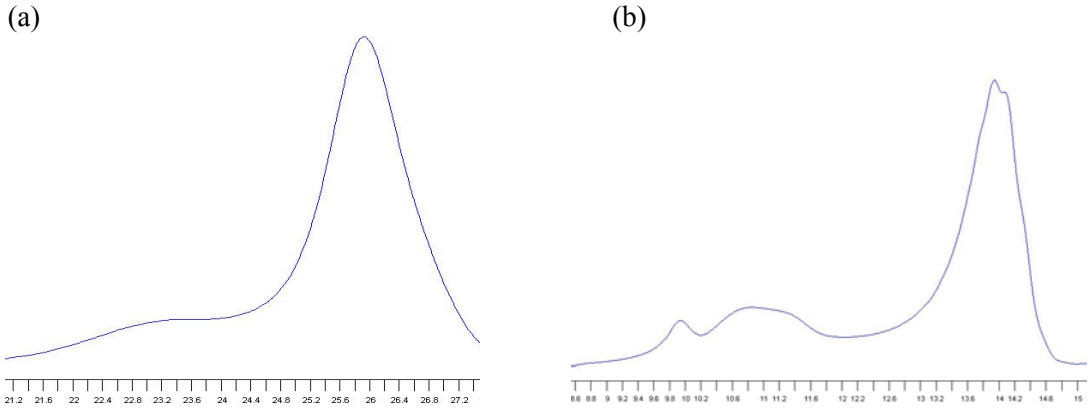

Figure 2.8. GPC curves of poly(caprolactone) produced with the MNP supported aluminum catalyst. Curves (a) and (b) are from the same sample measured through different columns. Columns for (a): American Polymer Standards column 10^2, 10^3, 10^5 Å. Columns for (b): PLgel Mixed E. Since better separation was achieved in the second case, the polymer molecular weights were calculated according to the data from column (b).

For the low MW fraction, the molecular weights of poly(caprolactone) increased linearly with conversions (Figure 2.9 A). Increasing the feed ratio of monomer to alcohol

while keeping other reaction conditions the same (Figure 2.9 A & Table 2.1), an increase in molecular weight was observed. However for the high MW fraction (Figure 2.9 B & Table 2.1), the polymer molecular weights were similar for different feed ratios. When the feed ratios increased from 22 to 50, the percentage of the high MW fragment was also increased.

Table 2.1. ROP of ε-caprolactone.[a]

Entry	[M]/[alcohol]	Conv. (%)	Mn (low, GPC)	Mw/Mn	Mn (high, GPC)	Mw/Mn
1	22	24	419	1.15	7328	1.21
2	22	54	792	1.08	10794	1.22
3	22	86	1235	1.04	12433	1.18
4	30	55	891	1.13	11894	1.25
5	30	93	1406	1.08	13404	1.16
6	50	28	617	1.22	7013	1.20
7	50	54	1153	1.08	10171	1.20
8	50	94	1943	1.05	12368	1.13

[a] Reaction conditions: toluene, 100°C, $[Al]_0$=1.69 mol%.

These phenomena are clearly associated with an inefficient chain transfer process. In the polymerization, the original isopropoxide ligand coordinated to the aluminum center initiated the polymerization and the polymer chains started to grow. Some of the active sites (defined as A sites) are suggested to easily exchange with chain transfer agents (free alcohol) in the reaction solution, leading to the predominant low molecular weight polymer product. However, some sites (defined as B sites) appear to be less able

to exchange with free alcohols and thus the polymer chains kept growing at these sites, resulting in high molecular weight polymer.

The molecular weights of polymer produced by A sites was determined by the ratio of [monomer (consumed by sites A)] / ([sites A] + [alcohol]). If we assume the number of A sites was not affected by the different [monomer] / [alcohol] ratios and that all the free alcohol was consumed by A sites, the molecular weights of polymer products would increase with the [monomer] / [alcohol] ratio. For the high MW fraction, since the chain transfer agent was not involved in the polymerization at B sites, the molecular weights should not be affected.

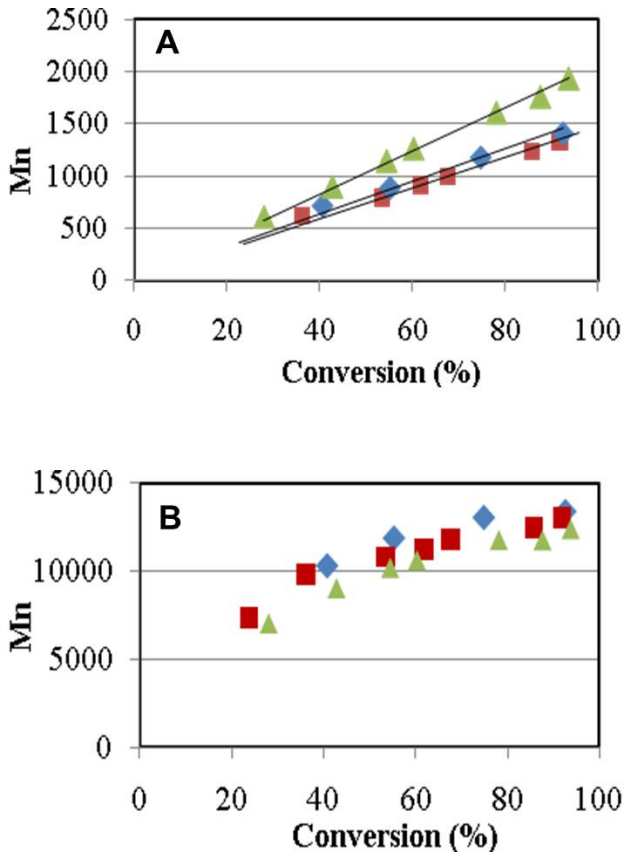

Figure 2.9. Mn (GPC) vs conversion for ROP of ε-CL. (A) low MW polymer; (B) high MW polymer. [M]/[^{i}PrOH]=22 (■),[M]/[^{i}PrOH]=30 (♦),[M]/[^{i}PrOH]=50 (▲).

Benzyl alcohol was used as the chain transfer agent in another set of experiments and the polymer samples were measured by GPC with both the UV and RI detectors. In the GPC traces (Figure 2.10) using the RI detector, a similar polymer distribution- a primary peak at low MW and a small amount of peaks at high MW, was observed. However in the GPC traces using the UV detector, only the low MW fraction could be observed. These observations are consistent with the hypothesis of the absence of chain transfer in the high molecular weight polymer. The benzyl alcohol, which could effectively exchange with A sites, produced low MW polymer with a benzyl end group that was visible with the UV detector. For B sites, the polymerization was initiated by the aluminum isopropoxide center and the chain transfer process was very slow, producing mainly high MW polymer with isopropyl end groups.

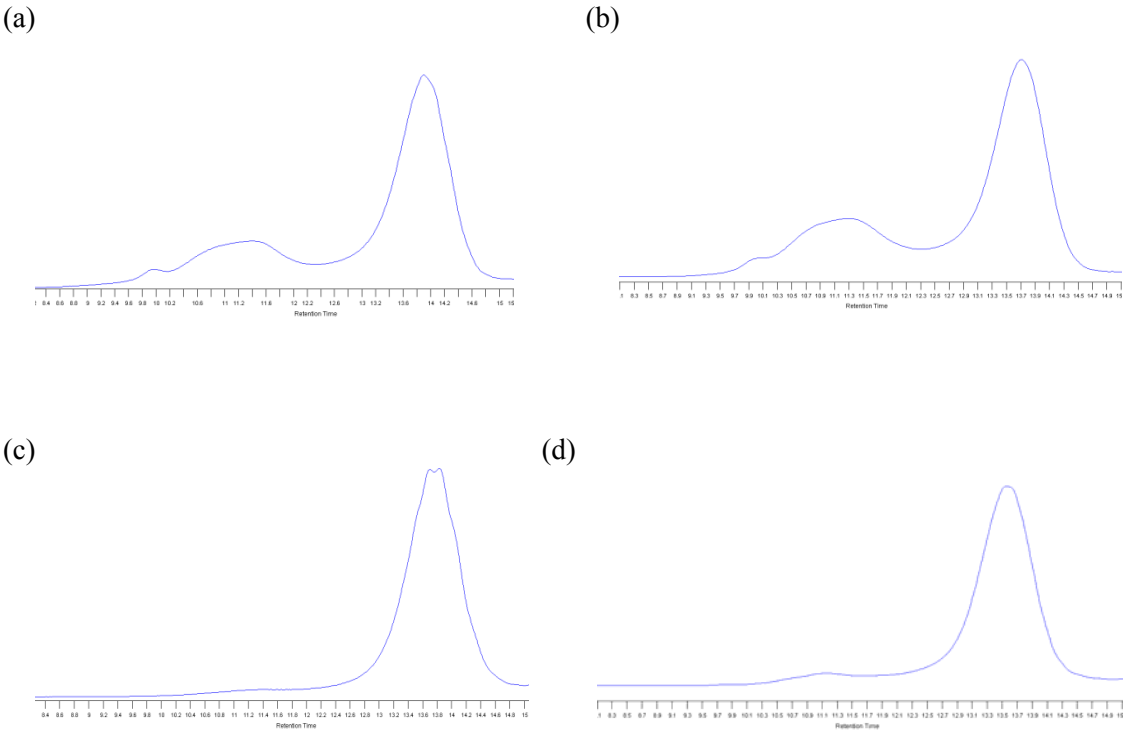

Figure 2.10. GPC curves of poly(caprolactone) produced with the MNP supported aluminum catalyst. (a) conversion = 73%, with RI detector; (b) conversion = 91%, with RI detector; (c) conversion = 73%, with UV detector; (d) conversion = 91%, with UV detector.

Table 2.2. EA results of fresh and recycled catalysts.

Catalysts	Co: Fe	Al : Co	Al : Fe
Fresh	1.96	0.110	0.060
After cycle 1	1.93	0.090	0.049
After cycle 3	1.96	0.085	0.046

2.3.5 Recyclability of the catalysts

The recyclability of the MNP supported aluminum catalyst was also investigated. After each run, the catalysts were separated from the reaction solution under an external magnet and then reused for polymerization after careful washing and drying. Each cycle allowed for high monomer conversions (over 90%) and produced poly(caprolactone) with similar molecular weights and PDIs (Table 2.3). Although the recycled catalysts showed lower reaction rates compared to the fresh ones, the catalytic activities of cycles 2 and 3 were quite similar (Figure 2.11), indicating the catalytic performance stabilized after the first run.

To understand the mechanisms associated with the decreased activity of the recycled catalysts, characterization of the recycled catalysts were performed. Fresh catalysts and recycled catalysts were sent for elemental analysis. EA (Table 2.2) results showed a small loss of aluminum in the recycled catalysts, while the content of the other two metals (cobalt, iron), which are the main components of the MNP supports, were essentially unchanged in the reused catalysts. These data suggest the cobalt iron oxide material was a stable support for the ROP of ε-caprolactone without significant support metal leaching, even under these somewhat harsh conditions (high temperature, long

time, etc.). However, the EA results also showed an 18% Al loss after cycle 1, and an additional 6% Al loss after cycle 3. This observation was consistent with the large activity decrease in cycle 2, and the observation of only a slight difference in the catalytic activity between cycles 2 and 3. The loss of aluminum might be associated with the recovery process of the catalysts. At the end of polymerization, a large amount of isopropanol was added to terminate the reaction, which may lead to the cleavage of aluminum species from the support. Because the mass of aluminum lost was small, it was undetectable in the final polymer.

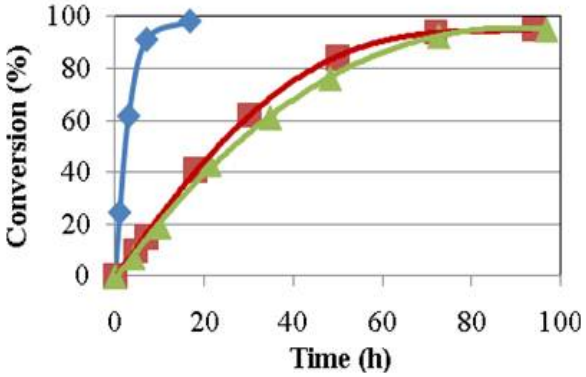

Figure 2.11. Kinetics for ROP of ε-caprolactone with fresh and recycled catalysts (cycle 1 = ♦, cycle 2 = ■, cycle 3 = ▲). Reaction conditions: toluene, 100 °C, $[Al]_0$=1.77 mol%, [M]/[^{i}PrOH]=22.

To assess changes in the organic content of the catalysts, the recycled catalysts were assessed by TGA. Compared to the fresh catalysts, the catalyst used for one cycle showed a moderate increase (6.6 wt %) in the organic content, while the organic contents of the catalyst after three cycles only increased slightly (1.0 wt %) compared to that after the first use. In the FT-IR spectra of the recycled catalyst (Figure 2.5), sharp peaks between 1600-1750 cm^{-1} corresponding to the C=O stretch could be easily identified. All these observations suggested there was still a small amount of polymer/oligomer residue in the recovered catalysts that was not removed by solvent washing. The polymer residue

may make some active sites inaccessible to reagents, and contribute to the decreased reaction rate between the fresh and recycled catalysts.

Table 2.3. ROP of ε-caprolactone with fresh and recycled catalyst. (Data in table represent low molecular weight fraction).

Cycle	Time (h)	Conv. (%)	Mn	Mw/Mn
1[a]	16.7	98	1087	1.10
2[b]	72	93	1035	1.06
3[c]	72.5	93.5	1224	1.06

[a] high MW fraction: Mn = 13032, PDI=1.26. [b] high MW fraction, Mn=5914, PDI=1.19. [c] high MW fraction, Mn=6167, PDI=1.17.

Particle agglomeration is a common problem with nanoparticles, and significant particle agglomeration would decrease the accessible surface area and thus negatively affect the catalytic performance of the catalysts. To investigate how the particle agglomeration affects the catalytic activity, the recycled catalysts were characterized by TEM and DLS and compared with the bare MNPs and the fresh catalyst. From the TEM images (Figure 2.12), the recycled catalysts have slightly increased agglomeration compared to the fresh catalysts. However, there was not much difference in the average particle size and the particle size distribution after one or three cycles. This TEM observation was also confirmed by DLS data (Table 2.4). Thus we suggest nanoparticle agglomeration may just have minor effect on the deactivation of the catalyst in going from the fresh catalyst to the recycled catalyst.

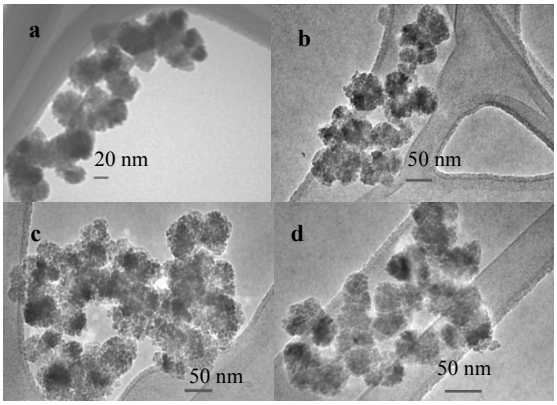

Figure 2.12. TEM images of fresh catalyst (a), catalyst after one cycle (b), catalyst after two cycles (c) and catalyst after three cycles (d).

Table 2.4. Hydrodynamic particle size of bare MNP and Al-MNP catalysts.

Entry	Hydrodynamic radius (nm)
Bare MNP	131.9 ± 8.2
Fresh catalyst	126.6 ± 2.7
Catalyst after cycle 1	152.0 ± 4.6
Catalyst after cycle 3	144.4 ± 4.4

2.4 Conclusions

Here we report a unique example of a MNP supported catalyst for polymerizations reactions involving a reaction mechanism that includes the covalent attachment and growth of polymers at the active sites (MNP supported catalysts for ATRP has been reported, which does not involve active site-polymer bonds).[3] This catalyst precludes the potential for deactivation mechanisms that are common with polymerization using porous supports, such as pore clogging with polymers and internal

diffusion limitations. Detailed investigation of the kinetics of ε-caprolactone polymerization, coupled with characterization of the polymer produced and the fresh and recycled catalysts allow for a good understanding of this new catalytic system. The catalyst can be easily separated from reaction solution under an external magnet field and reused, yielding poly(caprolactone) with negligible metal residue. Although kinetic studies showed the reaction rates were reduced in the recycled runs compared to the first cycle, the activities between subsequent recycles were similar. The recycled catalysts allow for high monomer conversions (> 90%) and produce poly(caprolactone)s with consistent molecular weights and PDIs. The loss of some active sites and the presence of polymer residue on the catalyst were likely the key contributors to the decreased activity of the recycled catalysts, based on a comprehensive characterization of the used catalysts.

2.5 Acknowledgment

The authors are grateful to the National Science Foundation (Grant CBET-055354) for financial support. W.L also thanks Dr. S. Choi and D. Kang for the TEM images.

2.6 References

(1) Hlatky, G. G. *Chem. Rev.* **2000**, *100*, 1347.

(2) Nguyen, J. V.; Jones, C. W. *J. Catal.* **2005**, *232*, 276.

(3) Ding, S. J.; Xing, Y. C.; Radosz, M.; Shen, Y. Q. *Macromolecules* **2006**, *39*, 6399.

(4) Munirasu, S.; Aggarwal, R.; Baskaran, D. *Chem. Commun.* **2009**, 4518.

(5) Tortosa, K.; Hamaide, T.; Boisson, C.; Spitz, R. *Macromol. Chem. Phys.* **2001**, *202*, 1156.

(6) Nomura, N.; Taira, A.; Tomioka, T.; Okada, M. *Macromolecules* **2000**, *33*, 1497.

(7) Ling, J.; Zhu, W. P.; Shen, Z. Q. *Macromolecules* **2004**, *37*, 758.

(8) Stevels, W. M.; Ankone, M. J. K.; Dijkstra, P. J.; Feijen, J. *Macromolecules* **1996**, *29*, 6132.

(9) Pietrangelo, A.; Hillmyer, M. A.; Tolman, W. B. *Chem. Commun.* **2009**, 2736.

(10) Du, H. Z.; Velders, A. H.; Dijkstra, P. J.; Zhong, Z. Y.; Chen, X. S.; Feijen, J. *Macromolecules* **2009**, *42*, 1058.

(11) Pappalardo, D.; Annunziata, L.; Pellecchia, C. *Macromolecules* **2009**, *42*, 6056.

(12) Nederberg, F.; Connor, E. F.; Moller, M.; Glauser, T.; Hedrick, J. L. *Angew. Chem. Int. Ed.* **2001**, *40*, 2712.

(13) Connor, E. F.; Nyce, G. W.; Myers, M.; Mock, A.; Hedrick, J. L. *J. Am. Chem. Soc.* **2002**, *124*, 914.

(14) Myers, M.; Connor, E. F.; Glauser, T.; Mock, A.; Nyce, G.; Hedrick, J. L. *J. Polym. Sci., Part A: Polym. Chem.* **2002**, *40*, 844.

(15) Nyce, G. W.; Glauser, T.; Connor, E. F.; Mock, A.; Waymouth, R. M.; Hedrick, J. L. *J. Am. Chem. Soc.* **2003**, *125*, 3046.

(16) Csihony, S.; Culkin, D. A.; Sentman, A. C.; Dove, A. P.; Waymouth, R. M.; Hedrick, J. L. *J. Am. Chem. Soc.* **2005**, *127*, 9079.

(17) Coulembier, O.; Mespouille, L.; Hedrick, J. L.; Waymouth, R. M.; Dubois, P. *Macromolecules* **2006**, *39*, 4001.

(18) Dove, A. P.; Li, H. B.; Pratt, R. C.; Lohmeijer, B. G. G.; Culkin, D. A.; Waymouth, R. M.; Hedrick, J. L. *Chem. Commun.* **2006**, 2881.

(19) Dove, A. P.; Pratt, R. C.; Lohmeijer, B. G. G.; Culkin, D. A.; Hagberg, E. C.; Nyce, G. W.; Waymouth, R. M.; Hedrick, J. L. *Polymer* **2006**, *47*, 4018.

(20) Lohmeijer, B. G. G.; Pratt, R. C.; Leibfarth, F.; Logan, J. W.; Long, D. A.; Dove, A. P.; Nederberg, F.; Choi, J.; Wade, C.; Waymouth, R. M.; Hedrick, J. L. *Macromolecules* **2006**, *39*, 8574.

(21) Pratt, R. C.; Lohmeijer, B. G. G.; Long, D. A.; Waymouth, R. M.; Hedrick, J. L. *J. Am. Chem. Soc.* **2006**, *128*, 4556.

(22) Zhang, L.; Nederberg, F.; Messman, J. M.; Pratt, R. C.; Hedrick, J. L.; Wade, C. G. *J. Am. Chem. Soc.* **2007**, *129*, 12610.

(23) Gazeau-Bureau, S.; Delcroix, D.; Martin-Vaca, B.; Bonrissou, D.; Navarro, C.; Magnet, S. *Macromolecules* **2008**, *41*, 3782.

(24) Kamber, N. E.; Jeong, W.; Gonzalez, S.; Hedrick, J. L.; Waymouth, R. M. *Macromolecules* **2009**, *42*, 1634.

(25) Kricheldorf, H. R.; Damrau, D. O. *Macromol. Chem. Phys.* **1997**, *198*, 1753.

(26) Kricheldorf, H. R.; Damrau, D. O. *Macromol. Chem. Phys.* **1997**, *198*, 1767.

(27) Kricheldorf, H. R.; Damrau, D. O. *Macromol. Chem. Phys.* **1998**, *199*, 1747.

(28) Zhong, Z. Y.; Dijkstra, P. J.; Birg, C.; Westerhausen, M.; Feijen, J. *Macromolecules* **2001**, *34*, 3863.

(29) Darensbourg, D. J.; Choi, W.; Karroonnirun, O.; Bhuvanesh, N. *Macromolecules* **2008**, *41*, 3493.

(30) Gowda, R. R.; Chakraborty, D. *J. Mol. Catal. A: Chem.* **2009**, *301*, 84.

(31) Wheaton, C. A.; Hayes, P. G.; Ireland, B. J. *Dalton Trans.* **2009**, 4832.

(32) Miola, C.; Hamaide, T.; Spitz, R. *Polymer* **1997**, *38*, 5667.

(33) Kageyama, K.; Ogino, S.; Aida, T.; Tatsumi, T. *Macromolecules* **1998**, *31*, 4069.

(34) Shen, Y. Q.; Zhu, S. P.; Zeng, F. Q.; Pelton, R. H. *Macromolecules* **2000**, *33*, 5427.

(35) Martin, E.; Dubois, P.; Jerome, R. *Macromolecules* **2003**, *36*, 7094.

(36) Wilson, B. C.; Jones, C. W. *Macromolecules* **2004**, *37*, 9709.

(37) Yu, K. Q.; Jones, C. W. *J. Catal.* **2004**, *222*, 558.

(38) Khan, J. H.; Schue, F.; George, G. A. *Polym. Int.* **2009**, *58*, 296.

(39) Kim, E.; Shin, E. W.; Yoo, I. K.; Chung, J. S. *J. Mol. Catal. A: Chem.* **2009**, *298*, 36.

(40) Oshimura, M.; Takasu, A.; Nagata, K. *Macromolecules* **2009**, *42*, 3086.

(41) Nguyen, J. V.; Jones, C. W. *Macromolecules* **2004**, *37*, 1190.

(42) Rondinone, A. J.; Samia, A. C. S.; Zhang, Z. J. *J. Phys. Chem. B* **1999**, *103*, 6876.

(43) Anwander, R.; Palm, C.; Gerstberger, G.; Groeger, O.; Engelhardt, G. *Chem. Commun.* **1998**, 1811.

(44) Endo, M.; Aida, T.; Inoue, S. *Macromolecules* **1987**, *20*, 2982.

(45) Aida, T.; Inoue, S. *Acc. Chem. Res.* **1996**, *29*, 39.

(46) Takizawa, K.; Tang, C.; Hawker, C. J. *J. Am. Chem. Soc.* **2008**, *130*, 1718.

(47) Heuschen, J.; Jerome, R.; Teyssie, P. *Macromolecules* **1981**, *14*, 242.

CHAPTER 3

CATALYTIC REGIOSELECTIVE EPOXIDE RING OPENING WITH PHENOL USING HOMOGNEOUS AND SUPPORTED ANALOGUES OF DIMETHYLAMINOPYRIDINE[†]

3.1 Introduction

The versatile reactivity of epoxides offers significant opportunity for the synthesis of many organic compounds.[1] In particular, terminal epoxides are easily prepared via a variety of routes and are versatile synthons.[2-8] Many important transformations are possible with 1,2-epoxides, with the catalytic asymmetric epoxide ring-opening (ERO) being one of the most well-studied reactions. This reaction has the versatility to produce numerous interesting structures due to the wide variety of nucleophiles that can be used, such as chloride ions,[9,10] amines,[11] carboxylates,[12] and others.[13-16]

For the asymmetric reaction, Jacobsen and others have used M-salen complexes with water as the nucleophile to kinetically resolve the epoxide, producing enantioenriched terminal epoxides and 1,2 diols that are easily separable from one another.[17-21] Jacobsen and others have also shown that M-salen catalyzed enantioselective ring-opening can be accomplished with a variety of nucleophiles using

---

[†] Reproduced with permission from N. A. Brunelli, W. Long, K. Venkatasubbaiah, C.W. Jones, *Top. Catal.* **2012**, in press. Copyright (2012), Springer.

suitable catalysts, with alcohols and phenols often being used.[22-28] While enantioselectivity for the ring-opening of terminal epoxides is required for many pharmaceutical or agrochemical applications, other bulk scale processes only require the high regioselectivity that both racemic M-salen and M-porphyrin catalysts can achieve, with nucleophilic attack favored at the less hindered alpha carbon, producing 1-alkoxy- or 1-aryloxy-2-alcohols.[29]

The regioselective epoxide ring-opening examples described above rely on metal-ligand complex catalysts. It would be advantageous to use simpler, low cost organocatalysts for these transformations if suitable activity and selectivity could be achieved.[30-32] Here we demonstrate the application of dimethyaminopyridine (DMAP) as a soluble, active and regioselective 1,2-epoxide ring-opening catalyst using a range of substituted phenols as the nucleophile.[31] Furthermore, in an effort to develop robust, recyclable epoxide ring-opening catalysts, we report the use of solid supported analogues of DMAP on polymeric, magnetic nanoparticle, and silica supports, building off of past work by us and others on supported, strongly-basic, DMAP-derived organocatalysts,[33-37] The combined use of the three heterogeneous catalyst supports (Figure 3.1) permits comparison of the increasingly utilized magnetic nanoparticle support in comparison to the more traditional and familiar polymer and silica supports.

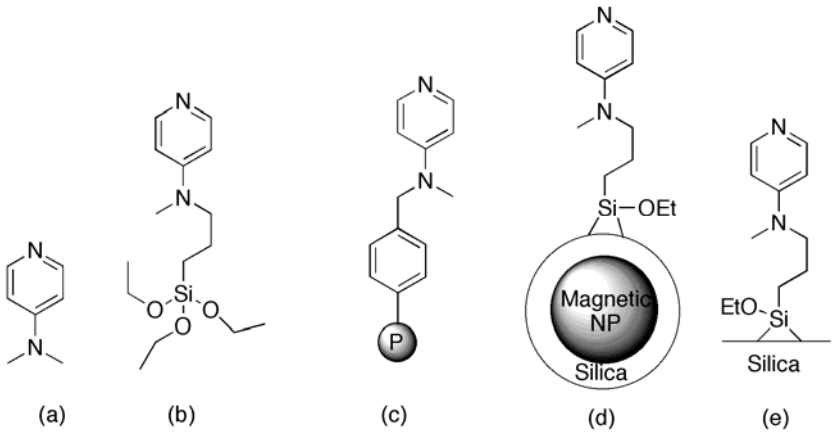

Figure 3.1. Base catalysts used for the epoxide ring opening, (a) homogeneous DMAP, (b) MPAP organosilane, (c) polyBMAP, (d) MNP_MPAP, and (e) SBA_MPAP.

3.2 Experimental Methods

3.2.1 Chemicals

Chemicals were used as received from Sigma Aldrich or VWR. Toluene (Sigma-Aldrich, anhydrous) was stored in a glovebox prior to use and used according to standard Schlenk conditions. Pluronic P123 EO-PO-EO triblock copolymer (poly(ethylene glycol)-poly(propylene glycol)-poly(ethylene glycol); $M_n \sim 5{,}800$) was obtained from Sigma-Aldrich. The polymeric catalyst was a commercially available resin containing a DMAP analogue, N-benzyl-4-(methylamino)pyridine (polyBMAP), at a loading of 3.0 mmol g^{-1}.[38]

3.2.2 Synthesis of N-methyl-N-(3-(triethoxysilyl)propyl)pyridin-4-amine

The synthesis procedure for N-methyl-N-(3-(triethoxysilyl)propyl)pyridin-4-amine was carried out as previously reported.[39] Under nitrogen, sodium hydride (3.0 g; 60 wt% in mineral oil) was washed with dry hexanes three times before drop-wise

addition of a solution containing 5.0 g of 4-methylaminopyridine and 70 mL dry THF. The solution temperature was raised to room temperature and stirred for 2 h before dropwise addition of a solution containing 11.1 g 3-chloropropyl triethoxy silane and 10 mL THF. The mixture was heated to 70°C for 15 h and then cooled to room temperature before filtering through celite. THF was removed on a rotovap. The compound was purified using a column, using the slurry method to pack the column with silica, eluting with 100 mL of methanol to remove water and to passivate the silanols of the silica, 200 mL DCM, and 100 mL hexanes before loading the compound into the column and eluting with a 95:5 DCM:triethylamine mixture. Fractions containing the product were combined, and the solvent was removed at reduced pressure. The material was further dried under reduced pressure (10 mTorr) overnight before analyzing by NMR and storing in a refrigerator. The NMR spectra were consistent with previous reported values.[40]

3.2.3 Mesoporous SBA-15 silica synthesis

The SBA-15 mesoporous silica was synthesized analogously to previous reports,[41] scaling the ingredients accordingly. Briefly, 24.0 g of the template polymer (P123; M_n ~ 5,800) was dissolved in a mixture of 120 mL concentrated hydrochloric acid and 636 mL distilled water in a 2 L Erlenmeyer flask heated to 40 °C in a silicone oil bath. Tetraethylorthosilicate (TEOS; 52.6 g) was added to the mixture with stirring for 20 h. The magnetic stir bar was removed, and the mixture was heated to 100 °C for 24 h. The resulting solid was cooled and filtered using a water aspirator, washing with copious amounts of water, and allowing the material to dry overnight. The dried material was calcined in a temperature-programmed furnace under flowing air at 550 °C for 6 h.

3.2.4 N-methyl-N-(3-(triethoxysilyl)propyl)pyridin-4-amine grafting

One gram of SBA-15 was dried in a 100 mL round bottom flask overnight at reduced pressure (10 mTorr) at 100°C. After cooling to room temperature, the septum-capped round bottom was degassed with UHP nitrogen for 30 minutes. Dry toluene (25 mL) was mixed with the N-methyl-N-(3-(triethoxysilyl)propyl)pyridin-4-amine (936 μL for the 3 mmol per gram sample). The mixture was injected via syringe into the round bottom with the silica powder while stirring. Stirring proceeded for 24 h at room temperature before removing the septum and heating at reflux for an additional 24 h using a condenser. The resultant material was cooled and filtered, washing with 100 mL of toluene, 100 mL of hexanes, and 100 mL of ethanol sequentially. It was dried overnight under reduced pressure (10 mTorr) at 100°C and labeled SBA_MPAP.

3.2.5 Magnetic nanoparticle synthesis

Oleic acid coated Fe_3O_4 nanoparticles were prepared in a similar manner to previous reports.[42,43] After synthesis, the Fe_3O_4 and oleic acid surfactant were dispersed in toluene (14.4 mg Fe_3O_4 mL^{-1}) for storage. The Fe_3O_4 solution (130 mL) was diluted into 2.5 mg mL^{-1} with 663 mL toluene before silica coating. A small amount of triethylamine (11.2 mL) was added into the solution, and then a mixture of 7.8 mL tetramethylorthosilicate and 62.7 mL of toluene was added dropwise while the nanoparticle solution was sonicated. Sonication was performed for 16 h in a water bath. The silica coated magnetic nanoparticles were separated using a strong magnet and washed repeatedly with toluene, methanol and water. The recovered material was dried under vacuum at 120°C for several hours. The organosilane functionalization was

achieved in a similar manner. First, 1.0 g SiO_2-Fe_3O_4 was mixed with 0.937 g N-methyl-N-(3-(triethoxysilyl)propyl)pyridin-4-amine and 43 g anhydrous toluene. The mixture was stirred at room temperature for 27 h, and then 10 ul distilled H_2O was added and the solution was refluxed at 120 ˚C for 30 h. The N-methyl-N-(3-(triethoxysilyl)propyl)pyridin-4-amine functionalized SiO_2-Fe_3O_4 (MNP_MPAP) was separated from the solution with a magnet and washed with toluene three times. The recovered material was dried overnight at 100°C under vacuum.

3.2.6 Materials characterization

Thermogravimetric analysis (TGA) was performed on a Netzsch STA409. Samples were analyzed in a nitrogen (30 sccm) diluted air (90 sccm) stream with a constant 10°C min^{-1} heating rate from 30 to 900°C. The organic loading was estimated from the percent weight loss in the range 150–900°C and subsequently confirmed with elemental analysis performed by Atlantic Microlab. The surface area, total pore volume and pore size distributions were determined by N_2 adsorption–desorption isotherms measured on a Micromeritics Tristar 2030 at (-196°C), with surface area determined by the Brunauer–Emmett–Teller (BET) method. Total pore volume and pore size were calculated using the Broekhoff-de Boer method with the Frenkel–Halsey–Hill (BdB-FHH) modification,[44] using the adsorption isotherm. Powder X-ray diffraction (XRD) was performed on a PAnalytical X'pert Pro diffractometer operating with a Cu KR source. Solution ^1H Nuclear Magnetic Resonance (NMR) measurements were performed using a Varian Mercury Vx 400 MHz with $CDCl_3$ as solvent. Solid state ^{13}C Cross Polarization-Magic Angle Spinning NMR (CP-MAS NMR) measurements were performed on a Bruker 300 MHz spectrometer with a spin rate of 5 kHz, using

adamantane as an external reference. FTIR spectroscopy was performed using a Brüker Vertex 80v with dual FTIR and FT-Raman benches with a KBr beamsplitter. Quantitative analysis of conversions and regioselectivity were performed on a Shimadzu GC-2010 gas chromatograph with flame ionization detector (GC-FID) equipped with an SHRX5 column (15 m, 0.25 lm film thickness, 0.25 mm i.d.), using the internal standard method to determine reactant conversion. Verification of organic products of the standard epoxide ring opening reaction was performed on a Shimadzu GCMS-QP2010S gas chromatograph with a mass spectrometer detector (GC–MS) equipped with an SHR5XLB column (30 m, 0.25 lm film thickness, 0.25 mm i.d.).

3.2.7 Catalysis

Initial homogeneous alcohol ring opening reactions (Figure 3.2) were performed in 15 mL pressure tubes. The pressure tubes were charged with 160 μL of solvent (DCM was initially used for most reactions, but difficulties with kinetic sampling necessitated the use of toluene for several reactions; no significant kinetic or selectivity differences were observed between use of DCM vs. toluene), 90 mg of phenol (0.96 mmol, 1.2 equivalents), 95.6 μL of 1,2-epoxyhexane (0.8 mmol), 9.8 mg of DMAP (0.08 mmol, 10 mol%), and 40 μL of dodecane as internal standard. The pressure tubes were immersed in a temperature-controlled silicone oil bath for 12 h, after which they were cooled under cold water for 5 minutes before removing a 10 μL sample for analysis. The small sample was diluted with 2 mL of DCM for GC analysis. For kinetic sampling, a 25 mL two neck round bottom flask equipped with a condenser and a septum was used. The reaction was scaled up by a factor of three, and toluene replaced DCM as the solvent.

For the heterogeneous recycle reactions, the pressure tubes were filled with 800 μL of toluene (the low catalyst loading for the magnetic nanoparticles necessitated the dilution), 90 mg of phenol (0.96 mmol, 1.2 equivalents), 96.5 μL of 1,2-epoxyhexane (0.8 mmol), and 40 μL of dodecane as internal standard. After taking a 10 μL initial sample, the catalyst (200 mg for MNP_MPAP, 26 mg for the polyBMAP, and 65.6 mg for SBA_MPAP) was added to the pressure tube. After addition of 10 mL of toluene to the pressure tube, the polymer catalyst was separated via centrifugation, pouring off the supernatant to isolate the polymer. This was repeated a total of 3 times, after which the catalyst was dried at 100 °C overnight at reduced pressure (10 mTorr) in the pressure tube. MNP_MPAP was separated using a magnet over a period of hours, washing three times with 10 mL of toluene for each separation, and dried at 100 °C overnight at reduced pressure (10 mTorr). The amount of reactant added in recycle runs was scaled based upon the weight of the catalyst after drying. SBA_MPAP was separated using filtration, washed with 10 mL of toluene three times, and dried at 100 °C overnight at reduced pressure (10 mTorr).

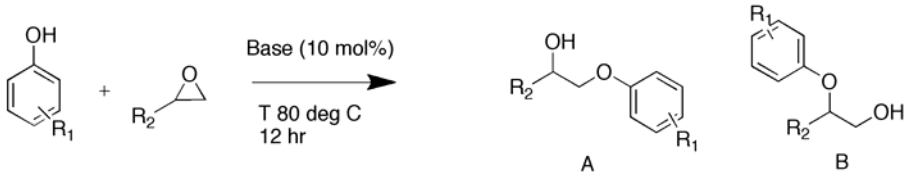

Figure 3.2 Base catalyzed epoxide ring opening.

3.3 Results and Discussions

3.3.1 Homogeneous reactions

The epoxide ring opening reaction was monitored for conversion after a fixed period of time for the standard reaction using DMAP as catalyst to convert 1,2-epoxyhexane and phenol. The conversion with the homogeneous catalyst increased with temperature (Table 3.1) reaching 94% conversion after 12 h at 80 °C. Two products were produced, 1-phenoxyhexan-2-ol and 2-phenoxyhexan-1-ol. The regioselectivity remained approximately constant at 93:7 over the temperature range investigated (i.e., 50 -120 °C). Therefore, the reaction temperature could be increased further to expedite the reaction while not impacting overall regioselectivity, unlike previous reports.[45,46] The choice of solvent had a modest impact on conversion (Table 3.2), but negligible impact on the regioselectivity of the reaction. While toluene, DCM, and TBME gave similar, high conversions after 12 h, acetonitrile or use of neat conditions resulted in lower conversions.

Table 3.1. Conversion and regioselectivity for the epoxide ring opening of epoxy hexane with phenol using homogenous DMAP (at 10 mol% as the catalyst after 12 h at various temperatures).

Temperature (°C)	Time (hrs)	Conversion (%)	A:B
50	12	24	94:6
70	12	67	93:7
80	12	94	93:7
100	5	96	92:8
120	2	94	92:8

Table 3.2. Conversion and regioselectivity comparison for different solvents for the epoxide ring opening of epoxy hexane using phenol with homogeneous DMAP (at 10 mol% as the catalyst at 80 °C after 12 h).

Solvent	Conversion (%)	A:B
Dichloromethane	94	93:7
Toluene	89	93:7
t-butyl methyl ether	89	93:7
Acetonitrile	69	92:8
None	65	92:8

The kinetics of the homogeneous catalyzed reaction was monitored by withdrawing samples periodically with a syringe, and the kinetic profile is shown in Figure 3.3. The volatility of DCM did not permit accurate sampling over a 12 h period due to solvent loss. Therefore, toluene was used for to monitor the kinetics of reaction. The initial rate of reaction was high, converting 38% of the limiting reactant, 1,2-epoxyhexane, within the first hour for an estimated initial turnover frequency of 0.63 min^{-1}. The apparent rate slowed significantly after 6 h, requiring 6 additional hours to proceed from 80% conversion to 94% conversion.

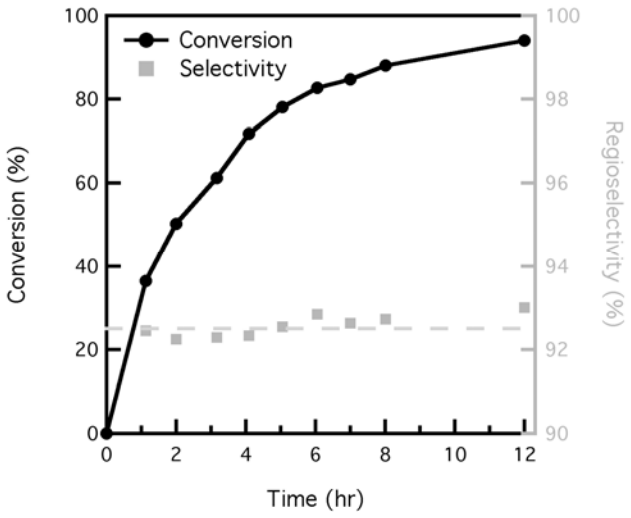

Figure 3.3. Kinetics of the reaction of 1,2-epoxyhexane with phenol catalyzed with homogeneous DMAP (10 mol%) at 80 °C in toluene. The conversion was determined through measuring the conversion of 1,2-epoxyhexane (limiting reagent) using a GC with dodecane as the internal standard. On the right axis, the regioselectivity is plotted of the product 1-phenoxyhexan-2-ol relative to 2-phenoxyhexan-1-ol.

Homogeneous DMAP was used as a catalyst with a variety of substrates (Table 3.3), examining differently substituted phenol-based nucleophiles and epoxides. A methyl substituent at the *para* position of the phenol had no effect on conversion and only a minor effect on regioselectivity. Moving the methyl substitution closer to the hydroxyl group decreased the conversion, but did not impact the selectivity, as evidenced with the *meta* and *ortho* methyl-substituted phenolic species. The decrease in conversion for the *ortho* substituted phenol can be attributed to steric hindrance of the nucleophile. Introducing an electron-withdrawing chloro group at the *meta* position slightly decreased conversion relative to phenol, in an amount approximately consistent with *meta* substitution of a methyl group. Therefore, this effect was not considered electronic in nature, as both electron-donating and electron-withdrawing substituents produced similar conversions. The electron-donating methoxy group in the *para* position similarly had a minor impact on conversion and selectivity. Overall, the substituent variations on the

nucleophile had relatively little impact on the reaction conversion, with only steric effects associated with *ortho* substitution contributing a minor effect, whereas the electronic character of the nucleophile had negligible impact on reactivity.

The substitutions on the epoxide had a significant impact on the reaction conversion. The reaction with 1-allyloxy-2,3-epoxypropane proceeded to almost complete conversion in 12 h with greater regioselectivity than the unsubstituted epoxide, indicating the electron donating properties of the oxygen atom in the ether bond reduce the nucleophilicity of the proximal carbon. Styrene oxide gave a higher conversion than 1-hexene oxide, but resulted in poor regioselectivity, with the phenol substitution occurring to a greater extent at the second position (B) than at the terminal position (A), as expected.[1,47]

Table 3.3. Conversion and regioselectivity of epoxide ring-opening reactions using homogeneous DMAP (at 10 mol% catalyst loading at 80°C after 12 h using different nucleophiles and epoxides).

R_1	R_2	Conversion (%)	A:B
H	n-butyl	94	93:7
4-CH_3	n-butyl	94	93:7
3-CH_3	n-butyl	92	93:7
2-CH_3	n-butyl	89	93:7
3-Cl	n-butyl	91	92:8
4-OCH_3	n-butyl	91	93:7
H	2-(allyloxy) methyl	99	99:1
H	phenyl	97	32:68

3.3.2 Heterogeneous catalysts

3.3.2.1 Materials characterization – SBA_MPAP

The functionalized mesoporous silica (listed in Figure 3.1 as SBA_MPAP where MPAP is the abbreviation for N-methyl-N-propyl-amino pyridine) was thoroughly characterized using standard techniques. Before silane grafting, the material was found to have a XRD pattern consistent with SBA-15 (Figure 3.4) and this pattern was not significantly altered upon grafting the organosilane onto the surface. While the XRD pattern was unchanged, the textural properties of the solid were significantly impacted (Figure 3.5). The mesoporous silica had a pore volume of 1.02 cm^3 g^{-1} of silica before organic grafting and 0.82 cm^3 g^{-1} of silica after grafting the organosilane on the surface. In parallel, the surface area decreased from 690 to 490 m^2 g^{-1} silica after grafting (Table 3.4). The significant decrease in pore volume indicates successful functionalization of the pore volume of the silica.

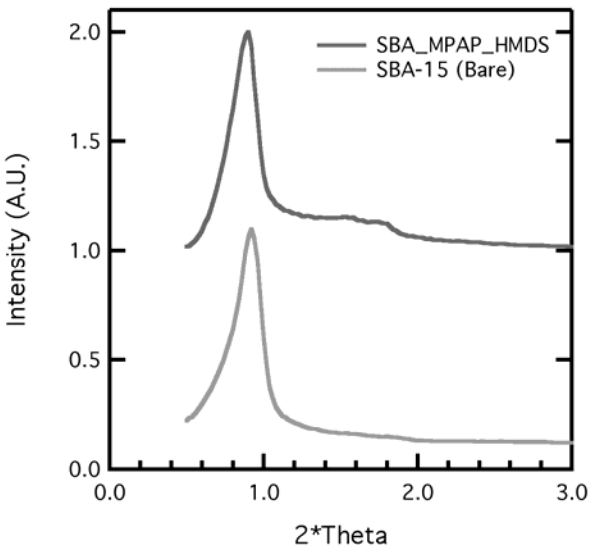

Figure 3.4. X-ray diffraction pattern of SBA-15 before (Bare) and after functionalization and silanol capping (SBA_MPAP_HMDS).

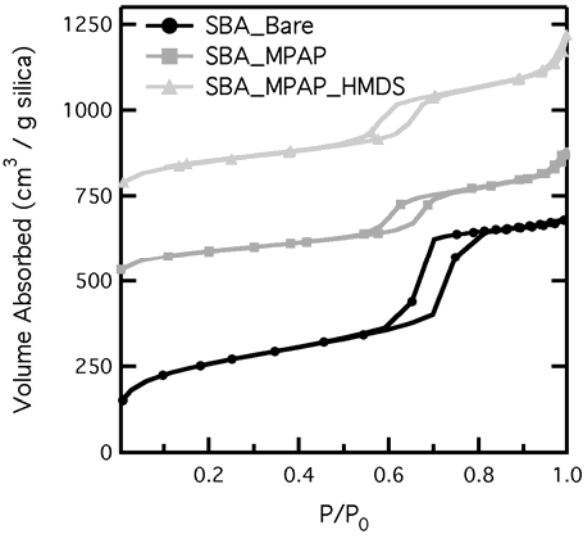

Figure 3.5. Nitrogen physisorption comparison of the silica material before and after grafting of the organosilane. The silica material after functionalization is also shown. The curves are offset by an additive factor (500 and 750 for SBA_MPAP and SBA_MPAP_HMDS, respectively) on the ordinate axis for clarity.

The grafting procedure was also monitored through TGA (Figure 3.6), NMR (Figure 3.7), and FTIR (Figure 3.8) spectroscopy. The estimated loading was found to be 1.17 mmol g^{-1} based on TGA analysis of the grafted organosilane combustion, assuming that the organic content originated from the N-methyl-N-propylpyridin-4-amine of the organosilane with, on average, one residual ethoxy.[48] This value is close to the loading calculated from elemental analysis of 1.21 mmol g^{-1}, but significantly lower than the amount of organosilane added during the functionalization (i.e., 3.0 mmol g^{-1}), due to the steric bulk of the organosilane inhibiting grafting to a higher loading. Finally, SBA_MPAP was analyzed with solid state NMR and FTIR to confirm the presence of the desired DMAP-analogue. The ^{13}C CP-MAS NMR spectrum was comparable to those previously reported for similar materials.[49] The FTIR spectra had peaks in the range of 3000-2900 cm^{-1} attributable to the aliphatic surface tether and the aromatic C-H bonds.

An additional set of peaks at 1660 cm^{-1}, 1610 cm^{-1}, and 1560 cm^{-1} correspond to skeletal vibrations of pyridine. Comparable peaks were observed for both the organosilane[40] and the SBA_MPAP. Overall, the combined results from the battery of characterization techniques confirm the presence of the supported organosilane.

Table 3.4. Physical and chemical characteristics of the different functionalized mesoporous and magnetic materials.

Material	SA_{BET} (m^2/ g_{Silica})	Pore Volume (cm^3/ g_{Silica})	Avg. Pore Dia. (nm)	TGA Loading (mmol/g)	EA %C	EA %N	EA Loading (mmol/g)	N/C (mol N/ mol C)
MNP_MPAP					5.42	1.12	0.40	0.18
MNP_MPAP Post-ERO					6.05	0.96		0.14
SBA_Bare	690	1.02	6.5	-	-	-	-	-
SBA_MPAP	490	0.82	6.5	1.17	14.30	3.41	1.21	0.20
SBA_MPAP Post ERO					21.08	2.67		0.11
SBA_MPAP-HMDS	470	0.80	6.1	-	16.69	3.49	1.25	0.18
SBA_MPAP-HMDS ERO_1					23.13	2.96		0.11
SB_MPAP-HMDS ERO_2				-	22.81	2.81		0.11
SBA-MPAP-HMDS-ERO_3				-	24.98	2.69		0.09

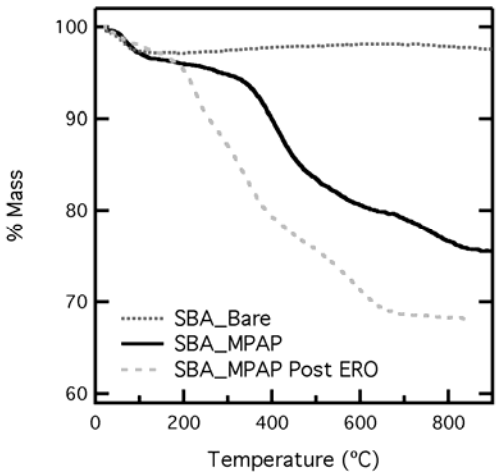

Figure 3.6. TGA curve for the mesoporous silica organosilane (SBA_MPAP) and the bare mesoporous material (SBA_Bare). After three ERO reaction cycles, the material was analyzed for the increase in organic content (SBA_MPAP Post ERO).

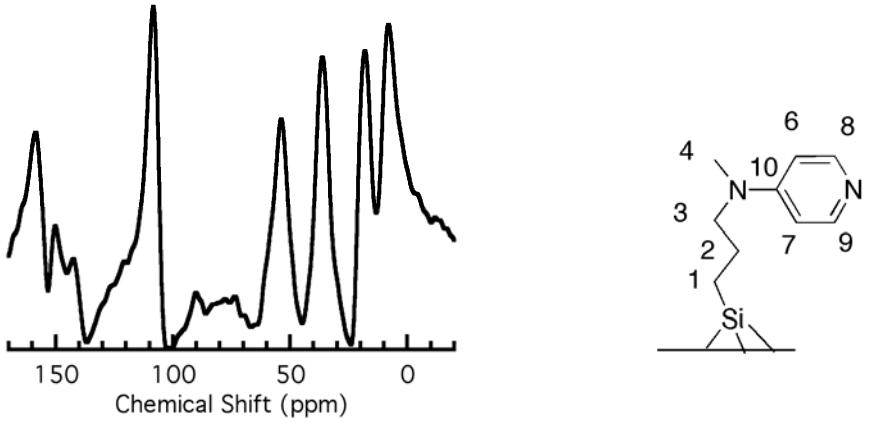

Figure 3.7. ^{13}C CP MAS NMR of SBA_MPAP. The peaks appear at δ (ppm) 8 (C1), 18 (C2), 36 (C4), 54 (C3), 108 (C6,C7), 150 (C8, C9), and 158 (C10).

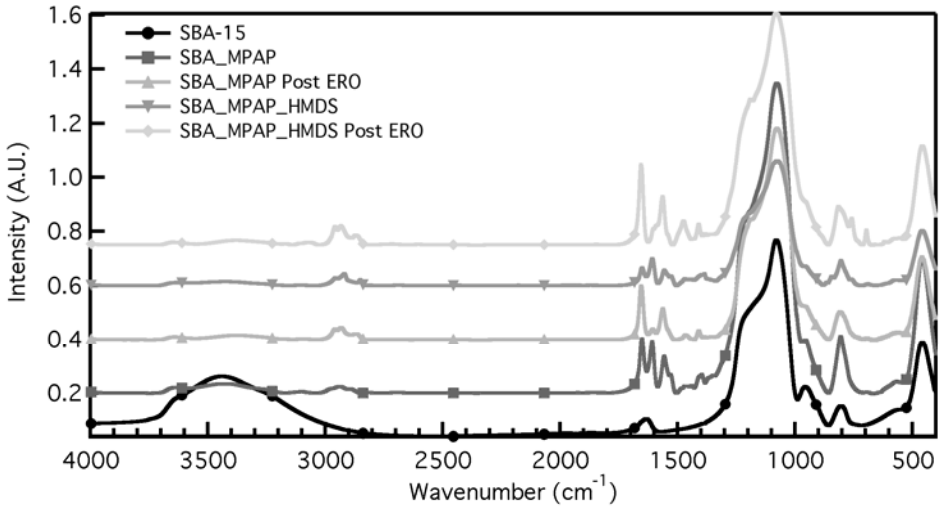

Figure 3.8. FTIR comparison of the bare silica (SBA-15), MPAP functionalized silica before reaction (SBA_MPAP) and after 3 reaction cycles (SBA_MPAP Post ERO), and the MPAP and HMDS functionalized silica before (SBA_MPAP_HMDS) and after 3 reaction cycles (SBA_MPAP_HMDS Post ERO).

3.3.2.2 Materials characterization – MNP_MPAP

The magnetic nanoparticles were produced in high yield with a coating of oleic acid to reduce agglomeration. The FTIR spectra (Figure 3.9) had peaks in the range of 3000-2800 cm^{-1} attributable to the long aliphatic tail of oleic acid as well as a peak at 1560 cm^{-1} that corresponded to the carbonyl stretch of the carboxylic acid group. The crystallinity of the particles was confirmed with XRD (Figure 3.10; the broad peaks are indicative of nanoparticles). The coated nanoparticles were analyzed using TEM, revealing a core particle size of ca. 8 nm with a shell thickness of ca. 6 nm, resulting in a core-shell particle size of 20 nm, as shown in Figure 3.11. The coating process displaced the oleic acid capping ligands, as the FTIR spectra demonstrate. While the nanoparticles were individually-coated initially, the nanoparticles agglomerated irreversibly over the course of the silica coating, resulting in an overall particle size on the order of 100 nm.

This coating process did not affect the crystallinity of the nanoparticles, as the XRD patterns indicated.

The silica-coated nanoparticles were subsequently functionalized with N-methyl-N-(3-(triethoxysilyl)propyl)pyridin-4-amine. While the loading for silica materials can be estimated from TGA, similar analysis for magnetic nanoparticles is more difficult due to the dehydration of the not fully condensed silica layer during TGA analysis (Figure 3.12), as well as small amounts of residual oleic acid. Instead, the loading was determined from the nitrogen content measured with elemental analysis to be 0.40 mmol g^{-1}. This loading is considerable given that previous composite silica-Fe_3O_4 nanoparticle with a comparable diameter and degree of agglomeration had loadings of 0.20 mmol g^{-1}.[34] As with the silica material, FTIR confirmed the presence of the organocatalyst on the surface with peaks at 1660 cm^{-1}, 1610 cm^{-1}, and 1560 cm^{-1}, which were comparable to those observed in the FTIR spectra of SBA_MPAP. The peak intensities were less than observed with SBA_MPAP due to the lower degree of functionalization.

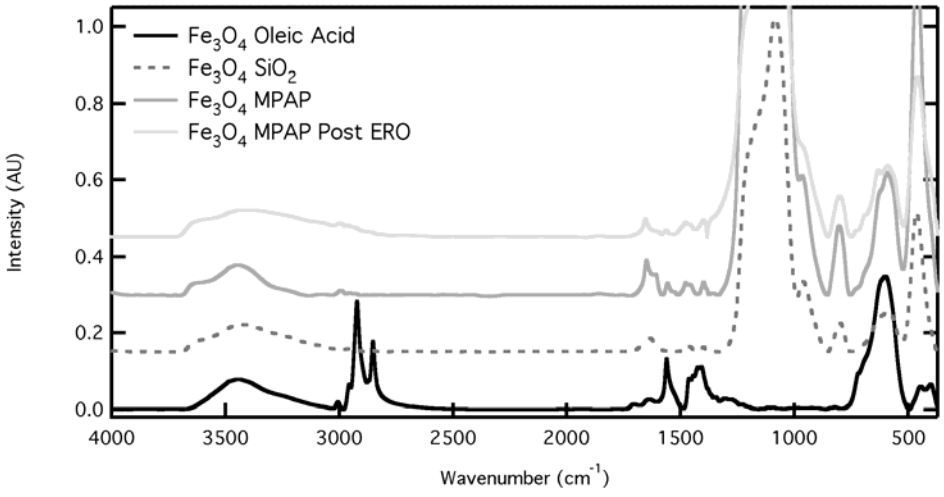

Figure 3.9. FTIR spectra of magnetic nanoparticles with oleic acid capping ligands (Fe_3O_4 Oleic Acid), after silica coating (Fe_3O_4 SiO_2), after functionalization with the PMAP organosilane (Fe_3O_4 PMAP), and after 3 reaction cycles (Fe_3O_4 PMP Post ERO).

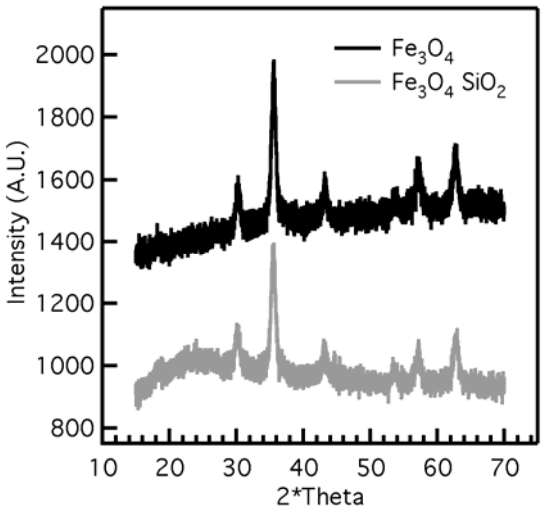

Figure 3.10. X-ray diffraction pattern of the as-synthesized Fe_3O_4 nanoparticles before (Fe_3O_4) and after silica coating (Fe_3O_4 SiO_2).

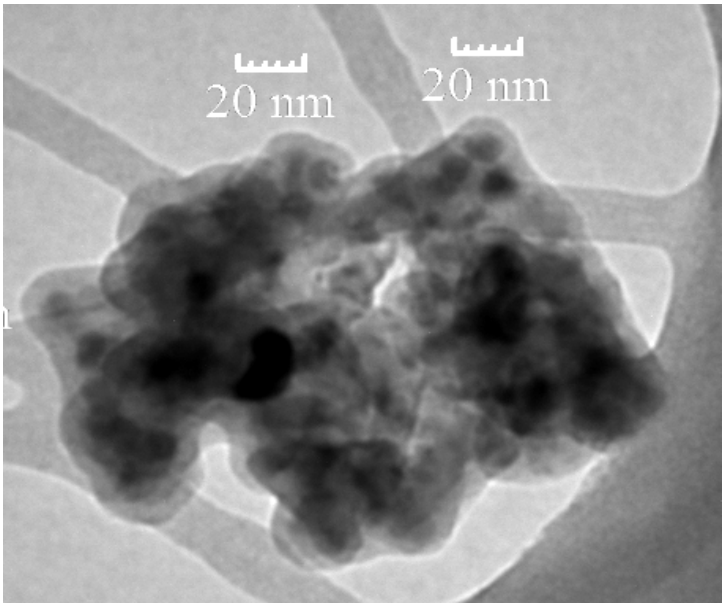

Figure 3.11. TEM image of the silica coated magnetic nanoparticles.

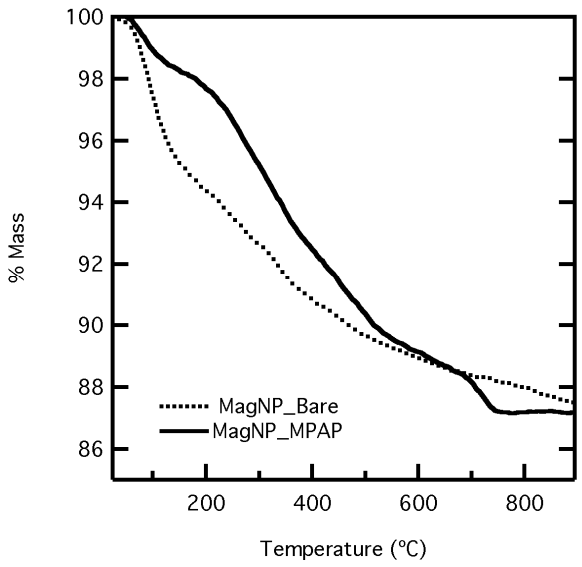

Figure 3.12. TGA curve for the as-synthesized Fe_3O_4 magnetic nanoparticles (MNP_Bare) and for organic functionalized, silica coated nanoparticles (MNP_MPAP).

3.3.3 Heterogeneous catalysis

For heterogeneous catalysis, the reaction mixture was diluted in comparison to the homogeneous case, as the magnetic nanoparticles formed viscous solutions due to the large mass required to achieve a 10 mol% catalyst loading (i.e. 200 mg). All heterogeneous reactions were therefore run at more diluted conditions for the sake of comparison. Both SBA_MPAP and MNP_MPAP required 6 days to achieve 80% conversion of 1,2-epoxyhexane, while polyBMAP achieved 88% conversion in 4 days (Table 3.5). MNP_MPAP was comparable to the mesoporous silica in terms of catalytic activity[50] and recyclability (*vide infra*).

Table 3.5. Conversion and regioselectivity comparison for different heterogeneous catalysts (at 10 mol% catalyst loading for the epoxide ring opening of 1,2-epoxyhexane with phenol at 80 °C after the specified time). All reactions were performed with 800 μL of toluene with two exceptions. SBA_MPAP_HMDS1 was run using 400 μL and SBA_MPAP_HMDS2 was run with 160 μL.

Catalyst	Cycle	Time (hr)	Conversion (%)	A:B
Polymer DMAP	1	96	88	93:7
	2	96	78	96:4
	3	96	80	93:7
MagNP DMAP	1	144	83	93:7
	2	144	55	93:7
	3	144	41	93:7
SBA-15 DMAP	1	144	79	92:8
	2	144	58	93:7
	3	144	48	93:7
SBA-15 DMAP HMDS	1	72	84	94:6
	2	72	85	94:6
	3	72	74	94:6
SBA-15 DPAP HMDS2	1	24	80	93:7
	2	24	80	93:7
	3	24	78	94:6

After reaction, the heterogeneous catalysts were recovered and reused in additional reactions to assess the recyclability and stability of the catalyst. Recycle experiments with polyBMAP resulted in conversions that were slightly lower than the fresh catalyst, but comparable to the initial conversion. SBA_MPAP and MNP_MPAP were found to decrease significantly in activity upon recycling. After 3 recycle reactions, the conversion decreased to approximately 40% after 144 h with no further decrease in conversion in a subsequent iteration. A small amount of product was irreversibly adsorbed onto the catalyst in these reactions that could not be removed despite washing three times with 15 mL of toluene, as indicated by the increase in carbon content in elemental analysis. This was expected to cause slightly inaccurate catalyst mass measurements with the MNP_MPAP for the recycle experiments (i.e. 0.5%), but is not

consistent with the dramatic decrease in catalytic activity (i.e., 50% loss in activity). Washing with DCM was attempted but the magnetic nanoparticles could not be precipitated as easily as when toluene was used as the washing solvent. Analysis with FTIR (Figure 3.9) indicated that the additional organic content had an aliphatic (3000-2800 cm^{-1}) and aromatic content (i.e., 1660 cm^{-1}) (*vide infra*). The combined analyses indicate that the product adsorbed to the surface of the catalyst, resulting in decreased activity.

With SBA_MPAP, separation by filtration was used to recover the catalyst, but this could not remove adsorbed product despite washing with hot toluene and subsequently a mixture of triethylamine and DCM (1:99). The accumulated product increased the carbon content by 8#wt%, as measured by elemental analysis. FTIR indicated the material had both an aliphatic portion and an aromatic portion, as the peaks in the range of 3000-2800 cm^{-1} increased and a peak at 1660 cm^{-1} appeared after reaction (Figure 3.8). Two possible reasons for the increased carbon content are the strong interaction of the products with the organocatalyst or the reaction of products with the support. The possibility that the ring-opened epoxide could react with the surface silanols was examined through performing the homogeneous reaction in the presence of bare mesoporous silica. After filtering the bare silica and washing with 100 mL of toluene, the organic content was roughly 30 wt% (Figure 3.13). This is larger than the 7 wt% increase observed for SBA_MPAP after 3 reactions. The greater amount of silanols for the bare silica should permit a greater degree of reaction with the surface, increasing the organic content. The FTIR spectra had similar features as the other samples analyzed after reaction (Figure 3.14), including peaks in both the aliphatic (3000-2800 cm^{-1}) and

the aromatic (1660 and 1580 cm^{-1}) regions associated with the presence of the reaction product. The results suggest that the product interacted strongly and essentially irreversibly with the surface silanols, rather than with the organic catalyst in SBA_MPAP. This interaction could block the active sites, decreasing the catalytic activity of both SBA_MPAP and MNP_MPAP.

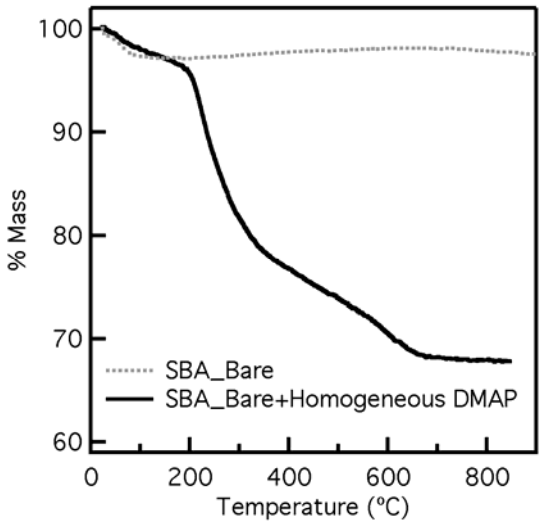

Figure 3.13. TGA curve for the bare mesoporous material before (SBA_Bare) and after one reaction cycle with homogeneous DMAP (SBA_Bare+Homogeneous DMAP).

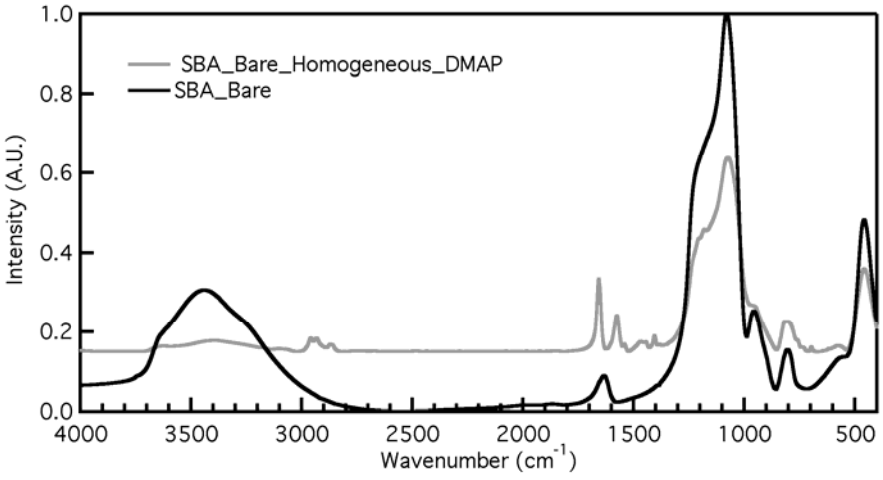

Figure 3.14. FTIR spectra of the bare mesoporous material before (SBA_Bare) and after one ERO reaction cycle with homogeneous DMAP (SBA_Bare_Homogeneous DMAP).

Therefore, the surface silanols were eliminated through treatment of SBA_MPAP with HMDS in dry toluene for two days under nitrogen, resulting in SBA_MPAP_HMDS. The capping was confirmed with ^{13}C CP-MAS NMR (Figure 3.15) with a new peak in the spectra with a shift of 0 ppm. To expedite the reaction, the amount of toluene was halved for a total amount of 400 μL. The decrease in solvent decreased the time for reaction to 72 h for both SBA_MPAP and SBA_MPAP_HMDS to achieve greater than 80% conversion. Reactions performed with SBA_MPAP_HMDS did not exhibit the dramatic loss of activity observed with the exposed silanols, reproducibly achieving high levels of conversion of approximately 80%. Yet, even with the capped silanols, the organic content of the catalyst increased after reaction, as demonstrated via TGA measurement and elemental analysis (Figure 3.16). The largest increase in organic content occurred during the first cycle, as the elemental analysis results indicate (SBA_MPAP_HMDS ERO_1 in Table 3.4). The FTIR spectra (Figure 3.8) indicated that the increased organic content was due to residual product, as peaks in the aliphatic region of 3000-2800 cm^{-1} increased and a peak in the aromatic region of 1660 cm^{-1} appeared. These results were consistent with a product that interacted with the organocatalyst or the capped oxide surface, but did not deactivate the catalyst to a significant extent over three cycles. Therefore, silanol capping was deemed necessary to retain high catalytic activity, but was not sufficient to prevent an increase in the organic content.

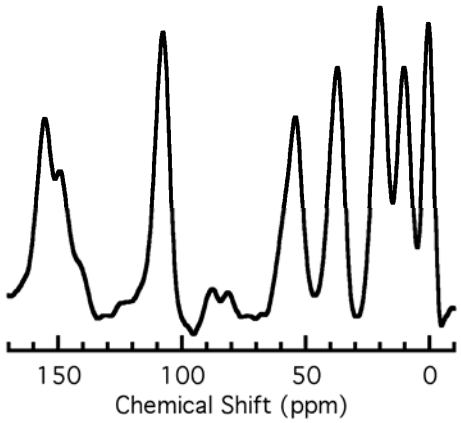

Figure 3.15. ^{13}C CP MAS NMR of SBA_MPAP_HMDS. The peaks associated with the organosilane appear as in Figure 3.7 with an additional peak at 0 ppm that corresponds to the trimethylsilane used to cap surfaces silanols.

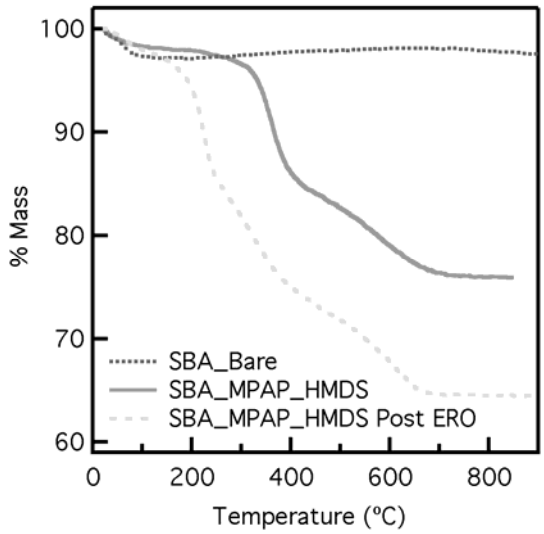

Figure 3.16. TGA curve for the mesoporous silica functionalized with the organosilane and with the silanols capped through an HMDS (SBA_MPAP_HMDS) and the bare mesoporous material (SBA_Bare). After three ERO reaction cycles with the functionalized silica, the recovered material was analyzed for the increase in organic content (SBA_MPAP_HMDS Post ERO).

3.4 Conclusions

We have demonstrated that DMAP was an active organocatalyst for epoxide ring opening reaction using phenolic nucleophiles, resulting in 94% conversion with 92%

regioselectivity for the 1-aryloxy-2-alcohol in as little as 2 h at 120 °C. Substituents on the phenol had little effect on conversion whereas those on the epoxide significantly affected conversion and regioselectivity. Of the heterogeneous catalysts, the polymeric catalyst performed the best, exhibiting faster conversion and better recyclability than the mesoporous silica and magnetic nanoparticle based catalysts. Improvement of the recyclability of the mesoporous silica based catalyst required coating the surface silanols with HMDS to retain catalytic activity. Overall, the magnetic nanoparticle catalyst was quite similar in activity to the silica based catalyst.

3.5 Acknowledgements

The authors would like to financial support from the US Department of Energy office of Basic Energy Sciences through Catalysis Science contract DE-FG02-03ER15459.

3.6 References

(1) Parker, R.; Isaacs, N. *Chem. Rev.* **1959**, *59*, 737.

(2) Cordeiro, P.; Tilley, T. D. *ACS Catal.* **2011**, *1*, 455.

(3) Na, K.; Jo, C.; Kim, J.; Ahn, W. S.; Ryoo, R. *ACS Catal.* **2011**, *1*, 901.

(4) Cuerva, J.; Justicia, J.; Oller-López, J.; Bazdi, B.; Oltra, J. *Mini-Reviews in Org. Chem.* **2006**, *3*, 23.

(5) Wong, O. A.; Shi, Y. *Chem. Rev.* **2008**, *108*, 3958.

(6) Rose, E.; Andrioletti, B.; Zrig, S.; Quelquejeu-Ethève, M. *Chem. Soc. Rev.* **2005**, *34*, 573.

(7) Dhakshinamoorthy, A.; Alvaro, M.; Garcia, H. *ACS Catal.* **2011**, *1*, 836.

(8) Feng, Y.; England, J.; Que, L. *ACS Catal.* **2011**, *1*, 1035.

(9) Denmark, S. E.; Barsanti, P. A.; Beutner, G. L.; Wilson, T. W. *Adv. Synth. Catal.* **2007**, *349*, 567.

(10) Tokuoka, E.; Kotani, S.; Matsunaga, H.; Ishizuka, T.; Hashimoto, S.; Nakajima, M. *Tetrahedron: Asymmetry* **2005**, *16*, 2391.

(11) Savle, P. S.; Lamoreaux, M. J.; Berry, J. F.; Gandour, R. D. *Tetrahedron: Asymmetry* **1998**, *9*, 1843.

(12) Jacobsen, E. N.; Kakiuchi, F.; Konsler, R. G.; Larrow, J. F.; Tokunaga, M. *Tetrahedron Lett.* **1997**, *38*, 773.

(13) Hansen, K.; Leighton, J.; Jacobsen, E. N. *J. Am. Chem. Soc.* **1996**, *118*, 10924.

(14) Konsler, R.; Karl, J.; Jacobsen, E. N. *J. Am. Chem. Soc.* **1998**, *120*, 10780.

(15) Adolfsson, H.; Moberg, C. *Tetrahedron: Asymmetry* **1995**, *6*, 2023.

(16) Pastor, I.; Yus, M. *Curr. Org. Chem.* **2005**, *9*, 1.

(17) Tokunaga, M.; Larrow, J. F.; Kakiuchi, F.; Jacobsen, E. N. *Science* **1997**, *277*, 936.

(18) Bonollo, S.; Lanari, D.; Vaccaro, L. *Eur. J. Org. Chem.* **2011**, *2011*, 2587.

(19) Kwon, M.; Kim, G. J. *Catal. Today* **2003**, *87*, 145.

(20) Larrow, J. F.; Hemberger, K. E.; Jasmin, S.; Kabir, H.; Morel, P. *Tetrahedron: Asymmetry* **2003**, *14*, 3589.

(21) Ready, J. M.; Jacobsen, E. N. *Angew. Chem. Int. Ed.* **2002**, *41*, 1374.

(22) Kim, Y.-S.; Guo, X.-F.; Kim, G.-J. *Chem. Commun.* **2009**, 4296.

(23) Kim, Y.-S.; Guo, X.-F.; Kim, G.-J. *Top. Catal.* **2009**, *52*, 197.

(24) Guo, X.-F.; Kim, Y.-S.; Kim, G.-J. *Top. Catal.* **2009**, *52*, 153.

(25) Kawthekar, R. B.; Ahn, C.-H.; Kim, G.-J. *Catal. Lett.* **2007**, *115*, 62.

(26) Zhu, X.; Venkatasubbaiah, K.; Weck, M.; Jones, C. W. *J. Mol. Catal. A* **2010**, *329*, 1.

(27) Matsunaga, S.; Das, J.; Roels, J.; Vogl, E. M.; Yamamoto, N.; Iida, T.; Yamaguchi, K.; Shibasaki, M. *J. Am. Chem. Soc.* **2000**, *122*, 2252.

(28) Joseph, M.; Jacobsen, E. N. *J. Am. Chem. Soc.* **1999**, *121*, 6086.

(29) Venkatasubbaiah, K.; Zhu, X.; Kays, E.; Hardcastle, K. I.; Jones, C. W. *ACS Catal.* **2011**, *1*, 489.

(30) Chen, J.; Shum, W. *Tetrahedron Lett.* **1995**, *36*, 2379.

(31) Christensen, S. P.; Flick, D. *US Patent App. 12/990,342* **2009**.

(32) Li, Y.; Tan, Y.; Herdtweck, E.; Cokoja, M.; Kuhn, F. E. *Appl. Catal. A* **2010**, *384*, 171.

(33) Shiels, R.; Jones, C. W. *J. Mol. Catal. A* **2007**, *261*, 160.

(34) Dalaigh, C.; Corr, S.; Gunko, Y.; Connon, S. J. *Angew. Chem. Int. Ed.* **2007**, *46*, 4329.

(35) D'elia, V.; Liu, Y.; Zipse, H. *Eur. J. Org. Chem.* **2011**, *2011*, 1527.

(36) Kwong; Huang, R.; Zhang, M.; Shi, M.; Toy, P. *Chem. Eur. J.* **2007**, *13*, 2369.

(37) Menger, F.; McCann, D. *J. Org. Chem.* **1985**, *50*, 3928.

(38) Tomoi, M.; Akada, Y.; Kakiuchi, H. *Die Makromolekulare Chemie, Rapid Commun.* **1982**, *3*, 537.

(39) Chen, H.; Huh, S.; Wiench, J.; Pruski, M.; Lin, V. S.-Y. *J. Am. Chem. Soc.* **2005**, *127*, 13305.

(40) Rubinsztajn, S.; Zeldin, M.; Fife, W. K. *Macromolecules* **1991**, *24*, 2682.

(41) Zhao, D.; Huo, Q.; Feng, J.; Chmelka, B.; Stucky, G. *J. Am. Chem. Soc.* **1998**, *120*, 6024.

(42) Sun, Y.; Ding, X.; Zheng, Z.; Cheng, X.; Hu, X.; Peng, Y. *Eur. Polymer J.* **2007**, *43*, 762.

(43) Gill, C. S.; Price, B.; Jones, C. W. *J. Catal.* **2007**, *251*, 145.

(44) Lukens Jr, W. W.; Schmidt-Winkel, P.; Zhao, D.; Feng, J.; Stucky, G. D. *Langmuir* **1999**, *15*, 5403.

(45) Terblans, Y. M.; Huyser, J. J.; Huyser, M.; Green, M. J.; Young, D. A.; Sibiya, M. S. *Can. J. Chem.* **2005**, *83*, 854.

(46) Terblans, Y. M.; Huyser, M.; Young, D. A.; Green, M. J. *Can. J. Chem.* **2006**, *84*, 859.

(47) Das, S.; Asefa, T. *ACS Catal.* **2011**, *1*, 502.

(48) Hicks, J.; Jones, C. W. *Langmuir* **2006**.

(49) Motokura, K.; Tomita, M.; Tada, M.; Iwasawa, Y. *Top. Catal.* **2009**, 579.

(50) Phan, N. T. S.; Jones, C. W. *J. Mol. Catal. A* **2006**, *253*, 123.

CHAPTER 4

HYBRID SULFONIC ACID CATALYSTS BASED ON SILICA-SUPPORTED POLY(STYRENE SULFONIC ACID) BRUSH MATERIALS AND THEIR APPLICATION IN ESTER HYDROLYSIS[‡]

4.1 Introduction

Acid catalysts are extensively used in many important chemical transformations, such as alkylation and etherification.[1-3] However traditional liquid acids, such as HCl, H_2SO_4, and HF, normally cause severe equipment corrosion and environmental pollution. Solid acids, such as zeolites, oxides, phosphates, heteropoly acids, and organic-inorganic composites, have emerged as green substitutes over the last decades for liquid acids because of their easy recovery, lower pollution and lack of corrosiveness.

Generally, the catalytic activity of solid acids is negatively impacted by aqueous media, with a few exceptions, such as some organic solid acids. In many important chemical transformations, water participates as a reactant or product, such as hydrolysis and esterification reactions. For example, production of biodiesel typically involves transesterification of triglycerides with short chain alcohols and esterification of free fatty acids from feedstocks with a large amount of water.[4,5] Catalytic reactions in aqueous

---

[‡] Reproduced with permission from W. Long, C.W. Jones, *ACS Catal.* **2011**, 1, 674. Copyright (2011) American Chemical Society.

systems are also very attractive from the perspective of replacing organic solvents. Compared to the use of organic solvents, catalytic reactions in aqueous systems have a lot of advantages including low cost, low toxicity and safety. Thus, it is desirable to synthesize new "water tolerant" acid catalysts and develop an understanding of acid catalyst stability in the presence of water.[6]

The two most-studied classes of organic solid acids are ion-exchange resins and inorganic oxide supported sufonic acids. Polymeric ion-exchange resins, such as the styrene-based sulfonic acids and perfluorosulfonic acid based polymer catalysts have been used commercially in many areas.[7] Sulfonic acid functionalized inorganic solids prepared via traditional post-grafting or silane co-condensation methods, such as silica supported alkyl sulfonic acids or arenesulfonic acids and Nafion/silica nanocomposites, have also been studied extensively.[8] Recently, surface initiated controlled polymerization has emerged as a new technique for material functionalization, endowing oxide surfaces with polymeric organic species. For example, surface initiated atom transfer radical polymerization (ATRP) is one of the most powerful and commonly used techniques to introduce uniform polymer layers on solid surfaces.[9,10] After immobilizing initiators onto the surface, the polymer chains are grown from the initiation position to form 'polymer brush' materials, first described as catalysts in 2008,[11,12] which can be used to achieve high catalyst loadings while allowing good accessibility to the active sites. [11-17] In the recent literature, grafting of poly(sodium styrene sulfonate) onto SBA-15[18] and ultra large pore SBA-15[19] via ATRP of sodium styrene sulfonate has been investigated. However in those two cases, low organic loadings and acidities were achieved. A poly(vinylsulfonic

acid)-grafted poly(styrene) resin has also been prepared via the surface initiated radical polymerization of vinylsulfonic acid and used for catalytic esterification reactions.[20,21]

Herein, a new polymer brush supported sulfonic acid is prepared via surface initiated ATRP of styrene followed by sulfonation of the polymer brush. Cab-O-Sil M5, a nonporous silica, is used as the support to avoid potential pore clogging issues associated with polymerization with porous materials as the supports.[22,23] For typical ATRP surface initiators, between the surface and the initiation site there is an ester or amide linkage that may be hydrolytically unstable under acidic or basic conditions. To alleviate this problem, an alkyl initiator with only carbon-carbon bonds between the surface and the grafted polymer is designed and synthesized (Figure 4.1). Ester hydrolysis of ethyl lactate is chosen as a model reaction to evaluate the activity and stability of the new acid catalyst. The product, lactic acid, is a very useful renewable chemical intermediate.[24] Lactic acid derived from fermentation processes requires extensive purification. Instead of the conventional sequential approach of reaction and separation,[25] catalytic distillation, whereby a water-tolerant acid catalyst is employed,[26-28] can be applied as a more efficient technique. In this work, new polymer brush supported sulfonic acid catalysts are used for the hydrolysis of ethyl lactate, with an emphasis placed on understanding the catalytic performance and stability of this new type of catalyst in the presence of excess water.

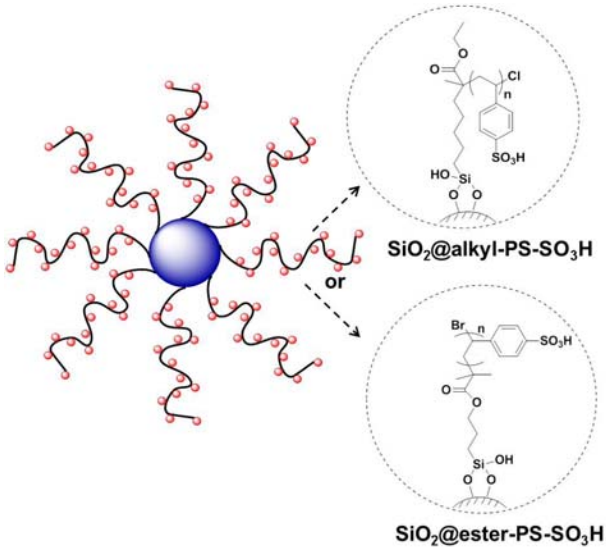

Figure 4.1. Silica-supported poly(styrene sulfonic acid) brush materials.

4.2 Experimental Section

4.2.1 Chemicals and materials

The following chemicals were commercially available and used as received unless otherwise noted: ethyl 2-chloropropionate (Alfa Aesar, 96%), 5-bromo-1-pentene (Alfa Aesar, 96%), lithium diisopropylamide (LDA, 2M in THF/heptane/ethylbenzene, Aldrich), THF (dried by passing through columns of activated copper oxide and alumina), toluene (J.T. Baker, anhydrous), dodecane (anhydrous, Sigma-Aldrich), hexamethylphosphoramide (HMPA, Aldrich, 99%), trimethoxysilane (Aldrich, 95%), Platinum(0)-1,3-divinyl-1,1,3,3,-tetramethyldisiloxane complex solution (Karstedt's catalyst, Aldrich, 0.1 M in poly(dimethylsiloxane) vinyl terminated), 1,1,4,7,10,10-hexamethyltriethylenetetramine (HMTETA, Sigma-Aldrich, 97%), (3-trimethoxysilyl)propyl 2-bromo-2-methylpropionate (Gelest, 95%), fuming sulfuric acid (Mallinckrodt, 20% SO_3), copper(I) bromide (purified by stirring in glacial acetic acid,

washed with ethanol and diethyl ether, dried under vacuum and stored inside glovebox), Cab-O-Sil M5 fumed silica (Cabot Corporation, BET surface area ~200 m^2/g), and styrene (dried over CaH_2, and purified by vacuum distillation). All air and moisture sensitive compounds were handled via Schlenk techniques or in a nitrogen glove box.

4.2.2 Synthesis of the new ATRP initiator silane

Ethyl 2-chloro-2-methyl-6-heptenoate (1a):

A flask containing dry THF was cooled to -78 °C and LDA (48 ml, 96 mmol) was added into the solvent. Ethyl 2-chloro propionate (10.2 ml, 80 mmol) was then added dropwise. The reaction solution was stirred for several minutes, and then HMPA (27.9 ml, 160 mmol) was injected quickly. The color of the solution changed from deep red to dark brown. Next, 5-bromo-1-pentene (9.5 ml, 80 mmol) was added slowly to the flask. The temperature was subsequently maintained at -78 °C for 1 h with stirring. Then the mixture was allowed to warm naturally to room temperature and stirred overnight. The next day, the reaction was quenched with 25 ml 5% HCl and 25 ml DI H_2O. 100 ml diethyl ether was added into the mixture for extraction. The organic layer was washed with 5% HCl (5 times) and brine (2 times), and then dried over $MgSO_4$. Finally, solvents were evaporated via rotary evaporation and the crude oil was purified by flash chromatography (95:5 hexane-EtOAc) to give 11.5 g product (yield: 70%). ^1H NMR (400MHz, $CDCl_3$): δ 1.29 (t, 3H), 1.48 (m, 2H), 1.72 (s, 3H), 2.0 (m, 4H), 4.21 (q, 2H), 5.0 (m, 2H), 5.77 (m, 1H). ^{13}C NMR (400MHz, $CDCl_3$): δ 14.14, 24.25, 27.82, 33.48, 41.59, 62.17, 69.10, 115.25, 137.98, 171.41.

Ethyl 2-chloro-2-methyl-7-(trimethoxysilyl) heptanoate (1b):

Ethyl 2-chloro-2-methyl-6-heptenoate (4.0 g, 19.5mmol) and trimethoxysilane (3.58 g, 29.3mmol) were added into the reaction vessel. Karstedt's catalyst (390 ul) was added into the mixture dropwise. The solution was stirred at 80 °C overnight. The crude mixture was purified with fractional vacuum distillation to give 3.2 g product (yield: 50%). ^{1}H NMR (400MHz, $CDCl_3$): δ 0.63 (m, 2H), 1.30 (t, 3H), 1.37 (m, 6H), 1.72 (s, 3H), 1.98 (m, 2H), 3.57 (s, 9H), 4.22 (q, 2H). ^{13}C NMR (400MHz, $CDCl_3$): δ 9.12, 14.10, 22.47, 24.62, 27.71, 32.86, 42.05, 50.56, 62.99, 69.18, 171.44.

Silica supported ATRP initiators

Cab-O-Sil M5 (2 g) was dispersed into toluene (86 g) with sonication in a 150 ml pressure tube. Ethyl 2-chloro-2-methyl-7-(trimethoxysilyl)heptanoate (4 mmol) was added slowly into the slurry and then the mixture was refluxed about 40 hr. The solid was recovered by filtration through filter paper and washed repeatedly with toluene, petroleum ether, methanol and diethyl ether. The recovered white powder was dried under vacuum at 100 °C for several hours and then stored in a glovebox for later use. TGA revealed that the organic loading of the supported chloro heptanoate (SiO_2@alkyl initiator) was 0.53 mmol/g.

(3-trimethoxysilyl)propyl 2-bromo-2-methylpropionate was immobilized to the silica surface with the same procedure. The organic loading of the supported bromo isobutyrate (SiO_2@ester initiator) was 0.23 mmol/g by TGA, which is lower than that of the SiO_2@alkyl initiator. The syntheses of SiO_2@alkyl initiator and SiO_2@ester initiator were repeated several times and the resulting loadings were consistent.

To obtain SiO_2@ester initiator with higher initiator loading, the ratio of initiator silane to Cab-O-Sil was increased from 2 mmol silane / g SiO_2 to 5 mmol silane / g SiO_2. The organic loading of SiO_2@ester initiator_2 was 0.44 mmol/g, as determined via TGA.

4.2.3 Preparation of catalysts

Surface-initiated ATRP

The surface-initiated ATRP was performed according to reported procedures[11] with minor modifications. Silica supported initiator (SiO_2@alkyl initiator, 899 mg) was suspended into anhydrous toluene (19.4 g) to get a slurry of 40 mg/ml. The molar ratios of reactants were as follows: styrene: SiO_2@alkyl initiator: CuBr: HMTETA = 50: 1: 1.2: 2.4. The mixture was stirred under nitrogen at 110 °C for 24 hrs. A small amount of dodecane was added as the standard to monitor the conversion of the polymerization. At the end, the polymerization solution was diluted with excess toluene and the solid product was recovered by centrifuge (8000 rpm, 30 minutes). This step was repeated at least three times to wash away the free polymer (if any formed) during the polymerization. Then the solid was washed repeatedly with a mixture of methanol and pyridine to remove the copper catalyst residue. The final recovered powder sample was dried under vacuum at 100 °C for several hours. For the SiO_2@ester initiator, all the experimental parameters and the synthesis procedure were the same except a higher ratio of styrene to SiO_2@ester initiator was used (80:1). For SiO_2@ester initiator_2, all the experimental parameters and the synthesis procedures were the same.

Synthesis of polymer brush supported sulfonic acids

The polymer brush materials were sulfonated following a published literature[29] with slight modifications. In a typical sulfonation, the polymer brush material (1 g) was added into a 50 ml flask. Fuming sulfuric acid (25 ml, 48 g) was weighed in a small vial and then transferred into the flask. The slurry was shaken for 10 minutes, and then was quenched by slowly adding the mixture into excess DI H_2O. The recovered acid catalyst was washed repeatedly with DI H_2O until the pH of the filtrate was above 6. The catalyst was dried under vacuum at 100 °C overnight.

4.2.4 Characterization

^{1}H and ^{13}C NMR spectra were acquired with a Varian Mercury Vx 400 ($CDCl_3$ solvent). Transmission electron microscopy (TEM) measurements were performed on a JEOL 100CX-2 and HF 2000. A Netzsch STA 409 was used for thermal gravimetric analysis (TGA) under a mixture of air and nitrogen with a heating rate of 10 °C/min. FT-IR spectra were obtained on a Bruker Vertex 80 optical bench using KBr Pellets. Surface areas were assessed via nitrogen physisorption analysis using a Micromeritics TristarII. Before measurement, the samples were degassed overnight under vacuum around 100 °C. X-ray Photoelectron Spectroscopy (XPS) were performed on a Thermo K-Alpha XPS using Al Kα irradiation with a flood gun. The samples were put on a powder sample holder, evacuated in a load lock, and then transferred to the analysis chamber (vacuum around E-08 mbar) for measurement. The spectra were referenced to the C1s peak at 284.8 eV. The reaction conversion was monitored by gas phase chromatography (GC) on a Shimadzu GC-2010 with a FID detector and a SHRX5 column. Elemental analyses

were performed by Columbia Analytical Services (Tucson, AZ). Titration was used to determine the acid loading of the catalysts. The polymer brush supported sulfonic acid (~ 15 mg) was dispersed into a saturated NaCl aqueous solution (~ 5 ml) for several hours under sonication. The solid was filtered and washed several times with brine. The collected filtrate (~20 ml) was titrated with 0.01 M NaOH with phenolphthalein as the indicator.

4.2.5 Catalytic hydrolysis of ethyl lactate

Typically, the catalyst (SiO_2@alkyl-PS-SO_3H, 48 mg, 1.25 mol% catalyst relative to the ethyl lactate, equivalent to 0.144 mmol H^+) was weighed into a 15 mL two-neck flask and was dispersed into 1 g DI H_2O via sonication (~ 30 min). 1,4-dioxane (1.03 g, internal standard) was added to the dispersed catalyst. The reaction flask with a condenser was immersed into an oil bath and preheated to 60 °C (~20 min). Ethyl lactate (1.37 g, 11.6 mmol) and DI H_2O (2.14 g) were mixed together and transferred into the two-neck flask to start the reaction. Samples (40 uL) were removed periodically via syringe and analyzed by GC-FID. The hydrolysis of ethyl lactate with SiO_2@ester-PS-SO_3H was performed following the same procedures. In all the reactions, 1.25 mol% of the catalyst was used, and the reactants and the standard were scaled according to the amount of catalysts used. At the end of the reaction, the catalyst was recovered by filtration and washed repeatedly with DI H_2O until the pH of the filtrate was above 6. The recovered catalysts were dried under vacuum overnight at 100 °C, and then reused in subsequent reactions. Recycle experiments were scaled according to the mass of the recovered catalysts.

4.3 Results and Discussions

4.3.1 Synthesis of the ATRP initiator silanes

For preparation of the polymer brush materials, the synthesis was carried out in two steps: (1) immobilization of the initiator on the solid support; (2) surface initiated polymerization. The most commonly used silane-functionalized ATRP initiators all have amide or ester linkages between the silicon atom and the polymerization initiation point, and therefore they may be unstable under acidic or basic aqueous conditions. For example, several reports from Rühe et al. describe a system whereby grafted polymers were detached from the surface by cleaving the ester bond in the initiator moiety between the surface and the polymer chain under reflux conditions with p-toluenesulfonic acid as the catalyst.[30,31] Since our target catalyst is a polymer brush supported sulfonic acid, to achieve better catalytic stability, a new initiator was designed and synthesized (Figrue 4.2). In this new initiator, instead of the ester linkage, there are only C-C bonds between the surface and the initiation position. The initiator precursor was functionalized by adding a pentene group next to the initiation position. A trimethoxysilane group was then added to the olefin via hydrosilylation in the presence of Karstedt's catalyst at 80 °C. A small number of samples were taken and checked with ^{1}H NMR during the course of the hydrosilylation to monitor the reaction. The peaks corresponding to the olefin group disappeared gradually. The final product was purified via fractional vacuum distillation. The distillate at 160 °C under 30 mmtorr contained the desired product, **1b**.

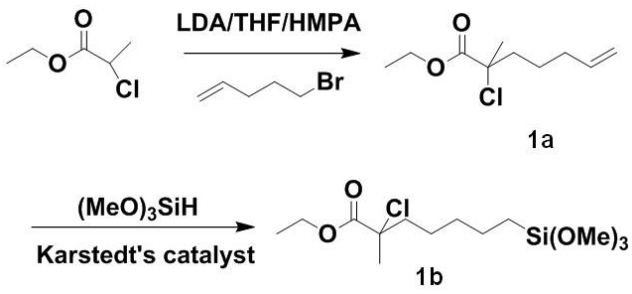

Figure 4.2. Synthesis of ethyl 2-chloro-2-methyl-7-(trimethoxysilyl) heptanoate.

4.3.2 Preparation of the supported initiator

Cab-O-Sil M5 is a fumed, nonporous silica with multiparticle aggregates. The average aggregate length is 0.2 – 0.3 μm and the surface area is ~ 200 m^2/g. ATRP initiator species were deposited onto the silica surface by refluxing the initiator silane and silica in toluene. Unreacted silane was removed by extensive washing with toluene, petroleum ether, methanol and diethyl ether. The organic loading of the silica supported initiator was estimated by TGA (Table 4.1). The immobilization of each initiator silane was performed following the same procedures and repeated multiple times. The loadings of the SiO_2@alkyl initiator were always higher than those of the SiO_2@ester initiator, which may be due to the different reactivities of these two initiator silanes. This results in slightly different initiator loadings on the surface of the silica support. The densities of the supported initiators were between 0.7- 1.6 / nm^2, which is lower than the silanol density of the fumed silica (2-4 OH/nm^2).[32]

Table 4.1. Loading and density of the supported initiator.

Materials	mmol of initiator/ g of sample	no. of initiators / nm^2 of surface*
SiO_2@alkyl initiator	0.53	1.6
SiO_2@ester initiator	0.23	0.70

FT-IR and XPS were used to further confirm the surface species in the hybrid material. In the FT-IR spectra (Figure 4.3), the peaks around 2930 cm^{-1} were assigned to aliphatic C-H stretches, and the C=O stretch was clearly visible at 1720 cm^{-1}. XPS analysis (Figure 4.4a) of the silica supported alkyl initiator also clearly revealed the characteristic peak of Cl 2p at 200.4 eV (for SiO_2@ester initiator, the Br 3d peak was evident at 69.6 eV).

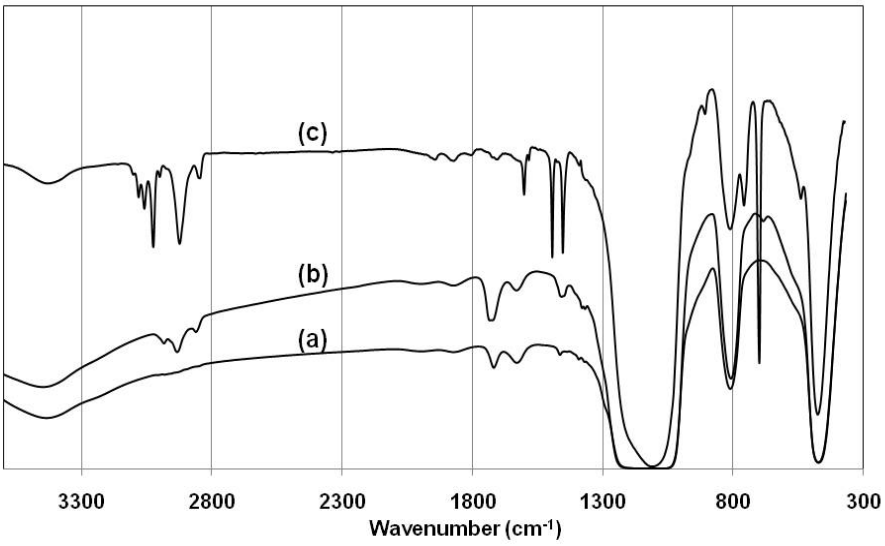

Figure 4.3. FT-IR of SiO_2@ester initiator (a); SiO_2@alkyl initiator (b); SiO_2@ester-PSt (c).

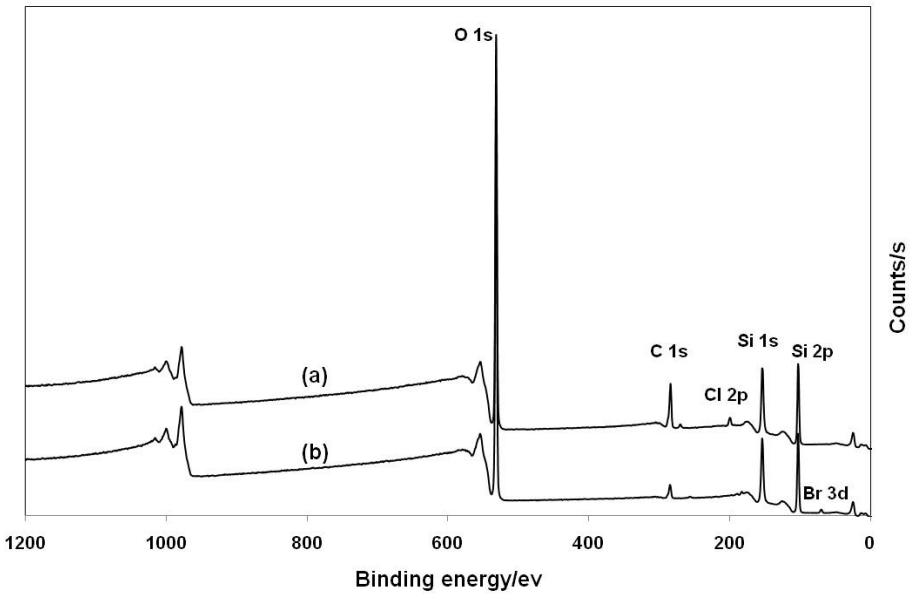

Figure 4.4. XPS spectra of SiO_2@alkyl initiator (a); SiO_2@ester initiator (b).

4.3.3 Surface initiated ATRP of styrene

The silica supported initiators were used for ATRP of styrene. Typically, the initiator functionalized silica was mixed with styrene, copper (I) bromide, ligand, toluene and internal standard at 110 °C for 24 h. The monomer conversion was determined at the end of polymerization via GC-FID. Since the initiator density and initiation efficiency of SiO_2@alkyl initiator were different from that of SiO_2@ester initiator, polymerization under identical conditions yielded significantly different polymer loadings and characteristics. To attempt to yield catalysts that had comparable polymer loadings using the two initiator-functionalized solids, the [monomer]/[initiator] ratio was tuned to yield the same ratio of the polymerized monomer to the supported initiator (= [styrene]/[SiO_2@initiator] × conversion). Although these values were similar for the two

materials, the polymer content of the produced SiO_2@alkyl-PS was still higher than that of the SiO_2@ester-PS because the initiator loading of the SiO_2@alkyl initiator was higher. The recovered polymer brush materials were washed extensively with toluene to remove free polymer to mitigate its potential effects on the subsequent catalytic investigations. The organic loadings of the polymer brush materials were estimated by TGA (Table 4.2). According to the calculations, the majority of the polymerized styrene was growing on the surface. Although a small amount of free polymer was likely formed, it could be removed by repeated washing. To ensure that the free polymer was removed, the washing procedures were repeated and it was found that the organic loadings of the polymer brush materials did not change. This suggests the two catalysts, SiO_2@alkyl-PS and SiO_2@ester-PS, were devoid of free polymer and all polymers were covalently bound to the oxide surface. FT-IR confirmed that the structure of the polymer layer in the solid materials was consistent with poly(styrene) (Figure 4.3c). Aromatic C-H stretches were observed around 3030 cm^{-1} and a significant growth of peaks associated with the polymer backbone, assigned to aliphatic C-H stretches around 2930 cm^{-1}, was also observed. In the TEM images, the Cab-O-Sil supported poly(styrene) material (Figure 4.5) displayed a fractal-like structure with a thin layer of polymer on the surface.

Table 4.2. Physical characteristics of the polymer brush materials prepared via surface initiated ATRP.

Materials	[M]/[SiO_2@initiator]	Conv.	$[M]_{polymerized}$/[SiO_2@initiator]	Organic loading	Organic loading after re-washing
SiO_2@alkyl-PS	50	64%	32	60.2%	61.7%
SiO_2@ester-PS	80	41%	32.8	41.1%	40.7%

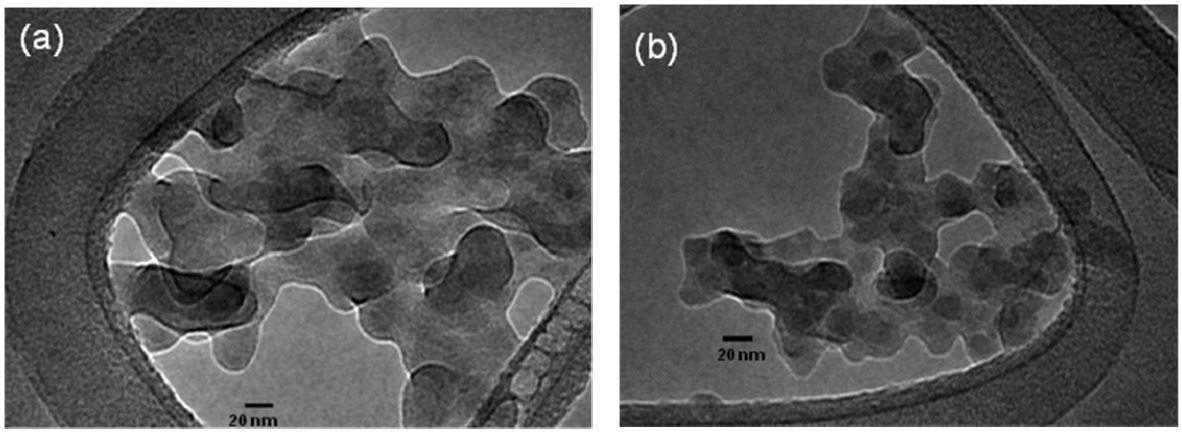

Figure 4.5. TEM images of SiO_2@alkyl-PS (a); SiO_2@ester-PS (b).

4.3.4 Sulfonation of the poly(styrene) brushes

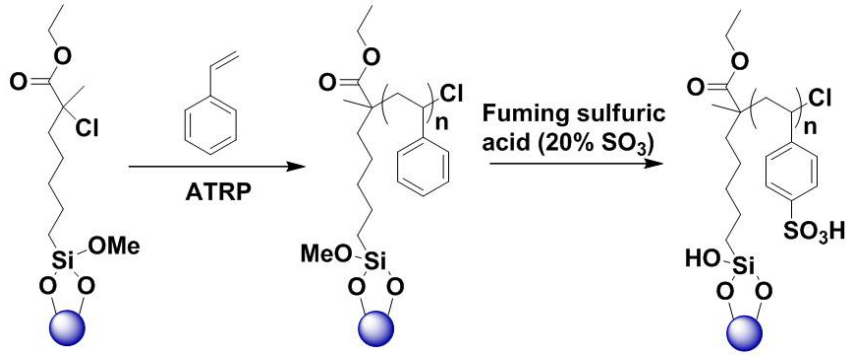

Figure 4.6. Preparation of SiO_2@alkyl-PS-SO_3H.

After treatment with fuming sulfuric acid,[29,33] -SO_3H groups were introduced into SiO_2@alkyl-PS (Figure 4.6) and SiO_2@ester-PS (the catalysts are denoted as SiO_2@alkyl-PS-SO_3H and SiO_2@ester-PS-SO_3H). Since the sulfonation reactions are typically electrophilic substitutions, the -SO_3H group is added to the ortho or para positions in the aromatic ring, and mono-substitution is preferred.[33] The successful sulfonation was verified by FT-IR, XPS, elemental analysis and titration. In the FT-IR spectra (Figure 4.7), the S=O stretches at 1008 cm^{-1} and 1037 cm^{-1} clearly indicated the existence of sulfonic acids.[34,35] In the XPS spectra (Figure 4.8), the S 2p peak at 169.1 eV was observed.[29] The XPS analysis showed that the S/C ratios of SiO_2@alkyl-PS-SO_3H and SiO_2@ester-PS-SO_3H were 0.146 and 0.140, respectively. The data suggest the SiO_2@alkyl-PS-SO_3H and SiO_2@ester-PS-SO_3H have similar surface sulfonation degrees. This value is also close to 0.125, which is the theoretical value of the S/C ratio assuming each aromatic ring bears one sulfonic acid group in the poly(styrene) polymers. The results from elemental analysis (Table 4.3) were consistent with the information interpreted from the XPS analysis. The compiled data reveal that both of the catalysts have similar sulfonation degrees and the S/C molar ratios were close to the theoretical ones.

The ion exchange capacity of the catalysts was determined by acid-base titration.[36,37] The acid loadings of SiO_2@alkyl-PS-SO_3H and SiO_2@ester-PS-SO_3H determined by titration were 3.0 mmol/g and 1.3 mmol/g, respectively. The results were consistent with the values from elemental analysis (Table 4.3). For polymer brush supported sulfonic acids prepared by the new synthesis strategy utilizing the alkyl-linked initiator, a much higher acid loading could be achieved, compared to other silica

supported sulfonic acids, which usually have acid loadings of less than 1 mmol/g. Furthermore, it should be noted that the carbon content of the SiO_2@alkyl-PS-SO_3H was reduced slightly from 130 mmol C/ g SiO_2 to 96 mmol C/ g SiO_2, after sulfonation. In contrast, the C content of the SiO_2@ester-PS-SO_3H decreased dramatically from 51 mmol C/ g SiO_2 to 19 mmol C/ g SiO_2 after sulfonation. This observation suggests the majority of the polymer matrix remained in the SiO_2@alkyl-PS-SO_3H catalyst after sulfonation, while a large percentage of polymers detached from the silica support in SiO_2@ester-PS-SO_3H during the sulfonation process. These observations show the polymer brush sulfonic acid catalyst based on the alkyl initiator has better stability compared to the material made with the ester initiator.

The thermal stability of the catalyst was determined by TGA. For example, in SiO_2@alkyl-PS-SO_3H (Figure 4.9), a three step decomposition pattern was observed. A slight mass loss around 100 °C was attributed to removal of water bound to the hydrophilic sulfonic acid groups. A second mass loss was observed around 310 °C, which is likely associated with desulfonation.[38] The final mass loss was likely due to decomposition of polymer matrix at around 560 °C.

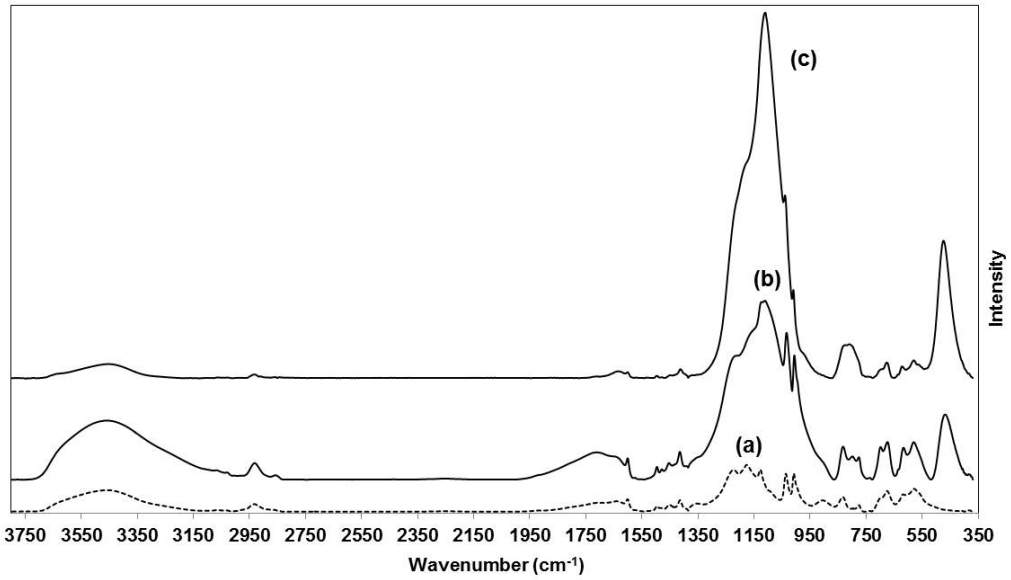

Figure 4.7. FT-IR of Amberlyst 15 (a); SiO_2@alkyl-PS-SO_3H (b); SiO_2@ester-PS-SO_3H (c). Amberlyst 15 is sulfonic acid resin based on cross-linked styrene-divinylbenzene copolymers.

Table 4.3. Compositions of solid polymer brush materials after sulfonation.

Catalysts	S (mmol/g)	C (mmol/g)	S/C	Sulfonation degree
SiO_2@alkyl-PS-SO_3H	3.26	27.6	0.118	~ 94%
SiO_2@ester-PS-SO_3H	1.51	13.02	0.116	~ 93%

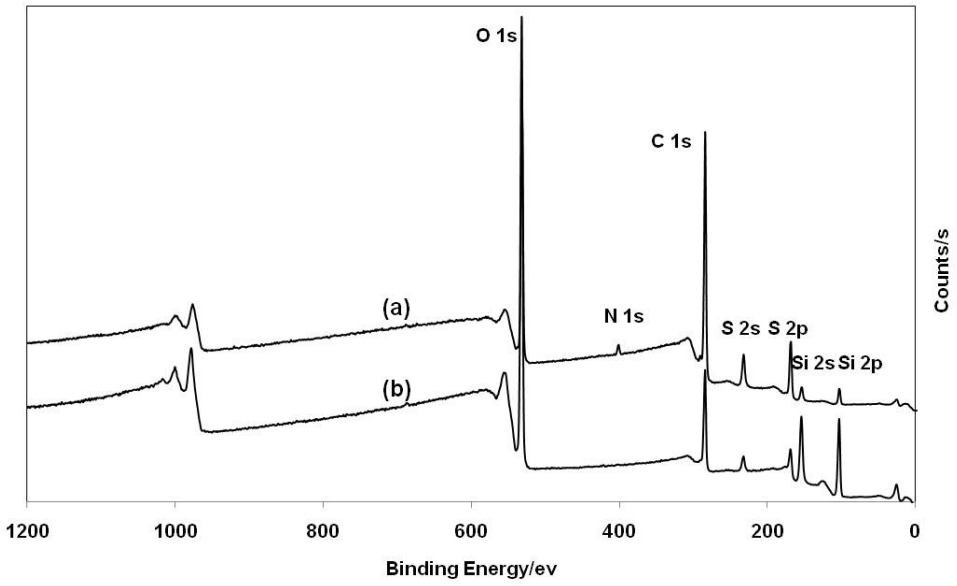

Figure 4.8. XPS spectra of SiO_2@alkyl-PS-SO_3H (a); SiO_2@ester-PS-SO_3H (b).

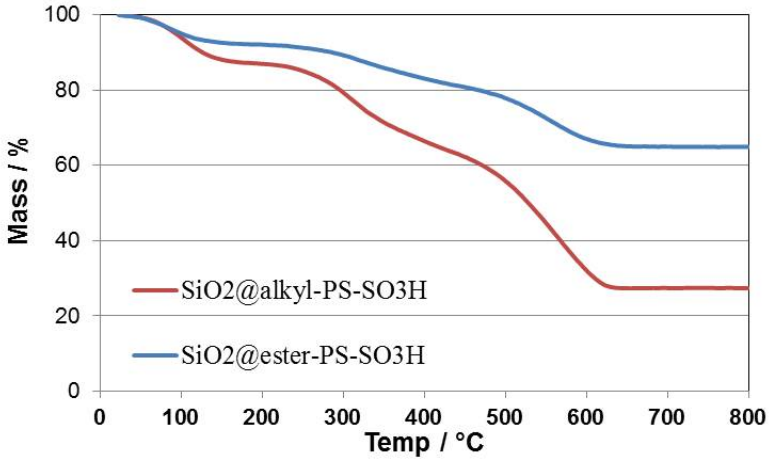

Figure 4.9. TGA of SiO_2@alkyl-PS-SO_3H.

4.3.5 Catalytic hydrolysis of ethyl lactate

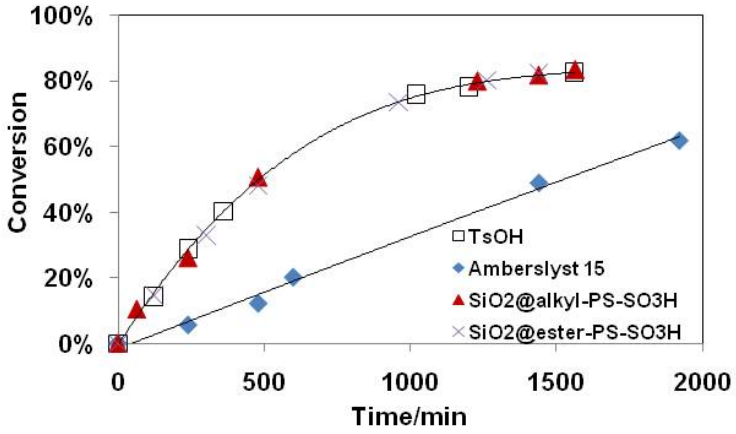

Figure 4.10. Kinetics of ethyl lactate hydrolysis. (1.25 mol% catalyst loading, 60 °C).

The catalytic activity and recyclability of the polymer brush sulfonic acid catalysts were demonstrated in the hydrolysis of ethyl lactate. The polymer brush supported sulfonic acids displayed similar activity (Figure 4.10) to their homogeneous analogue- p-toluenesulfonic acid, and a much higher reaction rate compared to Amberlyst 15, which is attributed to the easy accessibility of the active sites originating from the unique polymer brush architecture. For SiO_2@alkyl-PS-SO_3H, the catalyst showed good activity over three runs (Figure 4.11a), with only a slight decrease in the reaction rate upon recycle. Titration of the recovered SiO_2@alkyl-PS-SO_3H catalyst showed that the acid loading decreased from 3.0 mmol/g to 2.8 mmol/g after cycle 1 (7% loss) and then to 2.4 mmol/g after cycle 2 (20% loss). For SiO_2@ester-PS-SO_3H, the reaction rate in the first run was similar to that of the SiO_2@alkyl-PS-SO_3H (Figure 4.10). This suggests the two catalysts have similar accessibility of the active sites under these conditions, despite the different polymer surface coverage (reactions were run at the same acid loading). The SiO_2@ester-PS-SO_3H catalyst deactivated more quickly (Figure 4.11b) and the acid loading was reduced from1.3 mmol/g to 0.87 mmol/g after cycle 2 (33% loss).

The decrease of acid loading may be attributed to desulfonation or the detachment of the polymer chains from the surface. FT-IR (Figure 4.12 and 4.13) was used to assess the functional groups of the recycled catalysts. Compared to the fresh catalysts, the recycled ones did not have significant differences in the spectra. The peaks corresponding to the S=O stretches could still be clearly observed in the spectra of the recycled catalysts. For further understanding of the deactivation mechanisms, more quantitative analysis of the composition of the catalysts was performed by elemental analysis. It was found that the S/C ratio decreased gradually in the SiO_2@alkyl-PS-SO_3H, (Table 4.4), which indicated desulfonation[39] occurred during the ester hydrolysis reactions. The C/Si ratios also decreased slightly after recycle, which is probably due to the hydrolysis of the Si-O-Si bonds that connect the initiator group to the silica surface.[40,41] As for the SiO_2@ester-PS-SO_3H catalyst, it displayed similar trends (Table 4.5) except that the carbon content decreased more quickly (Figure 4.14).

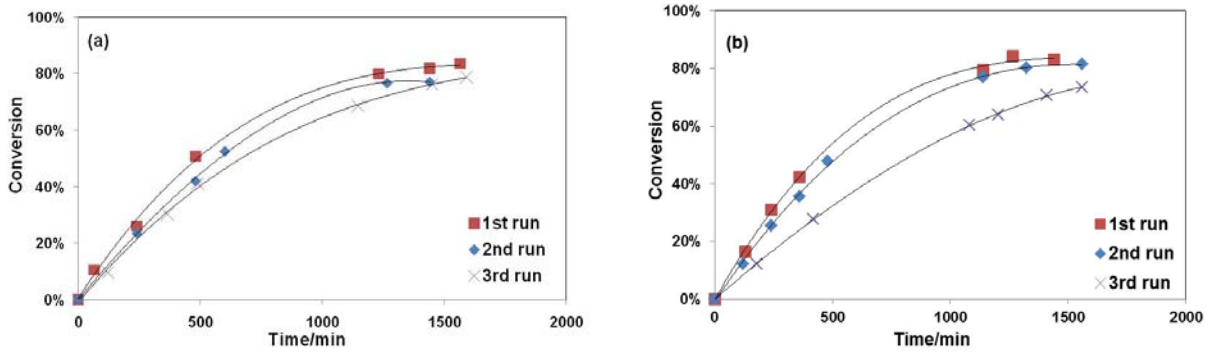

Figure 4.11. Kinetics of the catalysts during recycles: SiO_2@alkyl-PS-SO_3H (a); SiO_2@ester-PS-SO_3H (b). (1.25 mol% catalyst loading, 60 °C).

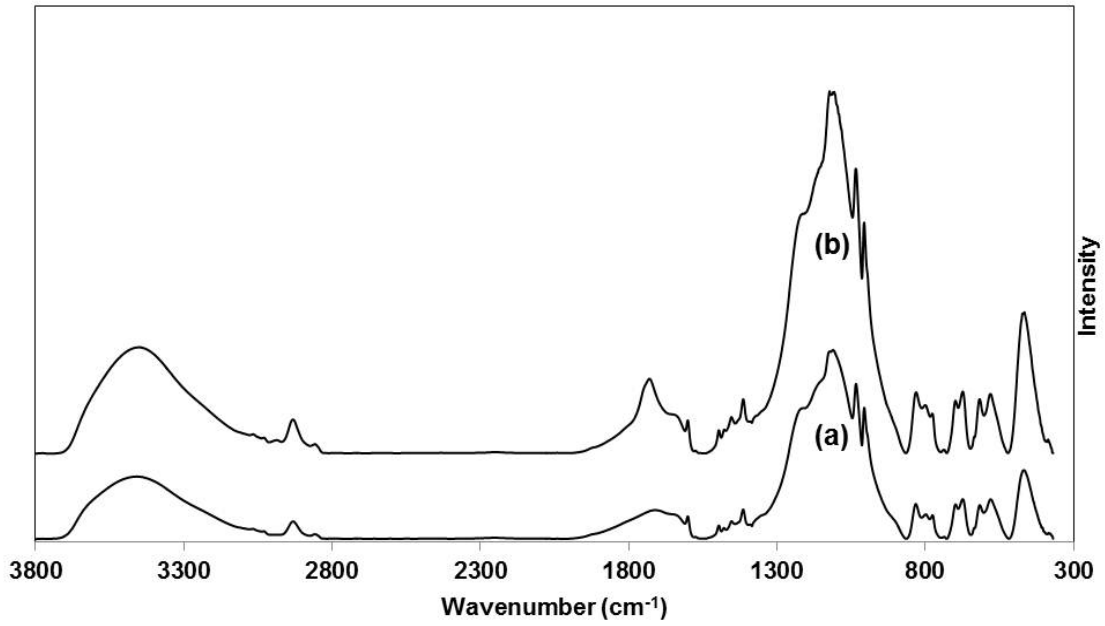

Figure 4.12. FT-IR spectra of SiO_2@alkyl-PS-SO_3H (a); SiO_2@alkyl-PS-SO_3H after run 1 (b).

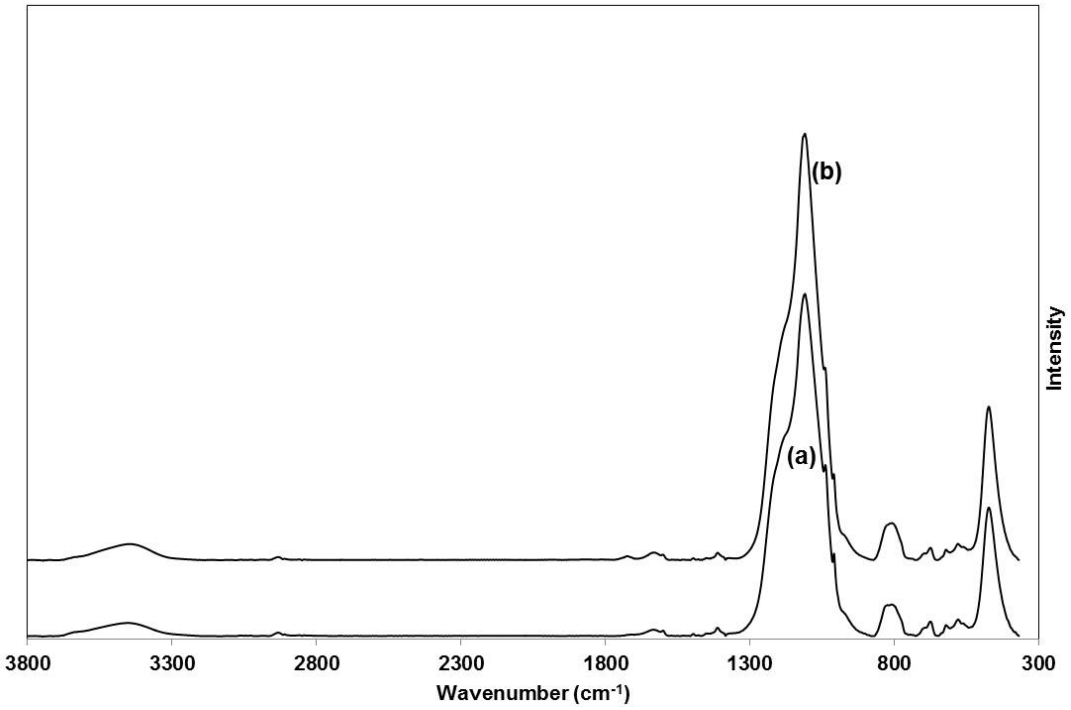

Figure 4.13. FT-IR spectra of SiO_2@ester-PS-SO_3H (a); SiO_2@ester-PS-SO_3H after run 1 (b).

Table 4.4. EA of the fresh SiO_2@alkyl-PS-SO_3H and the recycled ones.

Catalysts	C wt%	S wt%	Si wt%	S/C	C mmol/g SiO_2
Fresh	33.15	10.45	13.5	0.118	95.6
After 1st run	30.71	7.4	15.12	0.090	79.0
After 3rd run	32.83	7.5	20.01	0.086	63.9

Table 4.5. EA of the fresh SiO_2@ester-PS-SO_3H and the recycled ones.

Catalysts	C wt%	S wt%	Si wt%	S/C	C mmol/g SiO_2
Fresh	15.64	4.85	32.19	0.116	18.9
After 1st run	12.60	3.72	45.74	0.110	10.7
After 3rd run	8.45	1.395	48.72	0.062	6.75

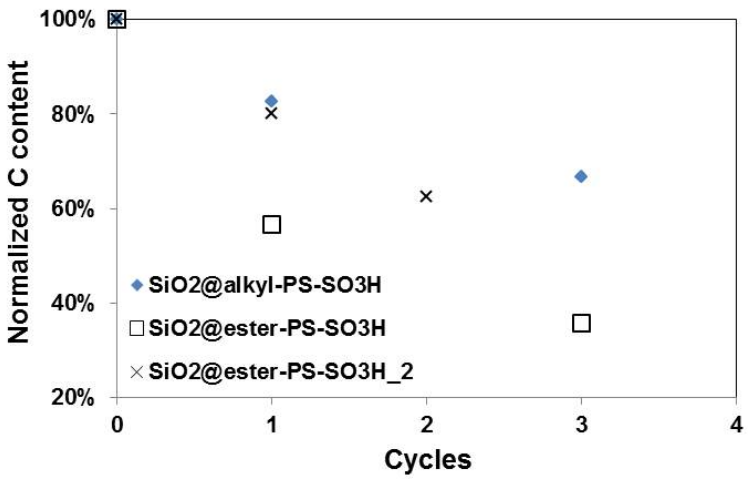

Figure 4.14. Normalized carbon content of the catalysts after each cycle (define the C mmol/g in the fresh catalyst as 100%).

Since polymer detachment was observed in both of the catalysts, to shed light on the effects of polymer coverage on the material stability, SiO_2@ester-PS_2 with a similar polymer loading to SiO_2@alkyl-PS was prepared. After sulfonation, the C content of the SiO_2@ester-PS-SO_3H_2 decreased from 118 mmol C/ g SiO_2 to 68 mmol C/ g SiO_2 (43% decrease, compared to 27% decrease in SiO_2@alkyl-PS-SO_3H and 65% decrease in SiO_2@ester-PS-SO_3H). The acid loading of the fresh catalyst was 2.8 mmol/g. The activity and stability of SiO_2@ester-PS-SO_3H_2 catalyst were tested in ethyl lactate hydrolysis test reaction. Consistently, the fresh catalyst displayed a similar reaction rate to the other two polymer brush supported sulfonic acids, but deactivated gradually during recycle, with a slightly higher deactivation rate than SiO_2@alkyl-PS-SO_3H (Figure 4.15). The C/Si ratio (Table 4.6) was also reduced in the reused catalysts. The trend of carbon loss (Figure 4.14) is faster compared to that of SiO_2@alkyl-PS-SO_3H, while slower than that of the original SiO_2@ester-PS-SO_3H. All the observations further indicated the polymer brush sulfonic acid based on the alkyl initiator had better stability compared to

the material made with the ester initiator. The improved stability of SiO_2@ester-PS-SO_3H_2 compared to SiO_2@ester-PS-SO_3H is suggested to be due to the increased initiator silane coverage on the surface and higher polymer content in the material, giving a denser coverage of protecting polymer around the support.

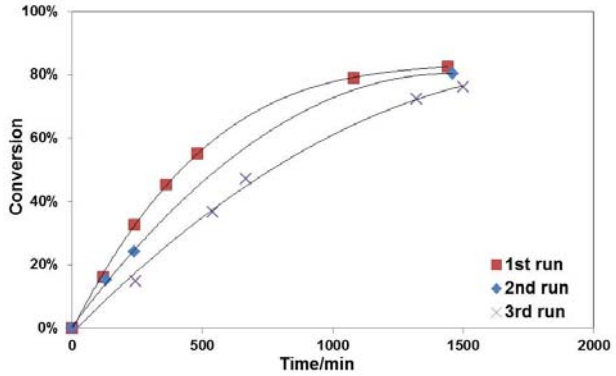

Figure 4.15. Kinetics of SiO_2@ester-PS-SO_3H_2 during recycles. (1.25 mol% catalyst, 60 °C)

Table 4.6. EA of the fresh SiO_2@ester-PS-SO_3H_2 and the recycled catalysts.

Catalysts	C wt%	S wt%	Si wt%	S/C	C mmol/g SiO_2
Fresh	26.43	7.09	15.12	0.100	68.0
After 1st run	28.05	6.70	20.03	0.089	54.5
After 2nd run	23.87	-	21.83	-	42.6

4.4 Conclusions

Silica particles functionalized with poly(styrene sulfonic acid) brushes were prepared via ATRP for use as acid catalysts containing highly accessible acid sites with high loading. The polymer brush catalysts were demonstrated in the hydrolysis of ethyl lactate and shown to be equally active to a homogeneous analogue, p-toluenesulfonic acid, as well as substantially more active than a traditional polymer resin catalyst, Amberlyst 15. A new ATRP initiator designed to be more hydrolytically stable was prepared and the resulting polymer brush catalyst, SiO_2@alkyl-PS-SO_3H, was shown to have improved stability relative to the catalysts made with a traditional ATRP initiator containing an ester group, SiO_2@ester-PS-SO_3H. Nonetheless, the catalysts deactivated slightly over several uses due to polymer loss and desulfonation. The polymer brush architecture is suggested to be a useful approach to preparation of polymeric catalysts with a high loading of accessible active sites and merits further development.

4.5 Acknowledgements

This work was partially supported by the U.S. Department of Energy, Basic Energy Sciences, for financial support through Catalysis Science Grant/Contract No. DE-FG02-03ER15459. The work was also partially supported by the U.S. National Science Foundation (Grant CBET-055354).

4.6 References

(1) Corma, A. *Chem. Rev.* **1995**, *95*, 559.

(2) Busca, G. *Chem. Rev.* **2007**, *107*, 5366.

(3) Wong, W.-L. H., Kam-Piu; Lee, Lawrence Yoon Suk; Lam, Kin-Ming; Zhou, Zhong-Yuan; Chan, Tak Hang; and Wong, K.-Y. *ACS Catalysis* **2011**, *1*, 116.

(4) Melero, J. A.; Iglesias, J.; Morales, G. *Green. Chem.* **2009**, *11*, 1285.

(5) Fang, D. Y., J.; Jiao, C. *ACS Catalysis* **2011**, *1*, 42.

(6) Okuhara, T. *Chem. Rev.* **2002**, *102*, 3641.

(7) Harmer, M. A.; Sun, Q. *Appl. Catal., A* **2001**, *221*, 45.

(8) Melero, J. A.; van Grieken, R.; Morales, G. *Chem. Rev.* **2006**, *106*, 3790.

(9) Barbey, R.; Lavanant, L.; Paripovic, D.; Schuwer, N.; Sugnaux, C.; Tugulu, S.; Klok, H. A. *Chem. Rev.* **2009**, *109*, 5437.

(10) Zhao, B.; Zhu, L. *Macromolecules* **2009**, *42*, 9369.

(11) Gill, C. S.; Venkatasubbaiah, K.; Phan, N. T. S.; Weck, M.; Jones, C. W. *Chem. Eur. J.* **2008**, *14*, 7306.

(12) Zhao, B.; Jiang, X. M.; Li, D. J.; Jiang, X. G.; O'Lenick, T. G.; Li, B.; Li, C. Y. *J. Polym. Sci., Part A: Polym. Chem.* **2008**, *46*, 3438.

(13) Jiang, X. M.; Wang, B. B.; Li, C. Y.; Zhao, B. *J. Polym. Sci., Part A: Polym. Chem.* **2009**, *47*, 2853.

(14) Gill, C. S.; Long, W.; Jones, C. W. *Catal. Lett.* **2009**, *131*, 425.

(15) Costantini, F.; Bula, W. P.; Salvio, R.; Huskens, J.; Gardeniers, H.; Reinhoudt, D. N.; Verboom, W. *J. Am. Chem. Soc.* **2009**, *131*, 1650.

(16) Costantini, F.; Benetti, E. M.; Tiggelaar, R. M.; Gardeniers, H.; Reinhoudt, D. N.; Huskens, J.; Vancso, G. J.; Verboom, W. *Chem. Eur. J.* **2010**, *16*, 12406.

(17) O'Lenick, T. G.; Jiang, X. M.; Zhao, B. *Polymer* **2009**, *50*, 4363.

(18) Li, C. M.; Yang, J.; Wang, P. Y.; Liu, J.; Yang, Q. H. *Micropor. Mesopor. Mat.* **2009**, *123*, 228.

(19) Martin, A.; Morales, G.; Martinez, F.; van Grieken, R.; Cao, L.; Kruk, M. *J. Mater. Chem.* **2010**, *20*, 8026.

(20) Okayasu, T.; Saito, K.; Nishide, H.; Hearn, M. T. W. *Chem. Commun.* **2009**, 4708.

(21) Okayasu, T.; Saito, K.; Nishide, H.; Hearn, M. T. W. *Green. Chem.* **2010**, *12*, 1981.

(22) Drese, J. H.; Choi, S.; Lively, R. P.; Koros, W. J.; Fauth, D. J.; Gray, M. L.; Jones, C. W. *Adv. Funct. Mater.* **2009**, *19*, 3821.

(23) Wilson, B. C.; Jones, C. W. *Macromolecules* **2004**, *37*, 9709.

(24) Zhang, J. Z., Y.; Pan, M.; Feng, X.; Ji, W.; Au, C. T. *ACS Catalysis* **2011**, *1*, 32.

(25) Sun, X. W., Q.; Zhao, W.; Ma, H.; Sakata, K. *Sep. Purif. Technol.* **2006**, *49*, 43.

(26) Sanz, M. T.; Murga, R.; Beltran, S.; Cabezas, J. L.; Coca, J. *Ind. Eng. Chem. Res.* **2002**, *41*, 512.

(27) Sanz, M. T.; Murga, R.; Beltran, S.; Cabezas, J. L.; Coca, J. *Ind. Eng. Chem. Res.* **2004**, *43*, 2049.

(28) Delgado, P.; Sanz, M. T.; Beltran, S. *Chem. Eng. J.* **2007**, *126*, 111.

(29) Feyen, M.; Weidenthaler, C.; Schuth, F.; Lu, A. H. *Chem. Mater.* **2010**, *22*, 2955.

(30) Prucker, O.; Ruhe, J. *Macromolecules* **1998**, *31*, 592.

(31) Rühe, J. K., W. *Polym. Rev.* **2002**, *42*, 91.

(32) Hubbard, A. T. *Encyclopedia of Surface and Colloid Science: Por-Z*; Marcel Dekker, Inc. : New York, 2002; Vol. 4.

(33) Kučera, F. J., J. *Polym. Eng. Sci.* **1998**, *38*, 783.

(34) Xing, R.; Liu, N.; Liu, Y. M.; Wu, H. W.; Jiang, Y. W.; Chen, L.; He, M. Y.; Wu, P. *Adv. Funct. Mater.* **2007**, *17*, 2455.

(35) Liu, F. J.; Meng, X. J.; Zhang, Y. L.; Ren, L. M.; Nawaz, F.; Xiao, F. S. *J. Catal.* **2010**, *271*, 52.

(36) Jones, C. W.; Tsuji, K.; Davis, M. E. *Nature* **1998**, *393*, 52.

(37) Gill, C. S.; Price, B. A.; Jones, C. W. *J. Catal.* **2007**, *251*, 145.

(38) Nasef, M. M.; Saidi, H.; Nor, H. M. *J. Appl. Polym. Sci.* **2000**, *77*, 1877.

(39) Melero, J. A.; Stucky, G. D.; van Grieken, R.; Morales, G. *J. Mater. Chem.* **2002**, *12*, 1664.

(40) Yang, H. Q.; Zhang, G. Y.; Hong, X. L.; Zhu, Y. Y. *Micropor. Mesopor. Mat.* **2004**, *68*, 119.

(41) Riachi, C.; Schuwer, N.; Klok, H. A. *Macromolecules* **2009**, *42*, 8076.

CHAPTER 5

AMINOPOLYMER-SILICA COMPOSITE SUPPORTED PALLADIUM CATALYSTS FOR SELECTIVE HYDROGENATION OF ALKYNES

5.1 Introduction

The selective hydrogenation of carbon – carbon triple bonds to double bonds is a catalytic challenge relevant to commodity chemical production (purification of olefin feeds for polymerization reactions) as well as for synthesis of fine and specialty chemicals.[1] Several approaches have been used to create catalyst that can selectively produce olefins from alkynes, such as manipulating metal nanoparticle dispersion and/or shapes or applying various surface modifiers, e.g. adjusting selectivity as a function of nanoparticle size in the hydrogenation of 1-hexyne.[2] Modifiers can be added during the catalytic reaction or incorporated into the original catalysts.[3] Although the former approach provides better operational flexibility, the latter one facilitates recovery of the potentially expensive modifying agents or ligands as well as simplifies the product purification processes.

The Lindlar catalyst [4] (Pd on $CaCO_3$ poisoned with lead) is a prototypical example of a highly selective supported metal catalyst for liquid phase selective hydrogenation of alkynes created by addition of an appropriate surface modifier. In the Lindlar catalyst, Pb is used as an irreversible dopant to promote the stereo-selective reduction of alkynes to cis-alkenes with accompanying low yields of trans-alkenes and

alkanes. A basic compound such as quinoline is often added during the reaction to slow the subsequent hydrogenation of the desired cis-alkene product to alkanes, thereby achieving a very high selectivity to cis-alkenes, even at high alkynes conversion.[1,5] More recently, several examples of use of new modifiers for the semi-hydrogenation of alkynes in liquid phase have been reported, such as addition of B and Bi to modify Pd for hexyne hydrogenation,[5] and use of poly(ethylenimine) (PEI) modified Pd for partial hydrogenation of various alkynes to alkenes.[6,7]

Applications of metal nanoparticles in catalysis have attracted tremendous attention in recent years because of their high efficiency, unique size/shape dependent catalytic properties, and the ability to catalyze a broad range of chemical reactions.[8–29] Naked, unsupported metal nanoparticles tend to aggregate due to their high surface energy, resulting in decrease of catalytic activity over time associated with nanoparticle sintering. To overcome this problem, polymers or surfactants have been used for preparation of soluble metal nanoparticles with good stability, for example, in the pioneering work of Crooks on dendrimer encapsulated noble metal nanoparticles.[8,30–36] Although polymer stabilized metal nanoparticles show unique catalytic properties in many cases, the inherent difficulties in separation of these soluble catalysts limits their wide applications. Thus, much effort has been directed towards development of new catalytic systems with good activity and selectivity as well as easy separation and recycle, such as mesoporous silica supported Pd nanoparticles,[37] magnetic nanoparticle supported Pd catalysts,[38] and palladium nanoclusters inside cross-linked polymer frameworks.[35,36,39] Polymer composites have also emerged as promising supports for metal nanoparticle catalysts because of the possibility of tuning catalytic properties using the polymeric

functional groups,[40] easy recovery compared to polymer/dendrimer encapsulated catalysts as well as "nano-scale" control of metal clusters.[18]

Herein, a new aminopolymer silica composite supported Pd catalyst is developed for the selective hydrogenation of alkynes in liquid phase. As noted above, the Lindlar catalyst is the most commonly used catalyst in the liquid phase semihydrogenation of alkynes or dienes. However, its outstanding selectivity is associated with use of undesirable lead compounds and other additives in order to achieve good selectivity, and thus it is desirable to develop alternative, greener catalysts for this catalytic transformation. Many alternative palladium catalysts have been explored in the literature for alkyne semihydrogenation, including Pd nanoparticles,[5,41–44] and molecular Pd complexes.[45–53] The various mechanisms leading to the selective hydrogenation of alkynes to alkenes over palladium catalysts are not yet fully understood. However, the traditional interpretation[1] based on metallic palladium indicates that the rates of hydrogenation of alkynes to alkenes, and the subsequent reduction of alkenes to alkanes are normally in the same order of magnitude, and selectivity is essentially governed by thermodynamic effects, more specifically the adsorption strength of different unsaturated C-C bonds on metal active sites. Selectivity would be greatly enhanced by increasing the adsorption of alkynes over alkenes, (Figure 5.1) which could be adjusted in the presence of modifiers.

In this work, an aminopolymer-silica composite is used to play two roles, first to modify the reactivity of the incorporated palladium nanoclusters through the ligating amine sites and second, to promote good dispersion of the nanoparticles. Mesoporous silica supported aminopolymer composites were prepared with both a grafting-to and

grafting-from method. After immobilization of a Pd (II) precursor onto the polymer composite, two reduction methods (H_2 reduction and $NaBH_4$ reduction) were investigated to generate palladium nanoparticles within the polymer composite matrix. The resulting catalysts were evaluated in the selective hydrogenation of alkynes. The catalytic activity, selectivity and recyclability were evaluated in detail to better understand the modification effect of the aminopolymers.

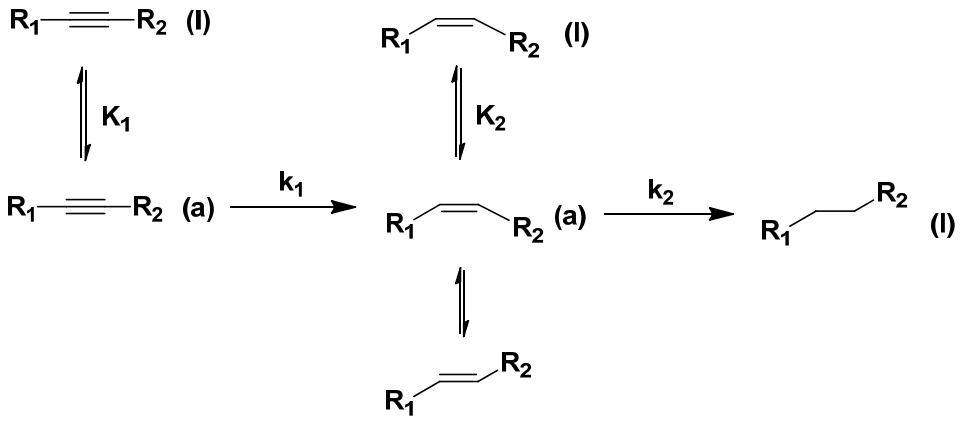

Figure 5.1. Reaction routes of selective hydrogenation of di-substituted alkynes.

5.2 Experimental Section

5.2.1 Chemicals and materials

The following chemicals were commercially available and used as received unless otherwise noted: Pluronic P123 EO-PO-EO triblock copolymer (poly(ethylene glycol)-poly(propylene glycol)-poly(ethylene glycol); $M_n \sim 5{,}800$, Sigma-Aldrich), tetraethylorthosilicate (TEOS, 98%, Sigma-Aldrich), hydrochloric acid (HCl, 37%, EMD), chloropropyl trimethoxysilane (Gelest), poly(ethylenimine) (branched, Sigma-Aldrich, Mn = 10,000, Mw = 25,000), palladium(II) acetate (98%, Sigma-Aldrich),

sodium borohydride (NaBH4, 99%, Sigma-Aldrich), ethanol (reagent grade, BDH), ammonia solution (28%, BDH), toluene (anhydrous, J.T. Baker), methanol (anhydrous, J.T. Baker), 1,4-dioxane (anhydrous, Alfa Aesar), diethylene glycol dibutyl ether (99+%, Acros), diphenyl acetylene (98%, Sigma-Aldrich), ethyl phenylpropiolate (98%, Sigma-Aldrich), 2,5-dimethyl-3-hexyne-2,5-diol (98%, Acros), propargyl benzoate (98%, Sigma-Aldrich)

5.2.2 Characterization

A Netzsch STA 409 was used for thermal gravimetric analysis (TGA) of materials under a mixture of air and nitrogen with a heating rate of 10 °C/min from room temperature to 900 ºC. Surface area, pore volume and pore size distribution were assessed via nitrogen physisorption analysis using a Micromeritics TristarII. Surface area was determined by Brunauer Emmett Teller (BET) method. Pore volume and pore size were calculated via Broekhoff-de Boer method with the Frenkel–Halsey–Hill modification (Bdb-FHH).[54] FT-IR spectra were obtained on a Bruker Vertex 80 optical bench using KBr Pellets. X-ray Photoelectron Spectroscopy (XPS) was performed on a Thermo K-Alpha XPS using Al Kα irradiation with a flood gun. A thin layer of powder was dispersed on the surface of carbon tape, evacuated in a load lock, and then transferred into the analysis chamber (vacuum around 10^{-8} mbar) for measurement. The binding energy of different elements was normalized according to the Si 2p peak at 103.6 eV. Transmission electron microscopy (TEM) measurements were performed on Tecnai F30 with an accelerating voltage of 300 kV. Ultraviolet-visible spectroscopy (UV/Vis) was performed on Agilent 8510 spectrophotometer for solution samples. Diffuse-reflectance UV/Vis on solid samples was measured with an Ocean Optics USB 2000

fiber optic spectrometer using a PTFE diffuse reflectance standard. The reaction conversions were monitored by gas phase chromatography (GC) on a Shimadzu GC-2010 with a FID detector and a SHRX5 column. Elemental analyses were measured by Columbia Analytical Services (Tucson, AZ) and Atlantic Microlab (Atlanta, GA).

5.2.3 Preparation of aminopolymer-silica composites

SBA-15 synthesis

The mesoporous silica SBA-15 was synthesized according to published procedures[55,56] and the reagents were scaled accordingly. The polymer template (Pluronic P123, 4 g) was dispersed in HCl (120 ml) and DI H_2O (636 ml). After the polymer was dissolved completely, TEOS (46.26 g) was added and the solution stirred for 20 h at 40 °C. The solution was heated to 100 °C and maintained at this temperature for 24 h without stirring. At the end of synthesis, the mixture was quenched with DI H_2O, filtered and washed repeatedly with DI H_2O. The recovered solid was dried in the oven at 80 °C overnight, and then calcined at 500 °C for 6 h.

MCF synthesis

Siliceous mesocellular foam (MCF) was synthesized according to a reported procedure with slight modifications.[57] The polymer template (Pluronic P123, 16 g) was dissolved in a mixture of HCl (47.4 g) and DI H_2O (260 g). The solution was heated to 40 °C, and then 1,3,5 – trimethyl benzene (16 g) was added. After 2 h mixing, TEOS (34.6 g) was added. The mixture was stirred for 5 min and then maintained quiescently at 40 °C for 20 h. NH_4F (184 mg) in 20 ml DI H_2O was added as mineralization agent, and the

solution was swirled briefly before aging at 100 °C for 24 h. The resulting solid was recovered by filtration, washed repeatedly with DI H2O, dried and calcined at 550 °C for 6 h.

Preparation of HAS

Aziridine was synthesized and purified according to reported methods.[58,59] (Caution: Aziridine is a carcinogen hazard. Please only handle it in a ventilated fume hood and wear proper personal protection equipment.) Hyperbranched aminosilica (HAS) was synthesized following published procedures.[59] SBA-15 (1 g, dried under vacuum at 150 °C overnight before use) was dispersed into 50 ml toluene, and the mixture was stirred for 1 h. Aziridine (2 g) was added into the solution under stirring and acetic acid (4 drops) was added to catalyze the polymerization. The solution was stirred at room temperature for 24 h in a capped pressure vessel. The resulting material was recovered, washed repeatedly with toluene and methanol, and dried under vacuum around 65 °C overnight.

Preparation of SiO_2-gt-PEI

An aminopolymer silica composite was also prepared with a grafting-to method following published procedures with some modifications.[60] Silica (2 g, dried under vacuum at 150 °C overnight before use) was first dispersed into dry toluene (100 ml). Chloropropyl trimethoxysilane (3.7 g) was added into the slurry slowly and the mixture was heated to 150 °C for 24 h. The solid was recovered by filtration through filter paper and washed with copious amounts of toluene, petroleum ether, methanol and diethyl ether. Finally the white powder was dried under vacuum at 100 °C overnight.

PEI (6 g) was dissolved completely in DI H_2O (6 g) and ethanol (100 ml) and then the solution was degassed with argon for 30 min. The silica supported propyl chloride material was added into the solution under argon and stirring was continued at room temperature for 30 min. The mixture was stirred at 90°C for 24 hrs. The resulting material was recovered, washed with DI H_2O, ammonia solution, methanol and dried under vacuum around 65 °C overnight.

5.2.4 Preparation of supported palladium catalysts

The aminopolymer silica composite (1 g) was dispersed into anhydrous methanol (47 ml) under argon with stirring for about one hour. Then $Pd(OAc)_2$ (23.5 mg) was transferred into the solution under argon and the mixture was stirred at room temperature for 24 h. The resulting slightly yellow powder was recovered by filtration, washed three times with methanol and dried under vacuum at room temperature. The resulting material was later reduced via two methods, (i) the H_2 reduction method or (ii) the $NaBH_4$ reduction method.

H_2 reduction

Pd(II)-HAS (500 mg) was dispersed in anhydrous methanol (24 ml) under inert gas with stirring for about 1 h. H_2 was introduced to the reaction system via a needle to the solution. The hydrogen pressure is 0.1 MPa and the flow rate was kept constant. The mixture was stirred under hydrogen for 64 h. At end of the reaction, methanol was removed under vacuum via a Schlenk line. The resulting powder was transferred into a glovebox, washed with anhydrous methanol and filtered inside the glovebox. The

recovered catalyst was dried under vacuum at room temperature and stored inside the glovebox for further use.

$NaBH_4$ reduction

DI H_2O (75 ml) was degassed with Ar for about 3 h before use. Pd(II)-HAS (800 mg) was dispersed into DI H_2O (65 ml) with stirring for 30 min. After adding a freshly prepared $NaBH_4$ solution (284 mg $NaBH_4$ in 10 ml DI H_2O), the color of the mixture was rapidly darkened. The solution was stirred for additional 2 h and the solids were recovered via filtration. The resulting catalyst was washed repeatedly with DI H_2O and methanol, dried under vacuum and stored under ambient conditions for further use. Other aminopolymer silica supported Pd catalysts were prepared following similar procedures.

5.2.5 Selective hydrogenation of alkynes

Catalytic reactions were performed in a three neck flask at room temperature and 0.1 MPa H_2. Hydrogen at a constant flow rate was introduced into the reactor through one side arm of the flask and another side arm was connected to a condenser with -15 °C coolant circulating through it to prevent evaporation of solvents. In a typical reaction with Pd-HAS (prepared by H_2 reduction), a small amount of catalyst (22 mg, 0.4 mol% Pd relative to the reactant) was transferred into the reactor inside a glovebox. Before reaction, the flask with the catalyst was purged with argon for about 20 min, and then H_2 for about 10 min. Substrate (0.5 mmol) was dissolved into anhydrous methanol (0.5 ml) and anhydrous1,4-dioxane (0.5 ml) with diethylene glycol dibutyl ether (50 ul) as the internal standard. The reactant solution was degassed first with inert gas and then transferred into the reactor via a syringe to start the reaction. A small aliquot of sample

was withdrawn at specific times, diluted and analyzed via GC-FID to monitor the course of the reaction.

For the catalysts prepared with $NaBH_4$ reduction, a much higher reaction rate was observed. To get reliable kinetic data, the catalyst amount was reduced to extend the reaction time for enough sampling points. Similarly, a small amount of catalyst (0.1 mol% Pd loading) was transferred into the flask, and the system was purged with argon for about 20 min, and then H_2 for about 10 min. Next, 1.5 ml anhydrous methanol was added to disperse the catalyst, and then the solution was treated under H_2 for 24.5 h (room temperature, 1 atm H_2 pressure). Reactant (1.5 mmol) was dissolved into anhydrous1,4-dioxane (1.5 ml) with diethylene glycol dibutyl ether (150 ul) under inert gas, and then the solution was transferred into the flask to start the reaction. At the end of reaction, the catalysts were recovered by filtration, washed with copious amount of methanol, and then dried under vacuum at room temperature. The recovered power was reused or kept for other characterization.

5.2.6 Catalyst regeneration

A small amount of recovered catalyst (Pd-SBA-gt-PEI-r, 45 mg) was transferred into a flask and the system was purged with Ar for 10 min. Freshly prepared $NaBH_4$ solution (0.1 M, 4.2 ml) was transferred into the flask quickly and the solution was stirred for 1 h. The material was recovered, washed with DI H_2O and MeOH, and dried under vacuum at room temperature.

5.3 Results and Discussions

5.3.1 Preparation and characterization of aminopolymer-silica composites

Aminopolymer-silica composites were prepared following two different methods: grafting-to and grafting-from approaches. (Figure 5.2) Mesoporous silica SBA-15 and MCF were synthesized and used as supports for preparation of the polymer composites. For the grafting-from method, silanol initiated *in-situ* ring-opening polymerization of aziridine[59,61] was performed on SBA-15 for synthesis of HAS. For the grafting-to method,[60,62] propyl chloride moieties were immobilized onto the surface of silica via silane chemistry and then branched poly(ethylenimine) (PEI) with known structure and molecular weight was grafted to the surface via nucleophilic substitution of Cl with amino groups of PEI.

The polymer content of the aminopolymer-silica composites was estimated by TGA (Table 5.1). HAS showed 22 wt% of polymer loading. For comparative analysis, SiO_2-gt-PEI materials with similar polymer contents were prepared via the grafting-to method. According to elemental analysis, a very small amount of Cl remained in the resulting materials, indicating the majority of the propyl chloride functional groups were reacted with PEI in the second step, and every polymer chain was anchored to multiple sites on the silica surface. In FT-IR spectra of the materials (Figure 5.3), the peaks around 2930 cm^{-1} were assigned to aliphatic C-H stretches, and the N-H vibration was clearly visible at 1580 and 1645 cm^{-1}. The peak at 1483 cm^{-1} was assigned to C-H vibrations,[63] which further confirmed the successful incorporation of the aminopolymer into the materials. The decrease of surface area, pore size and pore volume with the increasing

organic loading was observed in the nitrogen adsorption analysis (Table 5.2), confirming that the aminopolymer was constructed into the pores of mesoporous silica.

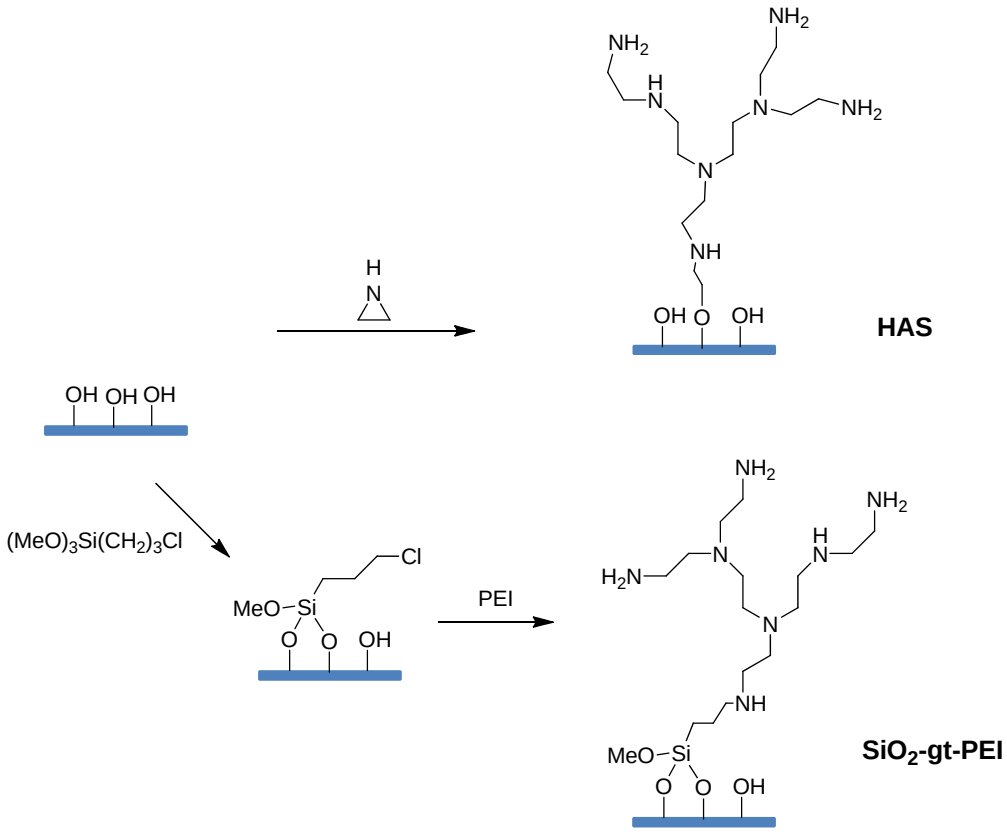

Figure 5.2. Preparation of aminopolymer-silica composites, HAS and SiO_2-gt-PEI.

Table 5.1. Compositions of aminopolymer-silica composites.

Materials	Organic loading [a] (w.t. %)	Polymer content [b]	Cl content (w.t. %)
HAS	21.7	21.7%	
SBA-Cl	11.1		4.25[c]
SBA-gt-PEI	27.9	24.2%	0.36[d]
MCF-Cl	12.3		4.71[c]
MCF-gt-PEI	30.8	27.0%	0.29[d]

[a] Determined by TGA, organic loading = w.t. % of organic groups/ (w.t. % of organic groups + w.t. % of silica).

[b] Polymer content = 1/ [w.t.% of silica / (w.t.% of organic groups – w.t.% of propyl group) +1].

[c] Calculated from the organic loading.

[d] Determined by elemental analysis.

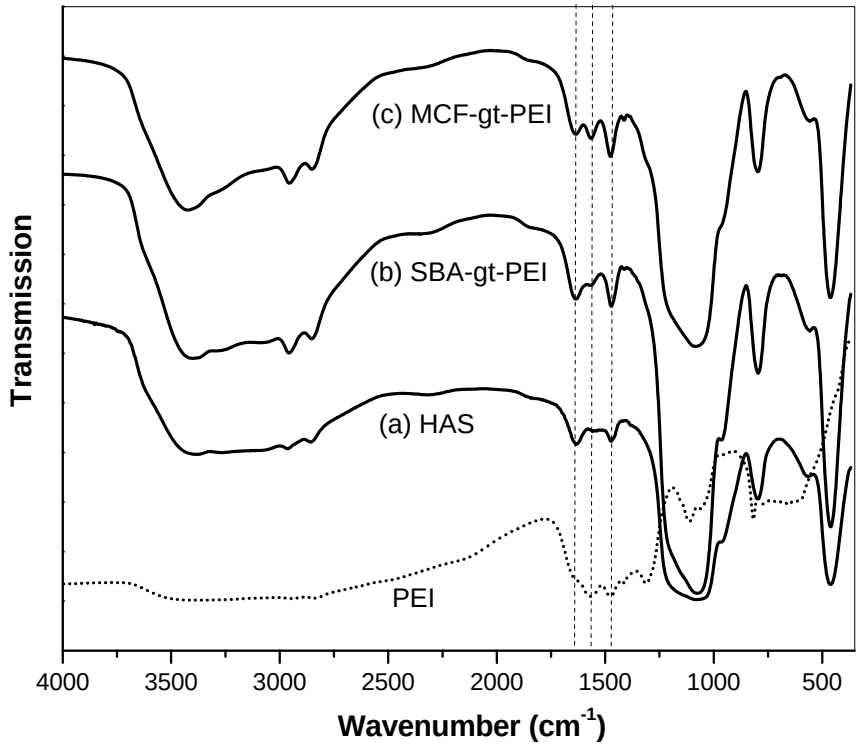

Figure 5.3. FT-IR spectra of HAS (a); SBA-gt-PEI (b); MCF-gt-PEI (c) and commercial PEI.

Table 5.2. Physical characteristics of the aminopolymer-silica composites.

Materials	S_{BET} (m^2/g)	Pore size (nm)	Pore volume (cm^3/g)
SBA-15	855	6.3	0.91
HAS	319	5.8	0.55
SBA-Cl	523	5.8	0.69
SBA-gt-PEI	277	5.1	0.44
MCF	693	38 (17)	2.6
MCF-Cl	477	39 (17)	2.1
MCF-gt-PEI	267	33 (13)	1.1

5.3.2 Preparation and catalytic performance of Pd-HAS

HAS was metallated with palladium acetate in MeOH for 24 h to introduce Pd(II) ions to the nitrogen ligands, and then the recovered material was washed with copious amounts of methanol to remove free or weakly bonded Pd(II) ions (Figure 5.4). Pd(II)-HAS was further reduced with hydrogen in MeOH (room temperature, 1 atm) to yield the resulting catalyst Pd-HAS (H_2 reduction) with 0.95 wt% Pd content.

Pd-HAS (H_2 reduction) was tested in the liquid phase selective hydrogenation of diphenylacetylene. The reaction proceeded smoothly at room temperature and 1 atm hydrogen pressure to achieve 97% conversion after 6 h in conjunction with 91% selectivity to cis-stilbene (Table 5.3, entry 1). To evaluate the applicable scope of the catalyst, it was also applied for the partial hydrogenation of three other substrates (Table 5.3), yielding good selectivity in the conversion of alkynes to alkenes in all cases,

especially for the aliphatic substituted internal alkyne - 2,5-dimethyl-3-hexyne-2,5-diol (Table 5.3, entry 3).

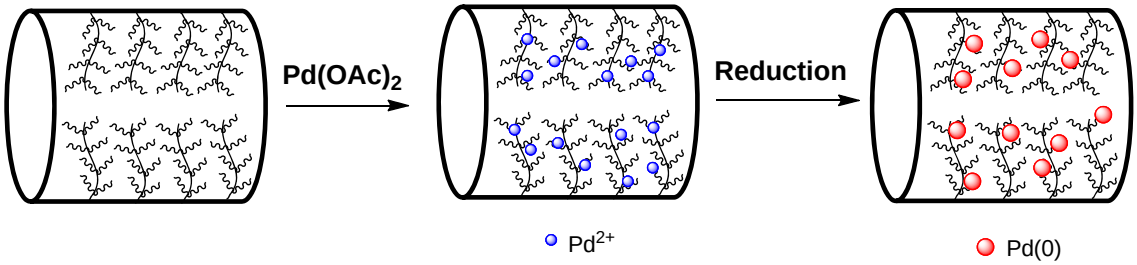

Figure 5.4. Preparation of aminopolymer-silica supported Pd catalysts.

Table 5.3. Catalytic performance of the Pd-HAS (H_2 reduction) catalyst with different substrates.

Substrates	Time/h	Conv. (%)	Selectivity [a]
Ph—≡—Ph	2	32	
	6	97	91:2:7
Ph—≡—CO_2Et	4	35	
	10	97	90:2:8
HO OH	2	36	
	6	94	97: 2:1 [b]
O O Ph	0.5	36	
	1.5	97	88:12

[a] Determined by ^{1}H NMR; for internal alkynes, selectivity = cis-alkene: trans-alkene: alkane; for terminal alkynes, selectivity = alkene: alkane.

[b] The alkane content was determined by GC-FID since the corresponding peak is overlapping with the peaks of the standard in ^{1}H NMR.

However the activity of Pd-HAS (H_2 reduction) was still relatively slower compared to other supported palladium catalysts used in similar selective hydrogenation reactions in literature (Table 5.4, vide infra).[64] After extensive characterization, the compiled results revealed that the majority of the Pd species in the fresh Pd-HAS (H_2 reduction) catalyst still existed as Pd(II)-N complexes. Under similar conditions, homogeneous Pd(II)-PEI could be readily reduced to Pd(0)-PEI,[43,65] as evidenced by the color change from yellow to black as well as the disappearance of Pd(II)-N peak at 300 nm in the UV/Vis spectra (Figure 5.5). In the UV/Vis spectra of soluble Pd(II)-loaded PEI (Figure 5.5), the peak at 400 nm is assigned to the d-d transition of Pd(II), which is shifted to 300 nm after coordination of Pd(II) to the N ligands in PEI. After reduction with H_2, the presence of a broad Plasmon absorbance and the shift in the baseline indicates the formation of Pd nanoparticles.[38] But as noted above, this mild reduction method is not efficient in the case of the insoluble Pd-HAS materials. Even after extended reduction with hydrogen at room temperature, the majority of Pd(II) was still not effectively converted to Pd nanoparticles (Figure 5.6) and only a very small amount of Pd(0) nanoparticles was formed, since the intensity of the peak at 400 nm did not change much after hydrogenation reduction. It is probably due to the limited mobility of the polymer composite anchored Pd(II) ions, hampering nucleation and nanoparticle growth.

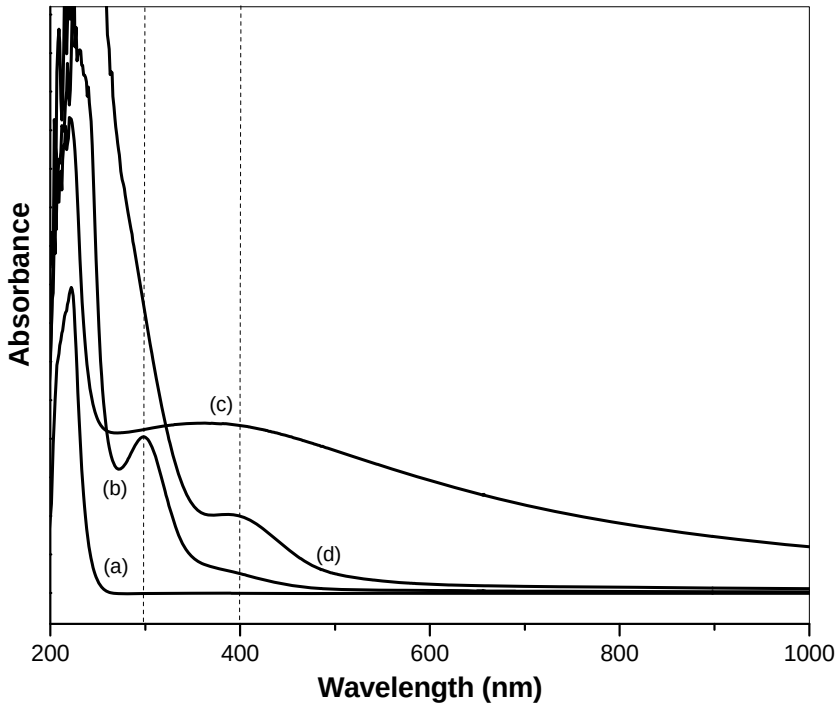

Figure 5.5. Solution UV-Vis of PEI (a); Pd(II)-PEI (b); Pd(0)-PEI (c); $Pd(OAc)_2$ (d).

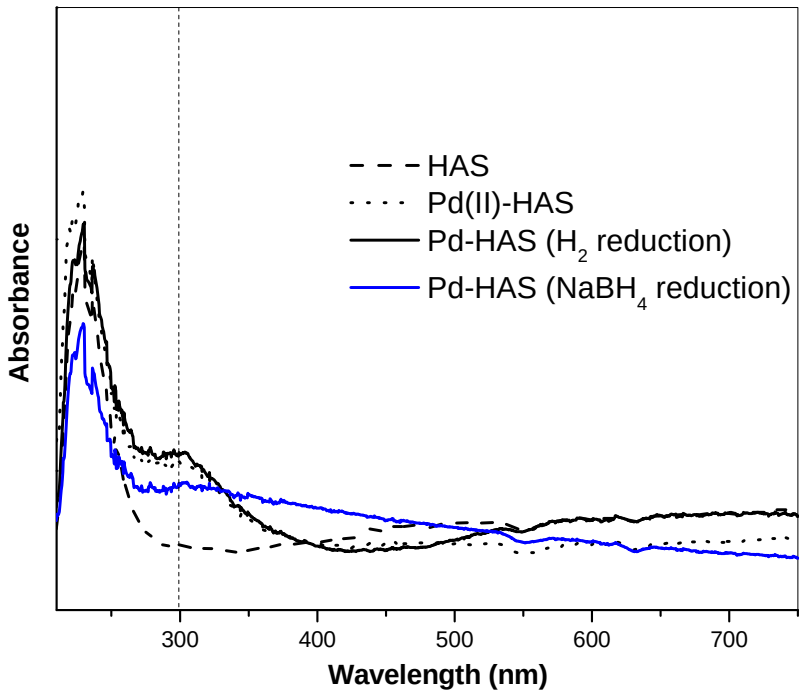

Figure 5.6. Solid UV-Vis of HAS (a); Pd(II)-HAS (b); Pd-HAS (H_2 reduction) (c); Pd-HAS ($NaBH_4$ reduction) (d).

$NaBH_4$ reduction was used as an alternative method for preparation of HAS supported Pd nanoparticles. The decreased intensity of the peak at 300 nm (Pd(II) ligated to amines), the appearance of a broad absorbance band as well as the grey color of the recovered catalysts indicated the formation of palladium nanoparticles (Figure 5.6). The material was further characterized with TEM and XPS. In the TEM image (Figure 5.7c), nanoparticles ~ 2 nm in diameter with a narrow particle distribution were clearly observed in the polymer composite. The Pd $3d_{5/2}$ binding energy (BE) at 336 eV (Table 5.6) in the XPS spectrum was assigned to metallic Pd, which is consistent with the literature.[66] The peak at 338.9 eV corresponding to Pd(II) was also observed in the XPS spectrum of Pd-HAS, which may be attributed to the oxidized palladium on the surface of the nanoparticle after exposure to air.

The Pd-HAS catalyst prepared with $NaBH_4$ reduction displayed similar selectivity (Table 5.4) but substantially higher activity than the Pd-HAS (H_2 reduction) catalyst, suggesting the efficient formation of small palladium nanoparticles with this reduction method. This observation also suggests that the activity in these catalysts is largely associated with Pd(0) nanoparticles, rather than molecular Pd(II) species ligated to the aminopolymer. The activity of Pd-HAS ($NaBH_4$ reduction) is higher or comparable to other efficient catalysts used for semi- hydrogenation of alkynes in the literature (Table 5.4). Although the soluble Pd-PEI [6,65] showed the best alkene selectivity as well as stereoselectivity (Z/E) in the literature, similar to or even better than Lindlar catalyst, its activity is very low, perhaps due to the large palladium particle size formed in Pd-PEI.

Table 5.4. Catalytic performance of aminopolymer-silica supported Pd catalysts and comparison to catalysts described in the literature.

Catalysts	Time/h	Conv. (%)	R [a] (h^{-1})	Selectivity [b]
Pd-HAS (H_2 reduction)	6	98	40	88:2:10
Pd-HAS ($NaBH_4$ reduction)	0.34	93	2389	91:4:5
Pd-SBA-gt-PEI	0.45	98	2170	90:4:6
Pd-MCF-gt-PEI	0.42	> 99	2387	91:4:5
Pd(0.7%) /SiO_2 [c]	1.0	96	819	75:2:23
Pd(3%)/C-amine [d]	0.5	99	1400	78:6:16
Lindlar catalyst-quinoline [e]	-	>99	-	93:2:5
Lindlar catalyst [f]	0.17	>99	1555	-
Pd/PEI [g]	12	>99	10	95:1:4

[a] R = moles of consumed reactant/ (mol of Pd * time), the total amount of Pd was used and dispersion of nanoparticle was not taken into consideration for the calculation.

[b] Determined by GC-FID after calibration. Selectivity = cis-alkene: trans-alkene: alkane

[c] Reaction performed in toluene, room temperature, under 1 atm H_2 flow, products determined by GC[67]

[d] Reaction performed in ethyl acetate, ethyl phenyl propiolate as the substrate, room temperature, under an H_2 balloon, 10 mol% octylamine added, products determined by GC and ^{1}H NMR[64]

[e] Reaction performed in methanol[68]

[f] Reaction performed in toluene, 25 ºC, 1-hexyne as the substrate, under 1 atm H_2 pressure, products determined by GC[5]

[g] Reaction performed in MeOH:dioxane =1:1, room temperature, under an H_2 balloon, products determined by ^{1}H NMR[6,65]

5.3.3 Catalytic performance of Pd-SiO_2-gt-PEI

For HAS materials prepared via *in-situ* polymerization of aziridine, the molecular weight of the resulting aminopolymer is normally several thousand Daltons.[69,70] Larger polymer molecular weights have thus far not been reported for HAS materials.[70] To allow for better control of the polymer structure within the composite support, we also investigated support materials via the "grafting to" approach. Specifically, pre-synthesized PEI with a known structure and molecular weight was used (branched, as in HAS materials, Mw ~ 25000, Mn ~ 10000, d = 4.6 nm by DLS) as the polymer component, taking into account two considerations: (1) the polymer size would fit into the pores of mesoporous silica used in this work (SBA-15 and MCF) and (2) the polymer should provide protection and encapsulation of the Pd nanoparticle without preventing access to the substrates. Given these constraints, the above polymer was chosen. Two types of mesoporous silica, SBA-15 and MCF, were used for preparation of SiO_2-gt-PEI. SBA-15 is highly ordered mesoporous silica composed of one dimensional cylindrical channels and is the same support used to create HAS materials. MCF consists of large hollow spherical cells and three-dimensional interconnecting cylindrical windows, providing enhanced pore connectivity and pore volume for loading of polymer-encapsulated Pd(0) nanoparticles.

The Pd(0) nanoparticles in Pd-SBA-gt-PEI and Pd-MCF-gt-PEI were synthesized in the same manner as the Pd-HAS ($NaBH_4$ reduction) material. The composition of the catalyst was determined by elemental analysis. For comparison, the catalysts were prepared with similar palladium contents and Pd:N ratios (Table 5.5). Palladium nanoparticles ~ 2nm in diameter with good dispersion in the 1D channels of SBA-15

were clearly observed in the HRTEM images of Pd-SBA-gt-PEI (Figure 5.7a). Similarly, the TEM images of Pd-MCF-gt-PEI showed well dispersed Pd nanoparticles (~2 nm) inside the large cells of the porous material (Figure 5.7b). The catalysts were also characterized with XPS to assess the oxidation state of the palladium. The binding energies of the Pd(0) species ($3d_{5/2}$) in Pd-SBA-gt-PEI and Pd-MCF-gt-PEI were 335.7 eV and 336 eV, respectively (Table 5.6), which is close to that of the Pd-HAS. The Pd(0):Pd(II) ratios were also consistent in the various catalysts, as would be expected if the ratio is associated with surface oxide vs. bulk metal species in materials having similar-sized nanoparticles.

Table 5.5. Composition of the catalysts. (determined by elemental analysis)

Catalysts	Pd (w.t.%)	C (w.t. %)	N (w.t. %)	Pd:N
Pd-HAS ($NaBH_4$ reduction)	0.7	9.8	5.3	0.017
Pd-SBA-gt-PEI	1.1	14.7	6.6	0.022
Pd-MCF-gt-PEI	0.94	17.2	7.9	0.016

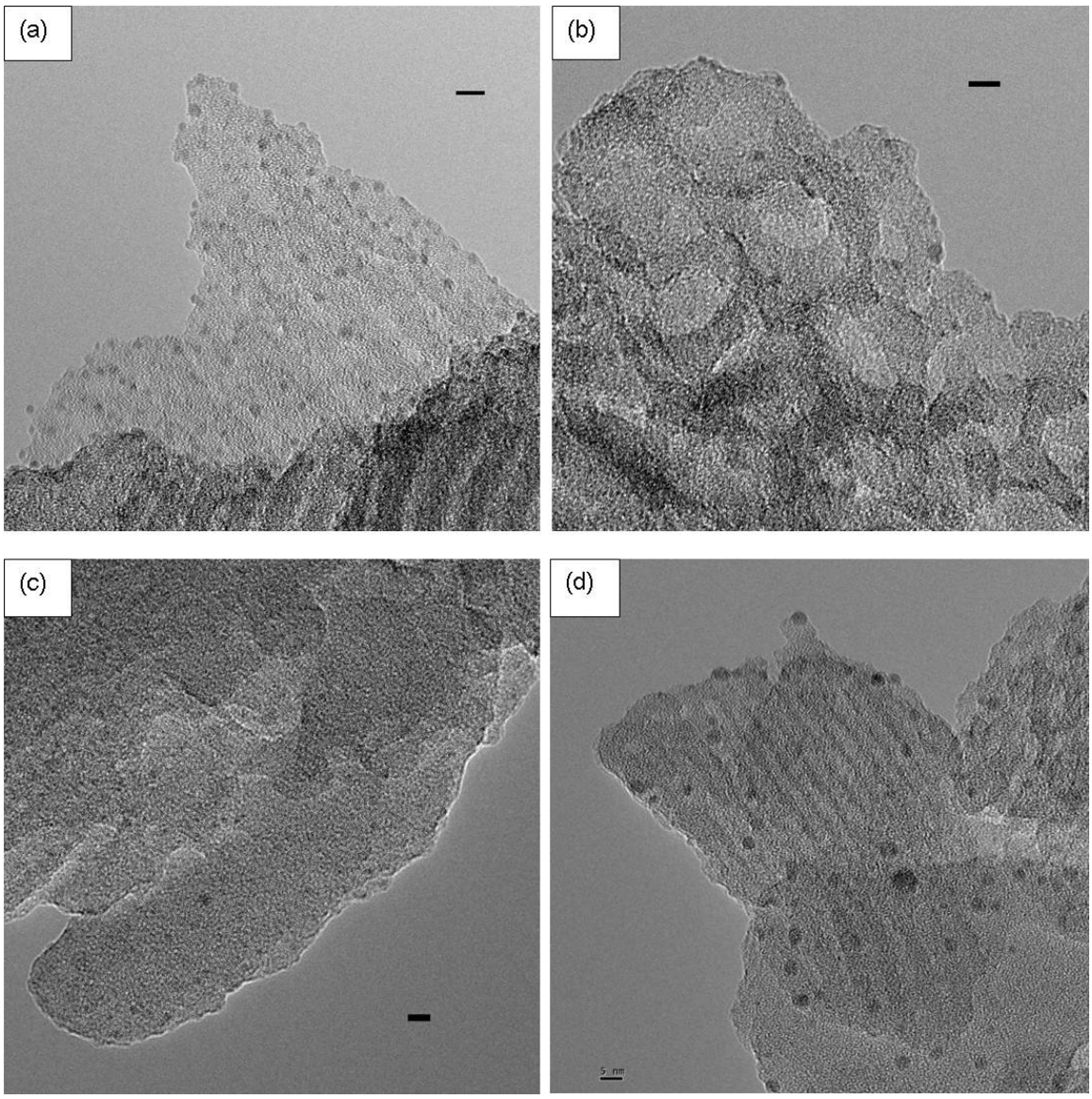

Figure 5.7. TEM of Pd-SBA-gt-PEI (a); Pd-MCF-gt-PEI (b); Pd-HAS ($NaBH_4$ reduction) (c); Pd-SBA-gt-PEI (used) (d). scale bar is 5 nm.

Table 5.6. Binding energies (BE) of different peaks in XPS spectra of aminopolymer-silica supported catalysts. [a]

Catalysts	Pd $3d_{5/2}$ (eV)		Pd(0):Pd(II)	C 1s [b] (eV)	N 1s (eV)
	Pd(0)	Pd(II)			
Pd-HAS ($NaBH_4$ reduction)	336.2	338.9	1:0.70	286.7	400.5
Pd-SBA-gt-PEI	335.7	338.4	1:0.76	286.2	399.8
Pd-MCF-gt-PEI	336.0	338.8	1:0.70		
Pd on SBA-15	335.5				
Pd/C [c]	335.6				
$Pd(OAc)_2$		337.9			
PdO [c]		338.1			
Bis(dibenzylideneacetone Palladium(0) [c]	337.1				

[a] The BE of different elements was corrected according to the Si 2p peak at 103.6 eV.

[b] The BE of C1s of the aminopolymer is higher than that of adventitious C (284.8 eV), which is also consistent with the reported value 286.35 eV.[71]

[c] The BE of Pd for Pd/C, PdO and bis(dibenzylideneacetone) palladium(0) is reproduced here from reference[66] for comparison.

Pd-HAS ($NaBH_4$ reduction), Pd-SBA-gt-PEI and Pd-MCF-gt-PEI were tested in the selective hydrogenation of diphenylacetylene under the same conditions. Reaction profiles were plotted to monitor the change of reactant and product concentrations over time. Figure 5.8 shows the reaction profile of diphenylacetylene conversion over Pd-HAS ($NaBH_4$ reduction). The yields of trans-stilbene and bibenzyl were very low until nearly complete conversion of diphenylacetylene was achieved in the first hydrogenation step. After the complete consumption of diphenylacetylene, cis-stilbene was quickly

transformed into bibenzyl, while the isomerization rate to trans-stilbene was very low. For Pd-SBA-gt-PEI (Figure 5.9), before the consumption of diphenylacetylene, the hydrogenation rate of diphenylacetylene and isomerization rate of cis-stilbene were close to those observed over Pd-HAS ($NaBH_4$ reduction). However, the subsequent hydrogenation to bibenzyl was suppressed compared to Pd-HAS ($NaBH_4$ reduction). Similar catalytic performance was observed in Pd-MCF-gt-PEI (Figure 5.10), except in this case the rate of the second hydrogenation step to produce alkane was even slower than that over Pd-SBA-gt-PEI, making this material the most selective catalyst evaluated here.

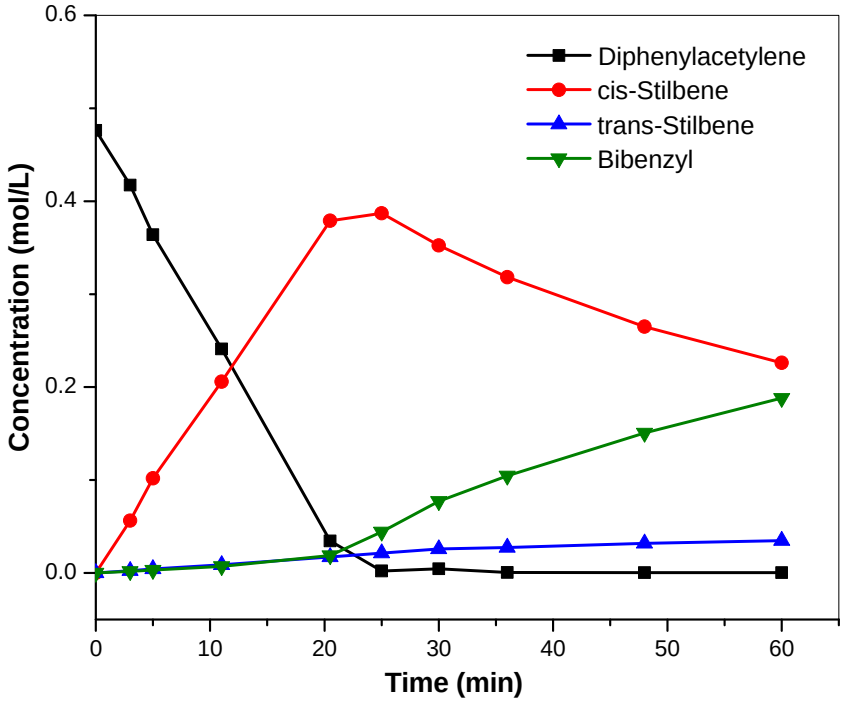

Figure 5.8. Reaction profiles of Pd-HAS ($NaBH_4$ reduction). (selective hydrogenation of diphenylacetylene in the mixture of MeOH and dioxane (v:v = 1:1), 0.1 mo% Pd, room temperature, 1 atm H_2)

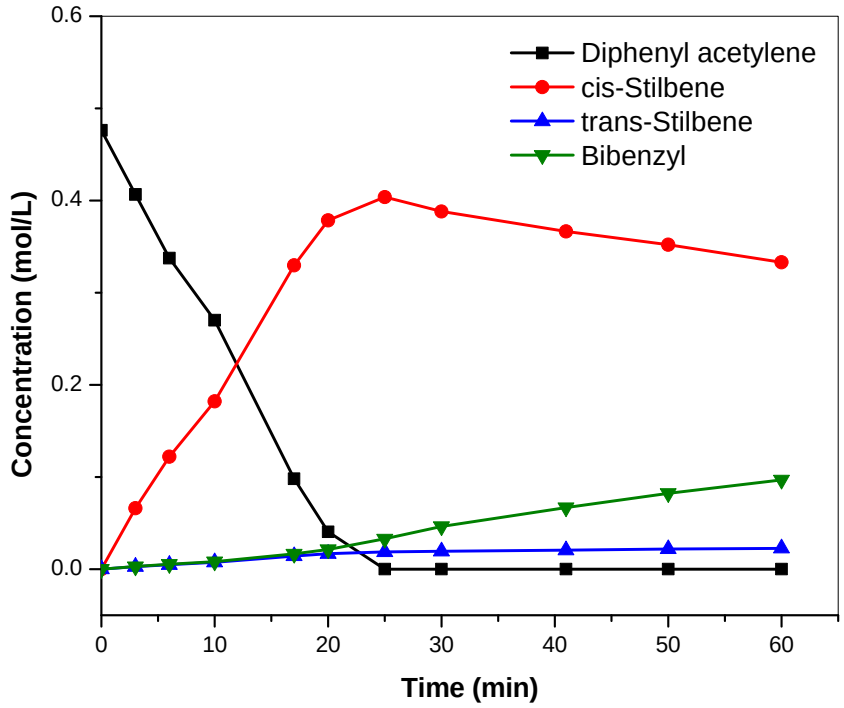

Figure 5.9. Reaction profiles of Pd-SBA-gt-PEI. (selective hydrogenation of diphenylacetylene in the mixture of MeOH and dioxane (v:v = 1:1), 0.1 mo% Pd, room temperature, 1 atm H_2)

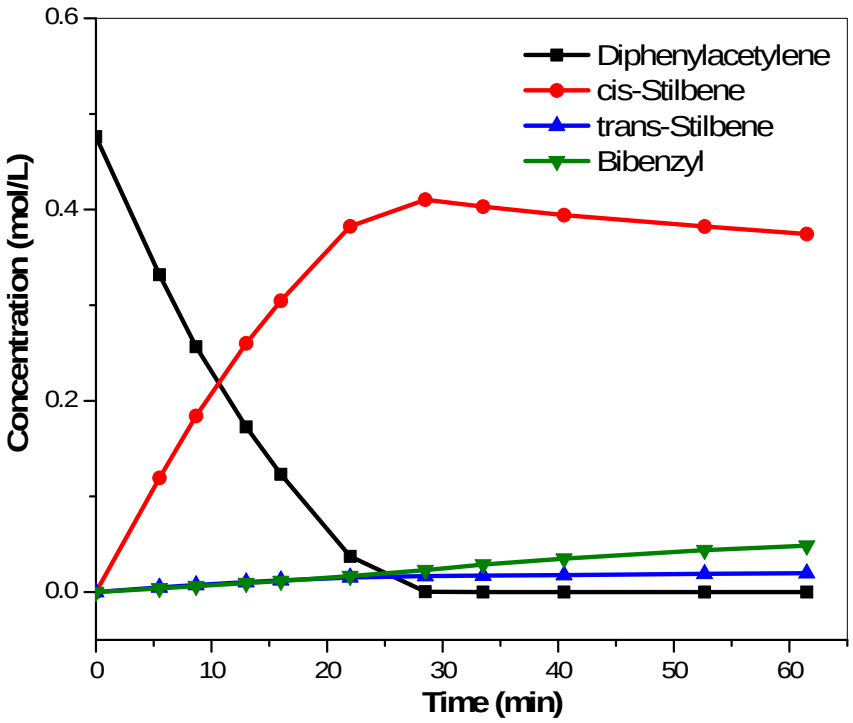

Figure 5.10. Reaction profiles of Pd-MCF-gt-PEI. (selective hydrogenation of diphenylacetylene in the mixture of MeOH and dioxane (v:v = 1:1), 0.1 mo% Pd, room temperature, 1 atm H_2)

The hydrogenation rate of diphenylacetylene (R_Y), hydrogenation rate of cis-stilbene (R_E), and selectivity at different conversions are summarized in Table 5.7. All three catalysts displayed a similar diphenylacetylene hydrogenation rate, R_Y, implying that similar types and amounts of surface palladium atoms were formed in these catalysts, and also consistent with the fact that similar palladium particle sizes were observed in TEM images. A very interesting observation is that the R_E of Pd-HAS ($NaBH_4$ reduction) is much higher than that of Pd-SBA-gt-PEI and Pd-MCF-gt-PEI. The MCF-supported catalyst, Pd-MCF-gt-PEI, showed the lowest cis-stilbene hydrogenation rate, giving a precipitous drop in the overall hydrogenation rate after complete consumption of the alkyne. According to the mechanism proposed by Molnar,[1] the high selectivity towards alkene production is due to the stronger adsorption of the alkyne on the palladium surface compared to the alkene (thermodynamic control), rather than a difference in the intrinsic kinetic constants of alkyne vs. olefin hydrogenation. For example, in the Lindlar catalyst, quinoline or other amines and sulfur compounds are added to the reaction mixture to compete for the palladium active sites with intermediate alkenes, thus hindering over-hydrogenation and increasing the selectivity. A recent paper by Kiwi-Minsker et al. offered a similar explanation for the selectivity of nitrogen modified Pd catalysts.[41] By modeling the experimental kinetic curves of the selective hydrogenation of 1-hexyne, they calculated the adsorption constants of the reactants and products in the reaction and showed the expected trend: K(alkyne) > K(nitrogen compound) >> K(alkene).

This mechanism is consistent with the experimental results in this work. In the first hydrogenation step, diphenylacetylene adsorbs on the surface of Pd nanoparticle and is transformed into alkenes without much effect of the aminopolymer due to the high

adsorption constant of alkyne, leading to similar values in R_Y in the three catalysts. However, when most of the diphenylacetylene was consumed, the aminopolymer competes with alkenes to re-adsorb onto the palladium surface, thus blocking the active sites and reducing the subsequent hydrogenation rate. The branched PEI used in "grafting to" catalysts could cover and passivate the palladium nanoparticle more effectively than the Pd-HAS ($NaBH_4$ reduction) catalyst, where the polymer was of lower molecular weight, such that over-hydrogenation was further suppressed. The lower R_E of Pd-MCF-gt-PEI than that of Pd-SBA-gt-PEI may be speculated to be because the immobilized aminopolymer may be able to swell and stretch out in a larger pore space associated with the large cell and window size in MCF, thus leading to a better coverage of the palladium nanoparticle surface.

Table 5.7. Catalytic performance of aminopolymer-silica composite supported Pd catalysts. [a]

Catalysts	R_Y [b] (h^{-1})	R_E [c] (h^{-1})	R_E/R_Y	Conv.(%)	Selectivity [d]
Pd-HAS ($NaBH_4$ reduction)	3027± 327	794 ± 13	3.8	50	93:4:3
				93	91:4:5
Pd-SBA-gt-PEI	2598 ± 96	230 ± 16	11.2	50	92:4:4
				98	90:4:6
Pd-MCF-gt-PEI	3216 ± 12	130 ± 5	24.7	55	93:4:3
				99	92:3:5

[a] Reaction conditions: selective hydrogenation of diphenylacetylene in the mixture of MeOH and dioxane (v:v = 1:1), 0.1 mol% Pd loading, room temperature, 1 atm H_2 pressure.

[b] R_Y = mols of consumed diphenylacetylene / (mol of Pd * time), R_Y calculated from the slop of the initial portion (conversion <50%) of the conversion-time plot. Each experiment was repeated twice and the ± value represents the difference between the average and the data.

[c] R_E = mols of consumed cis-stilbene / (mol of Pd * time)

[d] Determined by GC-FID after calibration. Selectivity = cis-alkene: trans-alkene: alkane

5.3.4 Investigation on recoverability and recyclability

Leaching of palladium active species from the catalyst support is one of the most common reasons for deactivation of supported palladium catalysts in liquid phase reactions. The Pd-SBA-gt-PEI was recovered after use and evaluated by elemental analysis. Table 5.8 shows that the palladium content of the reused catalyst was close to that of the fresh one, as well as the Pd:N ratios, indicating no or negligible palladium leaching occurred and the aminopolymer-silica composite is a stable support for this catalytic system. The recovered catalyst after selective hydrogenation was characterized by HRTEM. It can clearly be observed that the size of palladium nanoparticles was overall similar to that of the fresh Pd-SBA-gt-PEI, although there appears to be a moderate increase in size (Figure 5.7d). The recovered Pd-SBA-gt-PEI was reused for the selective hydrogenation of diphenylacetylene, displaying a slightly lower activity and similar selectivity compared to the fresh catalyst (Table 5.9). After treatment of the used catalyst with 0.1 M $NaBH_4$, the activity of the catalysts was fully regenerated. The reaction profiles of Pd-SBA-gt-PEI (regenerated) displayed similar reaction rates to the fresh catalyst, as well as same over-hydrogenation suppression trend.

Table 5.8. Comparison of compositions of the fresh and used catalysts. (determined by elemental analysis)

Catalysts	Pd:SiO_2 (w.t.%)	Pd:N	C:N
Pd-SBA-gt-PEI	1.7	0.022	2.6
Pd-SBA-gt-PEI (used)	1.8	0.024	2.6

Table 5.9. Comparison of activity of fresh, used and regenerated catalysts.

Catalysts [a]	R_Y (h^{-1})	Conv. (%)	Selectivity
Pd-SBA-gt-PEI	2598 ± 96	98	90:4:6
Pd-SBA-gt-PEI (used)	783 ± 105	96	91:4:5
Pd-SBA-gt-PEI (regenerated)	2661± 237	98	91:4:5

[a] Reaction conditions: selective hydrogenation of diphenylacetylene in the mixture of MeOH and dioxane (v:v = 1:1), 0.1 mol% Pd loading, room temperature, 1 atm H_2 pressure.

5.4 Conclusions

Aminopolymer-silica composite supported Pd(0) nanoparticle catalysts with good selectivity were successfully developed for the hydrogenation of alkynes in liquid media. Small palladium nanoparticles with narrow distribution were formed on the aminopolymer composite support using the $NaBH_4$ reduction method. The catalysts displayed high activity for the selective hydrogenation of diphenylacetylene while keeping excellent alkene selectivity and stereo-selectivity. Subsequent hydrogenation to alkanes was further suppressed on the Pd-SiO_2-gt-PEI catalysts compared to the Pd-HAS ($NaBH_4$ reduction), implying that better coverage of the surface of palladium nanoparticle surface with amino groups in the SBA-gt-PEI and MCF-gt-PEI composite catalysts prepared by the "grafting to" method using moderate molecular weight branched PEI more effectively reduced the adsorption constant of alkenes to improve the selectivity. No palladium leaching or significant nanoparticle agglomeration were observed in the used catalyst, and the catalytic activity could fully recovered after

regeneration of the used catalysts, indicating the excellent stability, recoverability and recyclability of the catalytic system.

5.5 Acknowledgements

This work was supported by the U.S. Department of Energy, Basic Energy Sciences, for financial support through Catalysis Science Grant/Contract No. DE-FG02-03ER15459.

5.6 References

(1) Molnar, A.; Sarkany, A.; Varga, M. *J. Mol. Catal. A: Chem.* **2001**, *173*, 185.

(2) Semagina, N.; Renken, A.; Kiwi-Minsker, L. *J. Phys. Chem. C* **2007**, *111*, 13933.

(3) Mallat, T.; Baiker, A. *Appl. Catal. A: Gen.* **2000**, *200*, 3.

(4) Lindlar, H. *Helv. Chim. Acta* **1952**, *35*, 446.

(5) Anderson, J.; Mellor, J.; Wells, R. *J. Catal.* **2009**, *261*, 208.

(6) Mori, S.; Ohkubo, T.; Ikawa, T.; Kume, A.; Maegawa, T.; Monguchi, Y.; Sajiki, H. *J. Mol. Catal. A: Chem.* **2009**, *307*, 77.

(7) Sajiki, H.; Mori, S.; Ohkubo, T.; Ikawa, T.; Kume, A.; Maegawa, T.; Monguchi, Y. *Chem. Eur. J.* **2008**, *14*, 5109.

(8) Carino, E. V.; Knecht, M. R.; Crooks, R. M. *Langmuir* **2009**, *25*, 10279.

(9) Mitran, E.; Dellinger, B.; McCarley, R. L. *Chem. Mater.* **2010**, *22*, 6555.

(10) Mizugaki, T.; Murata, M.; Fukubayashi, S.; Mitsudome, T.; Jitsukawa, K.; Kaneda, K. *Chem. Commun.* **2008**, 241.

(11) Wilson, O. M.; Knecht, M. R.; Garcia-Martinez, J. C.; Crooks, R. M. *J. Am. Chem. Soc.* **2006**, *128*, 4510.

(12) Tabuani, D.; Monticelli, O.; Chincarini, A.; Bianchini, C.; Vizza, F.; Moneti, S.; Russo, S. *Macromolecules* **2003**, *36*, 4294.

(13) Sulman, E.; Bodrova, Y.; Matveeva, V.; Semagina, N.; Cerveny, L.; Kurtc, V.; Bronstein, L.; Platonova, O.; Valetsky, P. *Appl. Catal. A: Gen.* **1999**, *176*, 75.

(14) Sidorov, S.; Bronstein, L.; Valetsky, P.; Hartmann, J.; Cölfen, H.; Schnablegger, H.; Antonietti, M. *J. Colloid Interface Sci.* **1999**, *212*, 197.

(15) Semagina, N. V.; Bykov, A. V.; Sulman, E. M.; Matveeva, V. G.; Sidorov, S. N.; Dubrovina, L. V.; Valetsky, P. M.; Kiselyova, O. I.; Khokhlov, A. R.; Stein, B.; Bronstein, L. M. *J. Mol. Catal. A: Chem.* **2004**, *208*, 273.

(16) Schlotterbeck, U.; Aymonier, C.; Thomann, R.; Hofmeister, H.; Tromp, M.; Richtering, W.; Mecking, S. *Adv. Funct. Mater.* **2004**, *14*, 999.

(17) Ping, E. W.; Wallace, R.; Pierson, J.; Fuller, T. F.; Jones, C. W. *Micropor. Mesopor. Mater.* **2010**, *132*, 174.

(18) Narayanan, R.; El-Sayed, M. A. *J. Phys. Chem. B* **2004**, *108*, 8572.

(19) Knecht, M. R.; Pacardo, D. B. *Anal Bioanal Chem* **2010**, *397*, 1137.

(20) Mastalir, Á.; Király, *Z. J. Catal.* **2003**, *220*, 372.

(21) Erathodiyil, N.; Ooi, S.; Seayad, A. M.; Han, Y.; Lee, S. S.; Ying, J. Y. *Chem. Eur. J.* **2008**, *14*, 3118.

(22) Burton, P. D.; Boyle, T. J.; Datye, A. K. *J. Catal.* **2011**, *280*, 145.

(23) Brayner, R.; Viau, G. *J. Mol. Catal. A: Chem.* **2002**, *183*, 227.

(24) Bronstein, L.; Chernyshov, D. M.; Volkov, I. O.; Ezernitskaya, M. G.; Valetsky, P. M.; Matveeva, V. G.; Sulman, E. M. *J. Catal.* **2000**, *196*, 302.

(25) Biradar, A. V.; Biradar, A. A.; Asefa, T. *Langmuir* **2011**, *27*, 14408.

(26) Bolfa, C.; Zoleo, A.; Sassi, A. S.; Maniero, A. L.; Pears, D.; Jerabek, K.; Corain, B. *J. Mol. Catal. A: Chem.* **2007**, *275*, 233.

(27) Kralik, M.; Biffis, A. *J. Mol. Catal. A: Chem.* **2001**, *177*, 113.

(28) Bhattacharjee, S.; Dotzauer, D. M.; Bruening, M. L. *J. Am. Chem. Soc.* **2009**, *131*, 3601.

(29) Bhattacharjee, S.; Bruening, M. L. *Langmuir* **2008**, *24*, 2916.

(30) Garcia, M. E.; Baker, L. A.; Crooks, R. M. *Anal. Chem.* **1999**, *71*, 256.

(31) Kim, Y.; Oh, S.; Crooks, R. M. *Chem. Mater.* **2004**, *16*, 167.

(32) Scott, R. W. J.; Datye, A. K.; Crooks, R. M. *J. Am. Chem. Soc.* **2003**, *125*, 3708.

(33) Yeung, L. K.; Crooks, R. M. *Nano Letters* **2001**, *1*, 14.

(34) Crooks, R. M.; Zhao, M.; Sun, L.; Chechik, V.; Yeung, L. K. *Acc. Chem. Res.* **2001**, *34*, 181.

(35) Zhao, M.; Crooks, R. M. *Adv. Mater.* **1999**, *11*, 217.

(36) Niu, Y.; Yeung, L. K.; Crooks, R. M. *J. Am. Chem. Soc.* **2001**, *123*, 6840.

(37) White, R. J.; Luque, R.; Budarin, V. L.; Clark, J. H.; Macquarrie, D. J. *Chem. Soc. Rev.* **2009**, *38*, 481.

(38) Amali, A. J.; Rana, R. K. *Green Chem.* **2009**, *11*, 1781.

(39) Corain, B. *J. Mol. Catal. A: Chem.* **2001**, *173*, 99.

(40) Guillet-Nicolas, R.; Marcoux, L.; Kleitz, F. *New J. Chem.* **2010**, *34*, 355.

(41) Crespo-Quesada, M.; Dykeman, R. R.; Laurenczy, G.; Dyson, P. J.; Kiwi-Minsker, L. *J. Catal.* **2011**, *279*, 66.

(42) Mastalir, Á.; Rác, B.; Király, Z.; Molnár, Á. *J. Mol. Catal. A: Chem.* **2007**, *264*, 170.

(43) Mori, S.; Ohkubo, T.; Ikawa, T.; Kume, A.; Maegawa, T.; Monguchi, Y.; Sajiki, H. *J. Mol. Catal. A: Chem.* **2009**, *307*, 77.

(44) Na-Chiangmai, C.; Tiengchad, N.; Kittisakmontree, P.; Mekasuwandumrong, O.; Powell, J.; Panpranot, J. *Catal. Lett.* **2011**, *141*, 1149.

(45) Kluwer, A. M.; Koblenz, T. S.; Jonischkeit, T.; Woelk, K.; Elsevier, C. J. *J. Am. Chem. Soc.* **2005**, *127*, 15470.

(46) Laren, M. van; Elsevier, C. J. *Angew. Chem. Int. Ed.* **1999**, *38*, 3715.

(47) Laren, M. W. V.; Duin, M. A.; Klerk, C.; Naglia, M.; Rogolino, D.; Pelagatti, P.; Bacchi, A.; Pelizzi, C.; Elsevier, C. J. *Organometallics* **2002**, *21*, 1546.

(48) Pelagatti, P.; Venturini, A.; Leporati, A. *J. Chem. Soc., Dalton Trans.* **1998**, 2715.

(49) Costa, M.; Pelagatti, P.; Pelizzi, C.; Rogolino, D. *J. Mol. Catal. A: Chem.* **2002**, *178*, 21.

(50) Scarel, A.; Axet, M.; Amoroso, F.; Ragaini, F. *Organometallics* **2008**, *27*, 1486.

(51) Liprandi, D.; Cagnola, E.; Quiroga, M. *Catal. Lett.* **2009**, *128*, 423.

(52) Evrard, D.; Groison, K.; Mugnier, Y.; Harvey, P. D. *Inorg. Chem.* **2004**, *43*, 790.

(53) Mizugaki, T.; Ooe, M.; Ebitani, K.; Kaneda, K. *J. Mol. Catal. A: Chem.* **1999**, *145*, 329.

(54) Lukens Jr, W. W.; Schmidt-Winkel, P.; Zhao, D.; Feng, J.; Stucky, G. D. *Langmuir* **1999**, 5403.

(55) Zhao, D.; Huo, Q.; Feng, J.; Chmelka, B.; Stucky, G. D. *J. Am. Chem. Soc.* **1998**, *120*, 6024.

(56) Zhao, D.; Feng, J. L.; Huo, Q.; Melosh, N.; Fredrickson, G. H.; Chmelka, B. F.; Stucky, G. D. *Science* **1998**, *279*, 548.

(57) Han, Y.; Lee, S. S.; Ying, J. Y. *Chem. Mater.* **2007**, *19*, 2292.

(58) Kim, H.; Moon, J.; Park, J. *J. Colloid Interface Sci.* **2000**, *227*, 247.

(59) Hicks, J. C.; Drese, J. H.; Fauth, D. J.; Gray, M. L.; Qi, G.; Jones, C. W. *J. Am. Chem. Soc.* **2008**, *130*, 2902.

(60) Kim, S.; Ida, J.; Guliants, V. V.; Lin, J. Y. S. *J. Phys. Chem. B* **2005**, *109*, 6287.

(61) Drese, J. H.; Choi, S.; Lively, R. P.; Koros, W. J.; Fauth, D. J.; Gray, M. L.; Jones, C. W. *Adv. Funct. Mater.* **2009**, *19*, 3821.

(62) Hughes, M.; Miranda, P.; Nielsen, D.; Rosenberg, E.; Gobetto, R.; Viale, A.; Burton, S. *Macromol. Symp.* **2006**, *235*, 161.

(63) Krämer, M.; Stumbé, J.; Grimm, G.; Kaufmann, B.; Krüger, U.; Weber, M.; Haag, R. *ChemBioChem* **2004**, *5*, 1081.

(64) Lee, Y.; Motoyama, Y.; Tsuji, K.; Yoon, S.; Mochida, I.; Nagashima, H. *ChemCatChem* **2012**, *4*, 778.

(65) Sajiki, H.; Mori, S.; Ohkubo, T.; Ikawa, T.; Kume, A.; Maegawa, T.; Monguchi, Y. *Chem. Eur. J.* **2008**, *14*, 5109.

(66) McEleney, K.; Crudden, C. M.; Horton, J. H. *J. Phys. Chem. C* **2009**, *113*, 1901.

(67) Komatsu, T.; Takagi, K.; Ozawa, K. *Catal. Today* **2011**, *164*, 143-147.

(68) Brunet, J.; Caubere, P. *J. Org. Chem.* **1984**, *49*, 4058.

(69) Drese, J. H.; Choi, S.; Lively, R. P.; Koros, W. J.; Fauth, D. J.; Gray, M. L.; Jones, C. W. *Adv. Funct. Mater.* **2009**, *19*, 3821-3832.

(70) Drese, J. H.; Choi, S.; Didas, S. a.; Bollini, P.; Gray, M. L.; Jones, C. W. *Micropor. Mesopor. Mater.* **2012**, *151*, 231.

(71) Dillon, E. P.; Crouse, C. A.; Barron, A. R. *ACS Nano* **2007**, *2*, 156.

CHAPTER 6

SUMMARY AND FUTURE WORK

6.1 Summary

As stated in the introduction part, the main goals of the thesis were to: (1) identify novel materials or architectures to build immobilized catalysts with new or unique properties; (2) intelligently design immobilized catalysts to tune the accessibility of active sites to achieve better activity/selectivity; (3) investigate the recoverability and recyclability of the catalytic systems and understand the deactivation mechanisms. With these goals in mind, valuable insights were gained during the course of this thesis work.

In the first project, Magnetic nanoparticle $CoFe_2O_4$ supported aluminum isoproxide was developed for ROP of ϵ-caprolactone. ROP of cyclic lactone monomers is a common route to produce biodegradable and biocompatible polyesters with wide applications in bio-renewable materials. MNP supported aluminum isopropoxide was demonstrated as a new catalyst for the ROP of ϵ-caprolactone. The catalyst can be easily separated from reaction solution under an external magnetic field and reused, yielding poly(caprolactone) products with negligible metal residues. Detailed investigation of the polymerization kinetics, along with characterization of the polymer products allowed for a better understanding of this new catalytic system. Comprehensive characterization of the used catalysts revealed that loss of a small amount of active sites and presence of polymer residue on the catalyst were probably the main reasons for the decreased activity with the recycled catalysts.

This was the first reported example of a MNP supported catalyst for polymerization involving a mechanism that includes the covalent attachment and growth of polymers at the active sites. Although MNP supported catalysts for ATRP have been reported before,[1] that catalytic system does not involve direct polymer-active sites bonds. MNP supported polymerization catalysts preclude the deactivation potential which is common in polymerization using supported catalysts on porous supports, such as pore clogging and internal diffusion limitations. However for this catalyst to be commercially viable, the catalyst activity and the control of the molecular weight of the polymer product should be further improved.

In the second project based on MNP supports, a silica-coated MNP-supported DMAP catalyst was synthesized and used for epoxide ring opening reactions using phenolic nucleophiles. The catalyst displayed good activity and region-selectivity, which is similar to that of mesoporous silica supported DMAP catalysts. This example also further demonstrated the versatile applications of magnetic nanoparticles in immobilized catalysts.

MNPs are promising catalyst supports[2,3] for a few reasons: magnetic separation; high external surface area; capacity for different surface modifications; easy dispersion in reaction solutions due to the nanoscale size. Some of these properties are impossible or very difficult to obtain using traditional materials. Along with further development in the following associated areas, such as controllable preparation of MNPs on a large scale, improved understanding on the surface chemistry of MNPs, MNPs will find wider applications in the field of immobilized catalysts.

The second class of immobilized catalysts investigated in this work is based on polymer-silica composite materials. Specifically, Chapter 4 describes the development and use of polymer brush supported sulfonic acid catalysts for acid catalysis. Silica-polymer brush supported sulfonic acids with high acid density, enhanced activity and improved stability were developed in this work and evaluated in hydrolytic reactions. One of the key disadvantages of traditional polymeric sulfonic acid catalysts based on crosslinked poly(styrene) resins is their poor swellability in aqueous media. Catalytic conversions involving water are of high importance in biomass conversion into chemicals and fuels. To create polymeric catalysts for enhanced utility in aqueous media, polymer composites based on silica supported poly(styrene sulfonic acid) brushes were prepared via ATRP as a new class of potentially water tolerant solid acid catalysts. With highly accessible acid sites and high acid loading, the polymer brush catalysts were used in the hydrolysis of ethyl lactate and displayed similar activity to a homogeneous analogue, *p*-toluenesulfonic acid, as well as substantially higher reaction rate than a commercial resin, Amberlyst 15. A new ATRP initiator with better hydrolytic stability was synthesized and used for preparation of the polymer brush catalysts. The resulting polymer brush catalyst exhibited improved stability. The activity of the recycled polymer brush catalysts decreased slightly in each cycle due to desulfonation and polymer loss. This work is among the first examples of the use of solid-supported polymer brushes as catalysts, with the first few catalysts based on polymer brush materials reported in 2008.[4,5]

The use of a different type of silica-polymer composite as a support for immobilized catalysts was described in Chapter 5. Specifically, aminopolymer-silica composite supported Pd catalysts were developed for the selective hydrogenation of

alkynes, which is an important class of chemical transformations with wide applications in industry. The catalysts displayed high activity for selective hydrogenation of diphenylacetylene while keeping good alkene and stereo-selectivity. Over-hydrogenation to alkanes at high conversions of alkynes was highly suppressed using a Pd-SiO_2-gt-PEI catalyst compared to the Pd-HAS catalyst, which was hypothesized to be due to better coverage of the palladium nanoparticle with amino groups in the SiO_2-gt-PEI catalyst, which effectively suppressed the adsorption of alkenes on the palladium nanoparticle surface. Negligible palladium leaching and nanoparticle agglomeration were observed in the used catalyst, and the catalytic activity could be fully recovered after regeneration. In this case, the aminopolymer composite was used as a template to stabilize the palladium nanoparticles with good dispersion, as well as a modifier to tune the catalyst selectivity.

All in all, the novel immobilized catalysts developed in this thesis work offered new catalyst candidates for several potential applications. It was also demonstrated that immobilized catalyst is not only about anchoring the active sites on the supports; with suitable materials and rational design, catalysts with improved activity and selectivity could be developed.

6.2 Suggested Future work

Palladium nanoparticles have been intensively studied recently due to their high efficiency, unique size/shape dependent catalytic properties, and the ability to catalyze a broad range of chemical reactions. For optimal performance, the nanoparticles must retain their structural stability during storage or while being used in specific catalytic

transformations. This stability is typically controlled by the ligands that are used to passivate the surface of the Pd nanoparticles. Different ligands/stabilizers, such as dendrimers, polymers, and surfactants have been used to prevent agglomeration of the nanoparticles while allowing for suitable interactions between reagents/products with surface palladium atoms. The ligands can also work as modifiers to tune the activity and selectivity of the catalysts, as shown in Chapter 6, by adjusting the electronic properties of the palladium surface, selectively poisoning active sites,[6] or acting as selective filters that allow for specific molecular orientation/entrance.[7]

Although molecular ligands or soluble polymer-stabilized palladium nanoparticles exhibit unique catalytic properties, the inherent difficulties in catalyst separation indeed limit their wide application. Polymer composites have emerged as promising supports for palladium nanoparticles, working as stabilizers while tuning the catalytic performance via support-active sites interaction, as noted above. Robust polymer composites could be prepared via *in-situ* polymerization in or on various materials (e.g. SiO_2, MNP, etc.),[8–10] or by direct grafting of pre-formed polymers onto the surface.[11,12] Unlike polymeric resins, polymer composites typically do not experience huge shrinking or swelling in solvents due to the structural rigidity imparted by the oxide support, and tend to be used at higher temperatures and have good long term stability. Following the work presented here on aminopolymer composite-supported Pd for selective hydrogenations, here are several interesting topics worth future exploration.

6.2.1 Further investigation on the modification effects of polymer composites

As described in Chapter 5, the over-hydrogenation from alkenes to alkanes was further hindered using Pd-SBA-gt-PEI compared to Pd-HAS, implying different modification effects derived from different structural properties imparted by different catalyst synthesis procedures. To improve the activity/selectivity, and develop a better understanding of the modification effects of the aminopolymer composites, the physical and chemical properties of the composites could be further tailored:

(1) Varying the molecular weights of the branched PEI to prepare a series of aminopolymer composites via the "grafting to" method to investigate how the palladium nanoparticle size and the corresponding activity / selectivity will be changed;

(2) Changing the degree of polymer cross-linking to modulate the swelling ability and accessibility of active sites;

(3) Incorporating other functional polymers with suitable ligands to the polymer composites, such as phosphinated polymers,[13] polyaniline,[14] etc., to modify the electronic properties of the palladium catalytic sites.

Further improvement of activity and selectivity of the catalysts via modulating the interaction between the palladium nanoparticle and the polymer composite can be achieved via rational modifying the physical and chemical properties of the polymer composites.

6.2.2 Characterization of the aminopolymer composite supported Pd nanoparticles using XAS

It is extremely difficult to probe the palladium and N ligand interactions with common characterization techniques. Specific information on formal oxidation state and local coordination environment could be obtained with X-ray absorption spectroscopy (XAS),[15,16] which is composed of two regions X-ray Absorption Near Edge Structure (XANES) and Extended X-ray Fine Structure spectrum (EXAFS). This technique can allow for in-situ reduction of the molecular palladium precursors, giving insight into the nature of the active palladium centers. Further characterization of aminopolymer composite-supported Pd nanoparticles via XAS should be performed to probe the interaction between surface palladium atoms and amino groups of the polymer composite to develop a better understanding of the catalytic performance.

6.2.3 Development of Pd nanoparticles on polymer brush sulfonic acids for the direct synthesis of hydrogen peroxide

Other polymer composites, for example silica-polymer brush materials developed in the thesis work, could also be used as the supports for palladium nanoparticles to achieve new catalytic applications, such as direct synthesis of hydrogen peroxide. Direct synthesis of hydrogen peroxide from hydrogen and oxygen has attracted tremendous attention in recent years.[17–26] To maintain the reaction outside the explosive region, the reaction mixture of H_2 and O_2 should contain less than 4% hydrogen.

The majority of the catalysts used in the direct synthesis of H_2O_2 are based on palladium. It is proposed that Pd nanoparticles with a high percentage of surface atoms with a low coordination number are favorable to achieve high activity and selectivity.[27] Small palladium nanoparticles tend to have more kink and step sites with a lower coordination number than the terrace atoms. In addition to the palladium, acids are often added into the reaction medium to prevent decomposition of H_2O_2. To reduce the corrosion by inorganic acids, acidic solid materials are often introduced as catalyst supports. Palladium catalysts immobilized on acidic resins and silica supported sulfonic acids have been developed as efficient catalysts for direct synthesis of H_2O_2.[17,25] It will be interesting to develop small palladium nanoparticles based on solid-polymer brush sulfonic acids for direct synthesis of hydrogen peroxide.

6.3 References

(1) Ding, S.; Xing, Y.; Radosz, M.; Shen, Y. *Macromolecules* **2006**, *39*, 6399.

(2) Lu, A.-hui; Salabas, E. L.; Schüth, F. *Angew. Chem. Int. Ed.* **2007**, *46*, 1222.

(3) Laurent, S.; Forge, D.; Port, M.; Roch, A.; Robic, C.; Vander Elst, L.; Muller, R. N. *Chem. Rev.* **2008**, *108*, 2064.

(4) Gill, C. S.; Venkatasubbaiah, K.; Phan, N. T. S.; Weck, M.; Jones, C. W. *Chem. Eur. J.* **2008**, *14*, 7306-13.

(5) Zhao, B. I. N.; Jiang, X.; Li, D.; Jiang, X.; Lenick, T. G. O.; Li, B.; Li, C. Y. *J. Polym. Sci., Part A: Polym. Chem.* **2008**, *46*, 3438.

(6) Crespo-Quesada, M.; Dykeman, R.; Laurenczy, G. *J. Catal.* **2011**, *279*, 66.

(7) Niu, Y.; Yeung, L. K.; Crooks, R. M. *J. Am. Chem. Soc.* **2001**, *123*, 6840.

(8) Kim, H.; Moon, J.; Park, J. *Journal of colloid and interface science* **2000**, *227*, 247.

(9) Choi, M.; Kleitz, F.; Liu, D.; Lee, H. Y.; Ahn, W.-S.; Ryoo, R. *J. Am. Chem. Soc.* **2005**, *127*, 1924-32.

(10) Moreno, J.; Sherrington, D. C. *Chem. Mater.* **2008**, *20*, 4468.

(11) Kim, S.; Ida, J.; Guliants, V. V.; Lin, J. Y. S. *J. Phys. Chem. B* **2005**, *109*, 6287.

(12) Hughes, M.; Miranda, P.; Nielsen, D.; Rosenberg, E.; Gobetto, R.; Viale, A.; Burton, S. *Macromolecular Symposia* **2006**, *235*, 161.

(13) Nishio, R.; Sugiura, M.; Kobayashi, S. *Organic & Biomolecular Chemistry* **2006**, *4*, 992.

(14) Gao, Y.; Chen, C.-an; Gau, H.-mou; Bailey, J. A.; Akhadov, E.; Williams, D.; Wang, H.-lin *Chem. Mater.* **2008**, *20*, 2839.

(15) Shimizu, K.; Koizumi, S.; Hatamachi, T.; Yoshida, H.; Komai, S.; Kodama, T.; Kitayama, Y. *J. Catal.* **2004**, *228*, 141.

(16) Nelson, R. C.; Miller, J. T. *Catalysis Science & Technology* **2012**, *2*, 461.

(17) Blanco-brieva, G.; Cano-serrano, E.; Campos-martin, J. M.; Fierro, J. L. G. *Chem. Commun.* **2004**, 1184.

(18) Blanco-Brieva, G.; Capel-Sanchez, M. C.; de Frutos, M. P.; Padilla-Polo, A.; Campos-Martin, J. M.; Fierro, J. L. G. *Ind. Eng. Chem. Res.* **2008**, *47*, 8011.

(19) Liu, Q.; Bauer, J. C.; Schaak, R. E.; Lunsford, J. H. *Angew. Chem. Int. Ed.* **2008**, *47*, 6221.

(20) Edwards, J. K.; Hutchings, G. J. *Angew. Chem. Int. Ed.* **2008**, *47*, 9192.

(21) Edwards, J. K.; Ntainjua, E.; Carley, A. F.; Herzing, A. a; Kiely, C. J.; Hutchings, G. J. *Angew. Chem. Int. Ed.* **2009**, *48*, 8512.

(22) Ntainjua N, E.; Piccinini, M.; Pritchard, J. C.; Edwards, J. K.; Carley, A. F.; Moulijn, J. a; Hutchings, G. J. *ChemSusChem* **2009**, *2*, 575.

(23) Edwards, J. K.; Solsona, B.; Ntainjua, E.; Carley, A. F.; Herzing, A. A.; Kiely, C. J.; Hutchings, G. J. *Science* **2009**, *323*, 1037.

(24) Brieva, G. B.; Campos-Martin, J. M.; de Frutos, M. P.; Fierro, J. L. G. *Catal. Today* **2010**, *158*, 97.

(25) Blanco-Brieva, G.; de Frutos Escrig, M. P.; Campos-Martin, J. M.; Fierro, J. L. G. *Green Chem.* **2010**, *12*, 1163.

(26) Kim, J.; Chung, Y.-M.; Kang, S.-M.; Choi, C.-H.; Kim, B.-Y.; Kwon, Y.-T.; Kim, T. J.; Oh, S.-H.; Lee, C.-S. *ACS Catalysis* **2012**, *2*, 1042.

(27) Campos-Martin, J. M.; Blanco-Brieva, G.; Fierro, J. L. G. *Angew. Chem. Int. Ed.* **2006**, *45*, 6962.